

2



AL-TR-89-051

AD:

Final Report
for the period
July 1986 to
July 1989

Dynamics of Electronically Excited Species in Gaseous and Condensed Phase

December 1989

Authors:
P.K. Swaminathan
M.J. Redmon
C.S. Murthy
B.C. Garrett
G.A. Natanson

Chemical Dynamics Corporation
9560 Pennsylvania Avenue
Upper Marlboro, MD 20772

F04611-86-C-0068

AD-A217 696

Approved for Public Release

Distribution is unlimited. The AFAL Technical Services Office has reviewed this report, and it is releasable to the National Technical Information Service, where it will be available to the general public, including foreign nationals.

Prepared for the: **Astronautics Laboratory (AFSC)**

Air Force Space Technology Center
Space Systems Division
Air Force Systems Command
Edwards Air Force Base, CA 93523-5000

90 01 17 100

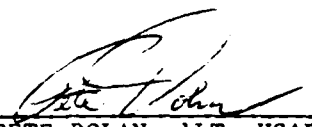
NOTICE


When U.S. Government drawings, specifications, or other data are used for any purpose other than a definitely related Government procurement operation, the fact that the Government may have formulated, furnished, or in any way supplied the said drawings, specifications, or other data, is not to be regarded by implication or otherwise, or in any way licensing the holder or any other person or corporation, or conveying any rights or permission to manufacture, use, or sell any patented invention that may be related thereto.

FOREWORD

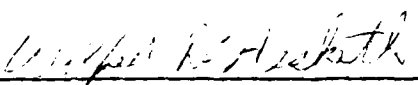
This final report was submitted by Chemical Dynamics Corporation on completion of Contract F04611-86-C-0068 for the Astronautics Laboratory (AFSC), Edwards AFB, CA. The Astronautics Laboratory Project Manager was Lt Pete Dolan.

This report has been reviewed and is approved for release and distribution in accordance with the distribution statement on the cover and on the DD Form 1473.


PETE DOLAN, 1LT, USAF
Project Manager


STEPHEN L. RODGERS
Chief, Applied Research in Energy
Storage Office

FOR THE DIRECTOR


WILFRED D. HESKETH
Acting Deputy Director
Astronautical Sciences Division

UNCLASSIFIED

SECURITY CLASSIFICATION OF THIS PAGE

REPORT DOCUMENTATION PAGE				Form Approved OMB No. 0704-0188	
1a. REPORT SECURITY CLASSIFICATION Unclassified			1b. RESTRICTIVE MARKINGS		
2a. SECURITY CLASSIFICATION AUTHORITY			3. DISTRIBUTION / AVAILABILITY OF REPORT Approved for public release; distribution unlimited		
2b. DECLASSIFICATION / DOWNGRADING SCHEDULE					
4. PERFORMING ORGANIZATION REPORT NUMBER(S) CD-TR-89-003			5. MONITORING ORGANIZATION REPORT NUMBER(S) AL-TR-89-051		
6a. NAME OF PERFORMING ORGANIZATION Chemical Dynamics Corporation		6b. OFFICE SYMBOL (If applicable)	7a. NAME OF MONITORING ORGANIZATION Astronautics Laboratory (AFSC)		
6c. ADDRESS (City, State, and ZIP Code) 9560 Pennsylvania Avenue Upper Marlboro, MD 20772			7b. ADDRESS (City, State, and ZIP Code) Edwards Air Force Base, CA 93523-5000		
8a. NAME OF FUNDING / SPONSORING ORGANIZATION		8b. OFFICE SYMBOL (If applicable)	9. PROCUREMENT INSTRUMENT IDENTIFICATION NUMBER F04611-86-C-0068		
8c. ADDRESS (City, State, and ZIP Code)			10. SOURCE OF FUNDING NUMBERS		
PROGRAM ELEMENT NO. 62302 F		PROJECT NO. 5730	TASK NO. 00	WORK UNIT ACCESSION NO. WI	
11. TITLE (Include Security Classification) Dynamics of Electronically Excited Species in Gaseous and Condensed Phase					
12. PERSONAL AUTHOR(S) P. K. Swaminathan, M. J. Redmon, C. S. Murthy, B. C. Garrett and G. A. Natanson					
13a. TYPE OF REPORT Final		13b. TIME COVERED FROM 86.07 TO 89.07	14. DATE OF REPORT (Year, Month, Day) 89 Dec		15. PAGE COUNT 154
16. SUPPLEMENTARY NOTATION					
17. COSATI CODES			18. SUBJECT TERMS (Continue on reverse if necessary and identify by block number)		
FIELD 0704	GROUP 2109	SUB-GROUP	HEDM, condensed phase, matrix isolation, lifetimes, energetic molecules, electronic excitation, semiclassical, simulations, stochastic dynamics, potentials		
19. ABSTRACT (Continue on reverse if necessary and identify by block number)					
<p>In order to assess the potential of energetic molecules to be advanced rocket propellants, the Air Force High Energy Density Materials Program requires theoretical methods to predict the lifetimes of energetic molecules in condensed phase. This research met this need by developing novel dynamical methods which can be used to elucidate the microscopic dynamics controlling lifetimes relevant to energy storage in isolated and matrix-embedded molecules. This has resulted in the capability to identify important quenching pathways in gas and condensed phases using computational methods. This research consisted of (1) developing novel semiclassical methods and computer simulation technology and (2) applications to the dynamics of electronically inelastic chemistry of light metastables, including helium and hydrogen in the gas and condensed phase.</p> <p style="text-align: center;">(Continued)</p>					
20. DISTRIBUTION / AVAILABILITY OF ABSTRACT <input checked="" type="checkbox"/> UNCLASSIFIED/UNLIMITED <input type="checkbox"/> SAME AS RPT. <input type="checkbox"/> DTIC USERS			21. ABSTRACT SECURITY CLASSIFICATION Unclassified		
22a. NAME OF RESPONSIBLE INDIVIDUAL Pete Dolan, 1Lt., USAF			22b. TELEPHONE (Include Area Code) (805) 275-5649		22c. OFFICE SYMBOL AL/LSX

19. Abstract (Continuation)

The key accomplishments in this research program include (1) development and validation of general and powerful semiclassical methods for energetic polyatomic species, (2) development of reduced heatbath models of condensed phase helium, (3) development of models of condensed phase hydrogen and (4) development of simulation procedures for solution-phase reaction and cluster formation of high energy density materials (HEDMs) with solvents. (11)

EXECUTIVE SUMMARY

This is the final report of a three year ARIES research program entitled "Dynamics of Electronically Excited Species in Gas and Condensed Phases". This research addressed the need of the Air Force High Energy Density Materials program to determine the lifetimes of potential advanced rocket propellants.

The key objective was to develop novel dynamical methods to be used in elucidating the microscopic dynamics controlling lifetimes important in energy storage in isolated and matrix-embedded molecules. This objective was met by (1) developing novel semiclassical methods and combining them with computer simulation technology; and (2) using these methods to computationally treat the electronically inelastic chemistry of light metastables, including helium and hydrogen, in the gas and condensed phase.

This report presents the new technologies and illustrative applications for which the relevant potential energy surface information existed. These applications successfully determined the mechanisms controlling helium metastable lifetimes in a transition from the gas to the condensed phase.

The methods validated by this research can be applied to problems where it is feasible to obtain the relevant interaction potentials and couplings. Different levels of implementation of the semiclassical methods are considered in this report. The levels vary from fully quantitative to semiquantitative levels of accuracy, and depend on the dynamical problem. In practice, the most relevant few-body potential energy surface information can be identified and obtained. The methods developed here can then be used to determine the underlying complex dynamical behavior of energetic molecules.



Accession For	
NAME	<input checked="" type="checkbox"/>
DATE	<input type="checkbox"/>
UNCLASSIFIED	<input type="checkbox"/>
JAN 1981	
Ft. Belvoir	
Dist	
A-1	

CONTENTS

INTRODUCTION	<u>Page</u> 9
TECHNICAL DISCUSSION	12
Gas Phase Methods and Calculations	12
Introduction	12
Semiclassical Methodology for Computing Multichannel Eikonal Wavefunctions in Molecular Collisions: A Reformulation and Extension	12
He-He* Scattering Calculations	40
Accurate Computations of Energy Transfer in Atom- Diatom Collisions: Comparative Study of Vibrational Excitations using Semiclassical Wavefunctions and Coupled Quantal States	55
The Quenching of Na(3^2P) by H ₂ : A Quantal IOS Calculation of Electronic-to-Vibrational Energy Transfer	68
Condensed Phase Modelling and Computer Experiments	93
Introduction	93
Monte Carlo Simulations of Helium Bubble States	94
Heatbath Models for Helium Bubble States	114
Condensed Phase Dynamics	136
Introduction	136
Dynamics of He* ($3S$) in Condensed Phase Bubbles	137

Extended Studies	141
Solvent Shift of $2^3\text{S} \rightarrow 2^3\text{P}$ Absorption Line	141
Studies on the H_2 matrix	141
CONCLUSIONS AND RECOMMENDATIONS	151
PUBLICATIONS, MEETINGS ATTENDED, OTHER INTERACTIONS AND PERSONNEL	152

ILLUSTRATIONS

<u>Figure</u>		<u>Page</u>
1	He-He* potential energy curves and couplings for two-state model.	40
2	Cross section for He(¹ P) quenching to He(³ S)	42
3	Opacity function for He(¹ P) quenching to He(³ S)	42
4	He ₂ Transition Pathways	51
5	He ₂ Two-state (a and X) radiative quenching model potentials	53
6	Angle Dependent O+HF(v) Vibrational Excitation (v=0 to v=1)	64
7	Angular Momentum Dependence of (v=0 to v=1) Vibrational Excitation in O+HF	65
8	Angular Momentum Dependence of (v=0 to v=1) Vibrational Excitation in Na+H ₂	66
9	Two Lowest Potential Energy Surfaces of NaH ₂ - Fixed R	79
10	Two Lowest Potential Energy Surfaces of NaH ₂ - Fixed γ	81
11	Nonadiabatic Coupling Term $f_{12}^{aA}(r,R,\gamma)$ - Fixed R	83
12	Mixed Adiabatic-Diabatic Potential Curves $V_{nn}^{dA}(r,R,\gamma)$	85
13	Eigenvalues $E_m^j(R,\gamma)$ of the H ₂ Internal Hamiltonian	87
14	Transition Probabilities $S_{mm}^{jl}(\gamma)^2$ versus IOS Angle γ	89
15	Long Range Potentials for He* in He Simulations	99
16	Structure of He* (c) Bubble	103
17	Structure of He* (a) Bubble	107
18	Structure of He* (a) Bubble for Different Treatments	109
19	Pressure Dependent Liquid Structure of He	121
20	Pressure Dependent Velocity Autocorrelation in Liquid He	123
21	Pressure Dependence of He(¹ S) Heatbath Parameters	125
22	Pressure Dependent Gaussian Friction Model of of He(¹ S) Heatbath	127
23	Deduced Velocity Correlations of He(³ S) in Solution	129

24	Schematic Illustration of Stochastic Model of Helium Bubble	137
25	(a and b) Model He(³ S) Dynamics at 0.5GPa	139
26	(a and b) Model He(³ S) Dynamics at 1.4GPa	139
27	Liquid Hydrogen Pair Correlations (P and L dimers)	142
28	Liquid Hydrogen Pair Correlations (T and X dimers)	142
29	Liquid Hydrogen Velocity Correlations	143
30	g-Coefficients (000,200,220) of Liquid Hydrogen Pair Correlations	147
31	g-Coefficients (221,222,400) of Liquid Hydrogen Pair Correlations	149

TABLES

<u>Table</u>	<u>Page</u>
1 Helium Metastable Lifetimes	10
2 He ₂ Electronic States in the Ω basis	46
3 He ₂ Total Coupling in the Ω basis	47
4 MC Results of He* in He at 300K	107
5 Thermodynamic Properties of Liquid ⁴ He at 300K	130
6 GLE Parameters for He and He* Solutes in Liquid He	131
7 Characteristics of Liquid Hydrogen Pair Correlation Functions	145

GLOSSARY OF KEY SYMBOLS

Δ_Q, ∇_R^2	Multidimensional Laplacians
$\frac{\partial}{\partial \cdot}$	Partial derivatives
∇	Multidimensional Gradient
δ_{ij}	Kronecker delta
$\hat{e}_{k\sigma}$	Photon polarization unit vector for wavevector k and polarization σ
$g_{(v)}^{s,s'}$	Momentum coupling for semiclassical change of coordinates
$g^{\mu\mu'}$	Covariant metric tensor
H	Hamiltonian operator
h, \hbar	Planck's constant, and divided by 2π
$h_{nv,n',v'}^{jl}$	Hamiltonian matrix element in close coupled equation
He^*	Electronically excited helium atom
$\tilde{J}(t, r_0, v)$	Modified function related to the semiclassical Jacobian $J(t, r_0, v)$
J_v	Semiclassical Jacobian
μ_r, μ_R	Reduced masses
$P^{(v)}(R)$	Momentum function for channel v at streamline coordinate R
\dot{P}, \ddot{P}	First and second time derivatives of P
$P_{\mu s}^v; Q_v^{\mu s}$	Elements of the semiclassical Jacobian matrix

$\sigma_{i \rightarrow j}$	Cross section for transition from state i to j
$t(v)$	Time for channel v
\hat{T}	Kinetic energy operator
u^T	Transpose of u
$V_v(Q)$	Adiabatic potential for channel v
$W_v(Q)$	Hamilton's characteristic function
$ \cdot $	Modulus valued
β_v^*	Complex conjugate of β_v
$\vec{a} \cdot \vec{b}$	Vector Dot (scalar) product of vectors \vec{a} and \vec{b}
\cdot	Tensor covariant product
$\langle \rangle$	Canonical ensemble average, quantum mechanical expectation value
β^+	Adjoint of β
div	Divergence operator
$arg[...]$	Argument of [...]
$mod[\pi]$	Modulo π
ϕ', ϕ''	First and second derivatives of ϕ

INTRODUCTION

High energy density material (HEDM) candidates necessarily involve excited or energetic molecular states. Their metastability in the gas phase can arise from spontaneous radiative decay, predissociation, or energy loss induced (via radiative and nonradiative relaxation, and reaction) in a collision with the ambient gas molecules. Any HEDM will be eventually used in a condensed phase environment for practical application. In the matrix environment, a variety of time dependent processes can occur that lead to decay of the stored energy. (1) the excitation may relax by radiative decay, (2) it may decay due to the relaxation induced by the coupling to the lattice phonons, (3) it may relax into modes localized at the site of the HEDM [such modes are strongly coupled to the HEDM states], (4) the stored excitation energy may be resonantly transferred to another excited molecule [this is the elementary step that leads to energy migration], (5) the excitation may be nonresonantly transferred to a chemically different matrix species, and (6) a chemical reaction of the excited HEDM may take place.

The main goal of this research program has been to develop the capability to identify important quenching pathways in gas and condensed phases using theoretical methods. In order to be able to treat electronically excited species, which are a key source of new metastable systems, we have concentrated on developing dynamical methodologies for electronically inelastic collision problems. We have addressed gas and condensed phase lifetime problems with helium metastables as prototypes.

Our key accomplishments in this research program include:

- (1) development and validation of general and powerful semiclassical methods for energetic species and polyatomic systems,
- (2) development of reduced heatbath models of condensed phase helium,
- (3) development of models of condensed phase hydrogen matrix, and
- (4) development of simulation procedures for solution-phase reaction and cluster formation of HEDM with solvents.

As an application, we present elucidation of the important dynamical mechanisms contributing to the observed helium metastable atom quenching propensities in gas and condensed phases using accurate *ab initio* input for the appropriate electronic potentials and couplings. A variety of processes have been addressed in validations or illustrative examples: (1) gas and condensed phase collision-induced radiative quenching, (2) gas and condensed phase collisional (nonradiative) quenching, (3) gas phase vibrational energy transfer, (4) gas phase electronic energy transfer, (5) condensed phase reaction with solvent medium, (6) pressure dependent solvation effects on different electronic states.

An illustrative example of our results concerns the dynamical mechanisms for the observed lifetime trends in helium metastables. Table 1 shows the known lifetimes of electronically excited $\text{He}^*(2^3\text{S})$ atoms and $\text{He}_2^*(a^3\Sigma_u^+)$ molecules in vacuum and condensed phase environments. The key trend to notice is the large change of lifetime (from 8000 sec to 15 μsec) that occurs upon transferring an excited atom into liquid, compared to the relatively small change (from 18 sec to 10 sec) found for the diatom. The large change in the vacuum lifetime of the atomic versus diatomic species is also noteworthy since this change is mostly accounted for by the spin-forbidden radiative quenching process constantly operative in the molecule. Unravelling the relevant mechanisms to

Table 1. Helium Metastable Lifetimes

Type	Species	Lifetime	Basis
Vacuum	$\text{He}^*(2^3\text{S})$	8000 s	PRL 30, 775 (1973)
Vacuum	$\text{He}_2^*(a^3\Sigma_u^+)$	18 s	JCP 90, 2504 (1989)
Intrinsic in ^4He Liquid	$\text{He}^*(2^3\text{S})$	15 μs (T-indep)	PRL 28, 792 (1972)
Intrinsic in ^4He Liquid	$\text{He}_2^*(a^3\Sigma_u^+)$	>10 s	JLTP 36, 47 (1979)
In ^4He Liquid at $\rho=10^{12}\text{cm}^{-3}$	$\text{He}_2^*(a^3\Sigma_u^+)$	30 ms	PRL 28, 792 (1972)
Timescales			
Key Process		Timescale	
$\text{He}^*(2^3\text{S})$ to $\text{He}(1^1\text{S})$ excitation transfer		10^{-8} s	
Cavity Formation in Helium Liquid		10^{-11} s	

explain the lifetime changes of the atomic species involves exploring systematically the electronically nonadiabatic dynamical processes that result in the quenching of $\text{He}(2^3\text{S})$ to $\text{He}(1^1\text{S})$ at the gaseous helium densities and at densities characteristic of condensed phase helium environments.

The 8000 sec isolated gas-phase lifetime of $\text{He}(2^3\text{S})$ is controlled by the dynamics of atomic spontaneous emission whose timescale is determined by relativistically induced magnetic multipole couplings in the atom. The shift to lower values of lifetime involves quenching dynamics in collisions with other helium atoms. This introduces nonadiabatic dynamics involving scattering on multiple electronic surfaces, notably the $a(^3\Sigma_u^+)$, $A(^1\Sigma_u^+)$, $b(^3\Pi_g)$, $B(^1\Pi_g)$, $c(^3\Sigma_g^+)$, and $C(^1\Sigma_g^+)$ states of He_2 . Dynamical studies of the important pathways leading to such an overall spin-forbidden quenching can now be studied employing Yarkony's new *ab initio* results (obtained in a parallel HEDM effort) for the relevant potential energy surfaces and nonadiabatic couplings of this metastable system. The possible dynamical pathways can be examined by considering emission of each of the photons at many possible energies (frequencies), thereby providing a thorough computational exploration of the radiative quenching spectra. However, an analysis of the important pathways may simply be based on selective dynamical results for key scattering propensities; in this report we illustrate the usefulness of such selected studies.

Radiative quenching of the gas phase $\text{He}_2(a^3\Sigma_u^+)$ state to the ground electronic state is a dissociative process and can be viewed as a half-collisional process. The gas phase lifetime of 18 sec has been explained in terms of radiative quenching by Chabalowski *et al.* [JCP 90, 2504 (1989)]. Collisional quenching of the diatomic HEDM by a third He atom can also be studied by our validated methods. However, the potential surfaces and electronic couplings are not yet available. Nevertheless, a reasonable understanding of what happens to helium metastables in condensed phases emerges from our approximate pairwise additive potential surfaces in the computer simulation studies described below. This is because helium metastables form bubbles in the condensed medium which reduce the proximity between excited species and solvent. As seen from Table 1, the timescale for $\text{He}^*(2^3\text{S})$ to $\text{He}(1^1\text{S})$ excitation transfer is orders of magnitude larger than the timescale for cavity formation in helium liquid. This is the reason why cavity formation occurs rather than excitation transfer, which would have led to energy migration. The formation of bubbles essentially traps the excitation energy (thus making the study of the bubble structure and dynamics relevant to HEDM's).

The following section of technical discussions is divided into four main parts. Each part contains the corresponding bibliography at its end. In Gas Phase Methods and Calculations, formal developments involving semiclassical computational methods are described, He-He* scattering calculations that include electronic inelasticity are presented, and two studies that involve vibrationally and vibronically inelastic collisions are described. In the Condensed Phase Modelling and Computer Experiments section computer simulations of the condensed phase structure surrounding metastable helium atoms in high pressure helium liquid are described and the construction of parameters for stochastic heatbath models from such simulations illustrated. This is

followed by the Condensed Phase Dynamics section, where the results presented are based on stochastic dynamics calculations of helium metastable atomic dynamics in a high-pressure helium matrix which forms microscopic bubbles around the metastable excited atom. The fourth part, Extended Studies, contains calculations of solvent shifts of the absorption line for the $\text{He}(2^3\text{S}) \rightarrow \text{He}^*(2^3\text{P})$ transition obtained from simulations; this part also contains preliminary results from liquid hydrogen simulations.

TECHNICAL DISCUSSION

Gas Phase Methods and Calculations

Introduction

There is a key need in HEDM research for theoretical methods of treating electronically excited energetic species in many-atom environments. Our efforts have developed novel semiclassical methodologies that show promise for use in these applications (unlike exact quantal methods, which are prohibitively expensive and usually intractable for problems of interest here). We have achieved a significant breakthrough in the semiclassical methodology during this period. The following subsection describes a new extended semiclassical formalism that has evolved from the present computational research. Applications are then presented of electronically inelastic helium scattering problems in early model studies as well as studies employing the accurate potentials and electronic couplings that became recently available for nonadiabatic $\text{He}^*\text{-He}$ collisions. This is followed by a subsection on numerical benchmark studies validating an extremely efficient implementation of the present semiclassical technology for vibrational excitation problems (in $\text{O}+\text{HF}$ and $\text{Na}+\text{H}_2$ collisions). The last subsection presents our quantum scattering work employed for benchmarking the $\text{Na}+\text{H}_2$ system.

Semiclassical Methodology for Computing Multichannel Eikonal Wavefunctions in Molecular Collisions: A Reformulation and Extension

1. Introduction

The standard quantum-mechanical description of collisional processes is based on the adiabatic separation of nuclear and electronic motions, and assumes that the electrons instantaneously adjust to nuclear motions because of a large difference in their masses. Encounters taking place on a single adiabatic surface can be described in the zeroth-order approximation simply by the classical equations of motion. However, transitions from one electronic surface to another are essentially quantum-mechanical processes which have no analogs in classical mechanics. As numerical solution of the Schrodinger equation is near the limit of capability of modern computers (even for four-atom nonreactive collisions on a single potential surface¹) there is presently no hope

to obtain necessary information about electronically inelastic scattering processes in polyatomic systems by performing exact quantum-mechanical calculations.

The gap between the quantum and classical treatments can however be filled by semiclassical theory. Construction of semiclassical solutions is simpler compared with solving the Schroedinger equation because they are often governed by a manageable number of ordinary differential equations of the first order [instead of the (usually large) complex set of partial differential equations exploited in quantum mechanics]. The semiclassical theory is often sufficiently accurate to reproduce specific quantum-mechanical features which are completely absent in a purely classical picture. In particular the semiclassical theory is powerful enough to describe the nonadiabatic transitions which are the main concern of the present research.

However, there is an obstacle that has been damping progress in this area for many years. The use of semiclassical equations implies that higher-order corrections are negligible compared with the kinetic energy of the system, so that they break down each time the kinetic energy becomes small, which occurs at classical turning points. As a result, the semiclassical wavefunctions become singular in such regions. The one-dimensional problem has a well-known solution within the WKB method² that gives the recipe for continuing the semiclassical wavefunction after its reflection at the turning point. This recipe, however, essentially exploits the conservation of flux in connecting the incoming and outgoing waves and this is insufficient in the multi-dimensional case because of a possible exchange of the probability density between different degrees of freedom. The current state-of-the-art theory in this area is mainly developed at the level of formal theorems³ which prove existence of the necessary solutions of the time-independent Schroedinger equation, but do not provide any practical numerical algorithms to find them. We can cite only two works^{4,5} where semiclassical scattering wavefunctions have been explicitly constructed in more than one dimension. These works exploit completely different approaches: a rather sophisticated numerical implementation of the formal theory as it is presented in Ref.3, and development of some approximate schemes still accurate enough to give the necessary quantitative answers. The latter more pragmatic view of the theory presently seems to be the only realistic way to approach the problems of practical interest. Our present research adopts the latter view.

Until now, much more attention has been to given to an alternative direction exploiting angle-action variables, following the pioneering works of Marcus⁶ and Miller⁷. However, the reported results in this direction are very limited. Even disregarding the fact that the latter approach is related with the Schroedinger equation only through the correspondence principle (and hence it remains unclear to what extent its predictions are equivalent to those of the asymptotic semiclassical theory^{3,8}) there is a purely practical reason for development of the semiclassical theory in terms of geometrical variables -- representation of realistic potential surfaces in angle-action variables is a complicated computational problem that makes the whole scheme infeasible for applications.

An additional problem arises when the semiclassical technique is applied to nonadiabatic processes. The problem arises from quantal interference between wavefunctions propagated on different potential surfaces.

The present subsection reports some new developments in overcoming both problems of the nonadiabatic semiclassical theory which make its implementation possible for realistic systems. Assuming adiabatic separation of nuclear motions in the semiclassical picture allows us to connect incoming and outgoing semiclassical solutions, correctly reproducing interference effects between different trajectories. By including this adiabatic hypothesis into the Self-Consistent Eikonal Method (SCEM)⁹ we have obtained a practical tool for treating electronically inelastic processes with a few degrees of freedom. It is shown that SCEM corresponds to a physical picture in which one approximates the flows of probability density on different adiabatic potential surfaces by the average flow obtained by weighting the individual flows with the probabilities for the system to be in the appropriate electronic state. We also discuss some additional terms that were previously ignored which arise in the forces governing nuclear motions for a system with two or more degrees of freedom and suggest a numerical algorithm for their evaluation.

For a more accurate treatment of electronic inelasticity in molecular collisions we developed a new extended approach called the Adiabatic Velocity Field Method (AVFM). This approach goes beyond the Ehrenfest effective potential approximation employed in SCEM without compromising on the advantages of the latter. This extended theory also exploits the eikonal ansatz for nuclear wavefunctions in each electronic state, but each wavefunction is propagated now along its own trajectory run on the appropriate adiabatic potential surface. One of the advantages of propagating classical trajectories on the particular adiabatic surfaces as prescribed by AVFM is that approximations (in addition to the short wavelength approximation) are made only in the nonadiabatic region. The equations outside the nonadiabatic region are the exact limit of the Schroedinger equation in the adiabatic representation as \hbar tends to zero; hence their solutions asymptotically reproduce specific features of the exact wavefunctions caused by local topology of the adiabatic potential surfaces. In particular, the new technique makes it possible to treat tunneling along the streamline coordinate R in electronically inelastic processes provided it takes place beyond the region of strong nonadiabatic couplings.

Semiclassical multichannel approximation in the mixed adiabatic/diabatic representation

Let us consider the multichannel problem described by a set of linear partial differential equations of the second order:

$$\left[\left(-\frac{\hbar^2}{2} \Delta_Q - E \right) \underline{1} + \underline{V}(Q) - \hbar^2 \underline{\vec{F}}(Q) \cdot \underline{\vec{\nabla}} + \underline{H}(Q) \right] \underline{\psi} = \underline{0}, \quad (1)$$

where $\underline{\psi}(Q)$ is the column formed by the functions $\psi_1(Q), \psi_2(Q), \dots, \psi_n(Q)$ sought for,

$$\Delta_Q = \sum_{\mu, \mu'} g^{-1/2} \frac{\partial}{\partial Q^\mu} g^{1/2} g^{\mu\mu'} \frac{\partial}{\partial Q^{\mu'}} \quad (2)$$

and $\underline{\vec{\nabla}}$ are respectively the covariant Laplacian (see next section for comments) and the gradient in the space of curvilinear coordinates Q . $\underline{V}(Q)$ is a $n \times n$ diagonal matrix having some potentials $V_v(Q)$ as its diagonal elements and $\underline{H}(Q)$ is the matrix of potential couplings with zeros at its main diagonal. The components of the vector $\underline{\vec{F}}$ are $n \times n$ real antisymmetric matrices describing nonadiabatic couplings. The set of curvilinear coordinates Q is composed of a streamline coordinate $Q^0 \equiv R$ and others $[Q^1 \equiv w^1, Q^2 \equiv w^2, \dots]$ describing some quasiperiodic degrees of freedom.

In the adiabatic representation $V_v(Q)$ are the adiabatic potentials and the matrix $\underline{H}(Q) \equiv \underline{0}$ so that

$$\left[\left(-\frac{\hbar^2}{2} \Delta_Q - E \right) \underline{1} + \underline{V}(Q) - \hbar^2 \underline{\vec{F}}(Q) \cdot \underline{\vec{\nabla}} \right] \underline{\psi} = \underline{0} \quad (3)$$

The main advantage of the adiabatic representation is that the last term in brackets in Eq. (3) vanishes in the limit as $\hbar \rightarrow 0$. As a result we come to the Hamilton-Jacobi equations governed by the adiabatic potentials. We can thus treat the coupling term as a perturbation. We show below that one needs an assumption of such a kind when continuing the semiclassical wavefunction through turning points of quasiperiodic motions. Another alternative is a system with only potential couplings which are relatively small compared with the potentials $V_v(Q)$. In the one-dimensional case it is sufficient to require that the couplings are negligible near the turning point of the streamline motion. We come to the problem of this type, when treating quasiperiodic degrees of freedom quantum-mechanically by representing the Schroedinger equation

$$\left(-\frac{\hbar^2}{2} \Delta_Q + V(Q) - E \right) \psi = 0 \quad (4)$$

in the matrix form

$$\left[\left(-\frac{\hbar^2}{2} \frac{d^2}{dR^2} - E \right) \underline{1} + \underline{V}(R) + \underline{H}(R) \right] \underline{\psi} = \underline{0}, \quad (5)$$

assuming that the streamline coordinate R is orthogonal to all others. As a result Eq.(4) takes the form

$$\left[\left(-\frac{\hbar^2}{2} \frac{d^2}{dR^2} + V_0(R) - E \right) \underline{1} + \underline{H}(R) \right] \underline{\psi} = \underline{0}. \quad (6)$$

Applying, by analogy, a similar expansion to an electronically inelastic process described by the Schrodinger equation, Eq. (2), we come to the set of ordinary differential equations in the mixed representation

$$\left[\left(-\frac{\hbar^2}{2} \frac{d^2}{dR^2} - E \right) \psi_{vv} - \hbar^2 \sum_{v' \neq v} \sum_{v''} F_{vv;v'v''}(R) \frac{d \psi_{v'v''}}{dR} + \sum_{v',s'} U_{vv;v'v'}(R) \psi_{v'v'} \right] = 0 \quad (7)$$

There are two questions which we need to address here. First of all, we construct asymptotic solutions of Eq. (1) as $\hbar \rightarrow 0$. This is a relatively easy problem which can be formulated in an arbitrary set of variables. It is much more difficult to find the connection formulas between different asymptotic solutions. (As stressed by Schiff¹⁰ the asymptotic solutions are of little use to us unless we know how to connect them together.) This part of the problem can be solved only with some additional assumptions concerning the motions under discussion. Here we restrict our discussion to systems with a single unbounded degree of freedom (a streamline motion) coupled with several quasi-periodic degrees of freedom such that each motion has a different time scale. There may be also some cyclic motions which do not create any difficulties on their own. All the bound motions are uncoupled at large values of the streamline coordinate R and are assumed to be adiabatically separable in the interaction region so that one can apply the usual WKB quantization rule.²

Let us illustrate these assumptions, using scattering of a diatomic molecule by an infinitely massive uncorrugated surface as an example. The cyclic motions are represented by the precession of the diatomic around the normal drawn from the center of mass of the diatomic to the surface. Relative oscillations of two atoms and the nutation of the diatom give us two quasi-periodic degrees of freedom. Since stretching vibration, described by the variable r , usually has a much larger frequency than the nutation we treat the former as a quasi-periodic motion with a frequency parametrically dependent on the nutational angle θ and the streamline coordinate R . On the other hand, the nutation is expected to be faster than streamline motion so that we can describe it as quasi-periodic motion with the frequency depending parametrically on R . We thus neglect the effect of small-amplitude oscillations of the interatomic distance r on the nutation of the diatomic and treat the diatomic as a rigid linear rotator in this particular context. We shall see below that one needs these assumptions only to formulate the connection formulas for the asymptotic solutions and we do not make any approximations in the classical Hamiltonian itself to be consistent with these assumptions.

Note that we included precession in our analysis only to be able to run trajectories in the Cartesian coordinates. One can directly start from the Schroedinger equation expressed in terms of the curvilinear coordinates R, r, θ . The appropriate kinetic-energy operator

$$\hat{T} = -\frac{\hbar^2}{2\mu_r} \frac{\partial^2}{\partial R^2} - \frac{\hbar^2}{2\mu_r r^2} \frac{\partial}{\partial r} r^2 \frac{\partial}{\partial r} - \frac{\hbar^2}{2\mu_r r^2} \frac{1}{\sin \theta} \frac{\partial}{\partial \theta} \sin \theta \frac{\partial}{\partial \theta} \quad (8)$$

is very similar to that for the $J=0$ atom-diatom nonreactive scattering problem:

$$\hat{T} = -\frac{\hbar^2}{2\mu_R} \frac{\partial}{\partial R} R^2 \frac{\partial}{\partial R} - \frac{\hbar^2}{2\mu_r r^2} \frac{\partial}{\partial r} r^2 \frac{\partial}{\partial r} - \frac{\hbar^2}{2} \left(\frac{1}{\mu_R R^2} + \frac{1}{\mu_r r^2} \right) \frac{1}{\sin \gamma} \frac{\partial}{\partial \gamma} \sin \gamma \frac{\partial}{\partial \gamma} \quad (9)$$

where r is the interatomic distance in the diatomic molecule, γ is the angle between the diatomic molecule and the vector \underline{R} drawn from the incident atom to the center of mass of the diatomic molecule, and $R=|\underline{R}|$. (Note that the volume elements $dR dr \sin \theta d\theta$ and $dR dr \sin \gamma d\gamma$ are defined in both cases in exactly the same way.) Therefore vibrational excitation of a diatomic molecule in a $J=0$ collision with an atom and scattering of diatomic molecules by incorrugated surfaces can be formally treated in terms of the nearly identical formalisms.

To extend the theory of semiclassical transition probabilities to the multichannel equation, Eq. (1), we start from Dirac-Marcus' representation^{6,11} of the wave functions $\psi_1(Q)$, $\psi_2(Q)$, ... $\psi_n(Q)$ as

$$\psi_v(Q) = A_v(Q) \exp[iW_v(Q)/\hbar], \quad v=1,2,\dots,n \quad (10)$$

where $A_v(Q)$ and $W_v(Q)$ are real functions which vary slowly with their arguments.

Substituting (2.10) into (2.1) with

$$\vec{P}^{(v)}(Q) \equiv \vec{\nabla} W_v(Q), \quad (11)$$

$$\left| \vec{P}^{(v)}(Q) \right|^2 \equiv \sum_{\mu,\mu'} P_{\mu}^{(v)}(Q) g^{\mu\mu'}(Q) P_{\mu'}^{(v)}(Q) \quad (12)$$

and neglecting the terms of the order of \hbar^2 , we come to the following set of differential equations of the first order:

$$i \frac{\hbar}{2} \text{div} \left[\psi_v^2 \vec{P}^{(v)} \right] = \psi_v^2 \left[V_v - E - \frac{1}{2} \left| \vec{P}^{(v)} \right|^2 \right] - i \hbar \psi_v \sum_{v'} \vec{F}_{vv'} \cdot \vec{P}^{(v')} \psi_{v'} \quad (13)$$

referred to below as the Semiclassical Multichannel Equations (SMEs). Note that *div* here implies use of the covariant derivatives of a vector \vec{I} so that

$$\text{div} \vec{I} = \sum_{\mu,\mu'} g^{-1/2} \frac{\partial}{\partial Q^{\mu}} g^{1/2} g^{\mu\mu'} I_{\mu'}. \quad (14)$$

One can easily verify that

$$\frac{1}{2} \left| \vec{P}^{(v)}(Q) \right|^2 + V_{\text{eff}}^{(v)}(Q) = E \quad (15)$$

with

$$V_v^{\text{eff}}(Q) \equiv V_v(Q) + \delta V_v(Q) \quad (16)$$

and

$$\delta V_v \equiv \hbar \sum_{v' \neq v} \vec{F}_{vv'} \cdot \vec{P}^{(v')} A_v \sin[(W_{v'} + W_v)/\hbar] / A_{v'} \quad (17)$$

and hence the function $W_v(Q)$ is Hamilton's characteristic function¹² for the effective potential, given by Eq. (15).

The SMEs have the trivial solution for the single-channel problem:

$$\frac{1}{2} \left| \vec{P}^{(1)}(Q) \right|^2 + V_1(Q) = E, \quad (18a)$$

$$\text{div} \left[\vec{P}^{(1)} \rho_1 \right] = 0 \quad (18b)$$

with

$$\rho_1(Q) \equiv A_1^2(Q). \quad (19)$$

However, what is taken for free in that case becomes a rather complicated problem if one has to include interference between the channels. Even the initial incoming values of effective potentials Eq. (16) cannot be unambiguously determined because the boundary condition for Hamilton's principal function $W_v(Q)$ is known only for the initially populated channel labeled below by index 1. As a result, quantum-mechanical correction Eq. (17) to the potential governing classical trajectories turns out to be an ill-defined function in the infinite-separation limit.

One of the ways to bypass this difficulty is to neglect quantum-mechanical correction Eq. (17), compared with the adiabatic potential $V_v(Q)$, bearing in mind that this correction is proportional to \hbar and hence it disappears in the limit $\hbar \rightarrow 0$. We refer to this approximation as the Adiabatic Velocity Field Method (AVFM). In the one-dimensional case the neglect of correction Eq. (17) leads us to the set of ordinary differential equations

$$i \frac{\hbar}{2} \frac{d}{dR} \left[\psi_v^2 P^{(v)} \right] = \psi_v^2 \left[W_v - E - \frac{1}{2} \left(P^{(v)} \right)^2 \right] - i \hbar \psi_v \sum_{v' \neq v} \vec{F}_{vv'} \cdot \vec{P}^{(v')} \psi_{v'}, \quad (20)$$

with

$$P^{(v)}(R) = \sqrt{2[E - V_v(R)]} \quad (21)$$

and

$$\psi_v|_0 = \delta_v [\rho^0]^{1/2} e^{i h k_1} \quad (22)$$

that can be solved by means of the finite-difference method provided that the coupling coefficients are negligibly small near the turning points and hence one can make use of the standard WKB connection formulae in each channel. The same assumption is used by us for the streamline motion in the multi-dimensional case; however the necessity to solve the set of partial differential equations makes the problem much more complicated.

Trajectory-following coordinate system (TFCS)

Let us now express each of Eqs. (13) in terms of its own set of the curvilinear coordinates $q_{(v)}$ with $q_{(v)}^s$ ($s > 0$) used for the initial values w_0^s of the quasi-periodic coordinate w^s on trajectories governed by the potential $V_v(Q)$ and parametrized by the time $t_{(v)} \equiv q_{(v)}^0$ different for each channel. Making use of the well-known expression for the covariant derivative (see Eq.(6.87) of Kyrala¹³ with $g^{1/2}$ for J here):

$$\text{div} \left[\psi_v^2 \vec{p}^{(v)} \right] = \sum_{s,s'} J_v^{-1} \frac{\partial}{\partial q_{(v)}^s} \left[g_{(v)}^{ss'} J_v p_{s'}^{(v)} \psi_v^2 \right], \quad (23)$$

where $g_{(v)}^{ss'}$ are the coefficients of momentum coupling in the new set of coordinates, J_v is the Jacobian of the transformation from $q_{(v)}$ to Q (positive by definition) and

$$p_s^{(v)} \equiv \frac{\partial W_v}{\partial q_{(v)}^s}. \quad (24)$$

Taking into account that

$$\dot{q}_{(v)}^s = \sum_{\mu} g_{(v)}^{ss'} p_{s'}^{(v)} \quad (25)$$

with

$$\dot{q}_{(v)}^0 = 1 \quad (26)$$

and

$$\dot{q}_{(v)}^s \equiv 0 \quad \text{for } s \geq 1 \quad (27)$$

we can represent Eq. (13) as

$$\begin{aligned} i\hbar \frac{d\zeta_v}{dt_{(v)}} = & \left[V_v - E - \frac{1}{2} |\vec{p}^{(v)}|^2 \right] \zeta_v \\ & - i\hbar J_v^{1/2} \sum_{v' \neq v} \vec{F}_{vv'} \cdot \vec{p}^{(v)} \zeta_{v'} J_{v'}^{1/2} \end{aligned} \quad (28)$$

where we put

$$\zeta_{v(t_{(v)}, w_0)} \equiv J_v^{1/2}(t_{(v)}, w_0) \psi_{v(t_{(v)}, w_0)} / A_1(0, w_0), \quad (29)$$

with index 1 used for the initially populated channel. Substituting Eqs. (16), (17) and (29) in (28) we find the following equation for the phase W_v :

$$\frac{dW_v}{dt_{(v)}} = 2 \left[E - V_v^{\text{eff}}(Q_{(v)}[t_{(v)}, w_0]) \right] \quad (30)$$

and hence

$$W_{v(t_{(v)}, w_0)} = 2 \int_0^{t_{(v)}} dt' \left\{ E - V_v^{\text{eff}}(Q_{(v)}[t'_{(v)}, w_0]) \right\} \quad (31)$$

or, in a more familiar form:

$$W_{\nu}(t_{(\nu)}, w_0) = \int_0^{t_{(\nu)}} \sum_{\mu} P_{\mu}^{(\nu)} dQ_{(\nu)}^{\mu} \quad (32)$$

Note that SMEs (13) are independent of the particular choice of the curvilinear coordinates Q as we assumed that the semiclassical approximation can be directly applied to covariant Laplacian Eq. (2). Use of the Podolsky transformation¹⁴ to get rid of the weight function in the volume element (represented in terms of the curvilinear coordinates in question) leads one to a quantum-mechanical correction of the order of \hbar^2 which does depend on the particular choice of variables. The correction is negligible compared with the adiabatic potential unless it is singular in the classically allowed region. For problems of interest here such complications come from nutational motion. Namely, if the Podolsky transformation is applied to the kinetic energy operator Eq. (8), this correction has the form

$$\delta U = - \frac{\hbar^2}{8\mu_r r^2} \frac{1}{\sin^2 \theta} \quad (33)$$

As it becomes negatively infinite at $\theta = 0, \pi$ the effective potential in absence of precession has infinitely deep holes which may trap trajectories. When discussing free nutational motion Landau and Lifshitz² merely neglect this term by narrowing the region of validity of the semiclassical approximation. There is however a much more ponderable argument against including this term in the effective potential. As primarily stressed by Langer¹⁵, to apply the WKB method one should first express the Schroedinger equation in terms of a variable which changes from $-\infty$ to $+\infty$. We show in Appendix A that no singular term appears if the interval $(0, \pi)$ is mapped onto the x -axis by the transformation $x = \ln \tan(\theta/2)$, and that the Bohr-Sommerfeld quantization rule gives the exact result for rotational frequencies when applied to free nutational motion described in terms of the new variable. The direct consequence of our analysis is that the kinetic energy operator for a diatom scattered by a corrugated surface should be taken in the form:

$$\hat{T} = - \frac{\hbar^2}{2\mu_r} \frac{\partial^2}{\partial R^2} - \frac{\hbar^2}{2\mu_r r^2} \frac{\partial}{\partial r} r^2 \frac{\partial}{\partial r} - \frac{\hbar^2}{2\mu_r r^2} \frac{\partial^2}{\partial \theta^2} + \frac{\hbar^2 m^2}{2\mu_r r^2 \sin^2 \theta} \quad (34)$$

whereas for the $J=0$ atom-diatom nonreactive scattering problem:

$$\hat{T} = -\frac{\hbar^2}{2\mu_R R^2} \frac{\partial}{\partial R} R^2 \frac{\partial}{\partial R} - \frac{\hbar^2}{2\mu_r r^2} \frac{\partial}{\partial r} r^2 \frac{\partial}{\partial r} - \frac{\hbar^2}{2} \left(\frac{1}{\mu_R R^2} + \frac{1}{\mu_r r^2} \right) \frac{\partial^2}{\partial \gamma^2}. \quad (35)$$

Rotational energies for initial and final states are given by the semiclassical expression Eq. (94).

To evaluate the Jacobian J_v we make use of the numerical algorithm developed by Stodden and Micha¹⁶, extending it to the equations of motion in curvilinear coordinates. To be more precise, we put

$$Q_{(v)}^{\mu s} \equiv \left(\frac{\partial Q^{\mu}}{\partial q_{(v)}^s} \right)_{t(v)}, \quad s > 0 \quad (36)$$

$$P_{\mu s}^{(v)} \equiv \left(\frac{\partial P_{\mu}^{(v)}}{\partial q_{(v)}^s} \right)_{t(v)} \quad s > 0 \quad (37)$$

and integrate the equations

$$\dot{Q}_{(v)}^{\mu s} = \sum_{\mu'} \left[g^{\mu\mu'} [Q_{(v)}] P_{\mu's}^{(v)} + P_{\mu'}^{(v)} \sum_{\mu''} Q_{(v)}^{\mu''s} \frac{\partial g^{\mu\mu'}}{\partial Q^{\mu''}} \right], \quad s > 0 \quad (38)$$

$$\begin{aligned} \dot{P}_{\mu s}^{(v)} &= \left(\frac{\partial F_{\mu}^{(v)}}{\partial q_{(v)}^s} \right)_{t(v)} \\ &= \sum_{\mu', \mu''} \left[2P_{\mu s}^{(v)} P_{\mu'}^{(v)} \frac{\partial g^{\mu\mu'}}{\partial Q^{\mu}} + P_{\mu'}^{(v)} P_{\mu''}^{(v)} \sum_{\mu'''} Q_{(v)}^{\mu'''} \frac{\partial^2 g^{\mu\mu'}}{\partial Q^{\mu} \partial Q^{\mu''}} \right] - \sum_{\mu'} Q_{(v)}^{\mu's} \frac{\partial^2 V_v}{\partial Q^{\mu'} \partial Q^{\mu}} \end{aligned} \quad s > 0 \quad (39)$$

together with the equations of motion

$$\dot{P}_{\mu}^{(v)} = F_{\mu}^{(v)} \equiv \sum_{\mu', \mu''} \frac{\partial g^{\mu \mu'}}{\partial Q^{\mu}} P_{\mu'}^{(v)} P_{\mu''}^{(v)} - \frac{\partial V_v}{\partial Q^{\mu}}. \quad (40)$$

4. Self-Consistent Eikonal Method (SCEM)

Let us now introduce the average flow with the kinetic energy given by the relation

$$\frac{1}{2} P^2(Q) = \frac{1}{2} \sum_v \rho_v(Q) \left| \vec{P}^{(v)}(Q) \right|^2 / \bar{\rho}(Q) \quad (41)$$

with

$$\bar{\rho}(Q) \equiv \sum_v \rho_v(Q). \quad (42)$$

Multiplying both sides of Eq.(15) by ρ_v , summing over v and taking into account that the vector coefficients $\vec{F}_{vv'}$ in Eq. (17) change their sign under the interchange of v and v' one can easily verify that the function $P(Q)$ satisfies the equation

$$\frac{1}{2} P^2(Q) + \bar{V}(Q) = E \quad (43)$$

with

$$\bar{V}(Q) \equiv \sum_v V_v(Q) \rho_v(Q) / \bar{\rho}(Q) \quad (44)$$

and hence we can define the velocity field of the average flow by means of the relation

$$\vec{P}(Q) \equiv \vec{\nabla} W, \quad (45)$$

where $W(Q)$ is Hamilton's characteristic function for the potential $\bar{V}(Q)$, namely,

$$\frac{1}{2} \left| \vec{\nabla} W \right|^2 + \bar{V}(Q) = E. \quad (46)$$

Let us now, in following Micha' work¹⁰, write functions Eq. (10) in the common eikonal form:

$$\psi_v(Q) = \chi_v(Q) \exp[iW(Q)/\hbar], \quad (47)$$

$$\tilde{\psi}_v(Q) = \tilde{\chi}_v(Q) \exp[iW(Q)/\hbar], \quad (48)$$

where we use the tilda to mark the diabatic wavefunctions to distinguish them from those in the adiabatic representation. Let us now neglect the difference between the Jacobians in the sum in the right side of Eq. (28), express the function $\tilde{\psi}_v(Q)$ in the right side of Eq. (29) in terms of

$$\beta_v(Q_{(v)}[t_{(v)}, w_0]) \equiv J_v^{1/2} \chi_v, \quad (49)$$

and substitute the resultant expression in Eq. (28), writing the semiclassical equations as

$$i\hbar \frac{d\beta_v}{dt_{(v)}} = \left[V_v - \bar{V} - \frac{1}{2} \left| \vec{\kappa}^{(v)} \right|^2 \right] \beta_v + \sum_{v' \neq v} \vec{F}_{vv'} \cdot \left(\vec{P} + \vec{\kappa}^{(v')} \right) \beta_{v'}, \quad (50)$$

where we put

$$\vec{\kappa}^{(v)}(Q) \equiv \vec{P}^{(v)}(Q) - \vec{P}(Q). \quad (51)$$

A similar equation in the diabatic representation takes the form

$$\frac{d\tilde{\beta}_v}{dt_{(v)}} = \left[H_{vv} - \bar{V} - \frac{1}{2} \left| \vec{\kappa}^{(v)} \right|^2 \right] \tilde{\beta}_v + \sum_{v' \neq v} H_{vv'} \tilde{\beta}_{v'}, \quad (52)$$

where $H_{vv'}$ are some diabatic potential couplings and the tilda is again used to distinguish between the two representations.

The main idea of the method is to run trajectories on the single potential surface approximating the potential $\bar{V}(Q)$ by means of the relations:

$$\bar{V}(Q) \approx \sum_v V_v(Q) \left| \beta_v^2(Q) \right| / \bar{\rho}(Q), \quad (53)$$

$$\bar{V}(Q) = \sum_{v,v'} H_{vv'} \beta_{v'}(Q) \beta_v^*(Q) / \bar{p}(Q), \quad (54)$$

with

$$\bar{p}(Q) \equiv \sum_v |\beta_v^2(Q)| = \sum_v |\beta_v(Q)|^2. \quad (55)$$

After neglecting the deviations $\vec{\kappa}^{(v)}$ of the momenta $\vec{P}^{(v)}$ from the average \vec{P} which cannot be evaluated on the trajectories in question we thus come to the following equations for the functions $\beta_v(Q)$ and $\beta_v^*(Q)$:

$$i\hbar \frac{d\beta_v}{dt} = [V_v - \bar{V}] \beta_v + \sum_{v' \neq v} \vec{F}_{vv'} \cdot \vec{P} \beta_{v'}, \quad (56)$$

$$i\hbar \frac{d\beta_v^*}{dt} = [H_{vv} - \bar{V}] \beta_v^* + \sum_{v' \neq v} H_{vv'} \beta_{v'}^*. \quad (57)$$

Note that both sets of equations conserve the right side of Eq. (55) along any trajectory governed by the potential $\bar{V}(Q)$. The equations are solved with the boundary conditions

$$\beta_v(0, w_0) = \beta_v^*(0, w_0) = \delta_{v1} [\rho^0(w_0)]^{1/2} \exp(-ik_1 R_0 + iW^0(w_0)/\hbar) \quad (58)$$

Compared with the discussion presented in Section 3, a certain simplification of the formalism comes from the fact that Eq. (44) does not contain the ratio of functions $A_v(Q)$ and $A_{v'}(Q)$ and hence one does not have to deal with the indeterminate forms necessary to evaluate the effective potentials V_v at $t=0$. It is worth pointing out that the neglect of the deviations of the momenta

$\vec{P}^{(v)}$ from the average \vec{P} in Eqs. (56) and (57) is the most serious assumption made so far because it changes the asymptotic behavior of wave functions after the couplings between the channels completely turn off. In the next section we show how one can eliminate this defect by running a separate trajectory in the field of each adiabatic potential, instead of a single trajectory in the field of the average potential $\bar{V}(Q)$.

The set of equations, Eq. (57), has been recently derived by Stodden and Micha¹⁷ by evaluating directly the time derivative of the Jacobian, Eq. (24). It should be emphasized that although similar sets of coupled differential equations have been derived in the literature, starting from the time dependent Schroedinger equation in either adiabatic¹⁸ or diabatic^{19,20}

representations, in the latter case one propagates some time-dependent coefficients in a basis-set expansion whereas we try to build the wavefunction itself. The crucial difference comes from turning points where the phases of the functions $\beta_v(Q)$ and $\bar{\beta}_v(Q)$ take a discontinuous change. When the eikonal method is applicable, it should give more accurate results since it treats translations semiclassically, rather than classically as in the time-dependent expansions.

The novelty of our approach when extended to the multi-dimensional case comes from the explicit use of the time-scale separation to carry those functions through the caustics. We show below that the equations of motion used by us in the multi-dimensional case differ from those derived in the literature¹⁷⁻¹⁹.

Potential Eq. (54) has a very interesting feature, namely, its first derivative with respect to time is given by the simple relation:

$$\dot{\bar{V}} \equiv \sum_{v,v'} \vec{P} \cdot \vec{\nabla} H_{vv'} \bar{\beta}_v \bar{\beta}_{v'}^* / \bar{\rho} . \quad (59)$$

To prove it we need just represent Eq. (54) and Eq. (57) as

$$\bar{V} \equiv \bar{\beta}^\dagger \underline{H} \bar{\beta} / \bar{\rho} \quad (60)$$

and

$$i\hbar \dot{\bar{\beta}} = (\underline{H} - \bar{V} \underline{1}) \bar{\beta} \quad (61)$$

and then substitute Eq. (61) in the derivative of Eq. (60) with respect to t , taking into account that the matrix $\underline{H} - \bar{V} \underline{1}$ commutes with \underline{H} . The direct consequence of the proved result is that the governing force in the one-dimensional case is given by the simple expression

$$\dot{P}^1 = \bar{\beta}^\dagger \frac{d\underline{H}}{dQ^1} \bar{\beta} / \bar{\rho} . \quad (62)$$

(We can always make g^{11} equal to a constant $1/\mu_R$ by the appropriate change of variables so that no additional term appears in the equation for the streamline motion.)

The governing potential force in the multi-dimensional case has a more complicated form:

$$\ddot{Q}^{\mu s} \equiv F_{\mu} = \underline{\beta}^{\dagger} \frac{\partial H}{\partial Q^{\mu}} \underline{\beta} / \bar{p} + \sum_{s>0} \frac{\partial q^s}{\partial Q^{\mu}} \left[2 \operatorname{Re} \left(\underline{\beta}^{\dagger} H \underline{\beta}_{,s} \right) / \bar{p} - \bar{p}_{,s} \underline{\beta}^{\dagger} H \underline{\beta} / \bar{p}^2 \right] \quad (63)$$

where we put

$$\underline{\beta}_{,s} \equiv \frac{\partial \underline{\beta}}{\partial q^s_{(v)}}, \quad (64)$$

$$\bar{p}_{,s} \equiv \frac{\partial \bar{p}}{\partial q^s_{(v)}}. \quad (65)$$

Evaluation of derivatives Eq. (64) along trajectories governed by the Ehrenfest potential Eq. (53) is discussed in Appendix B.

5. Adiabatic Velocity Field Method (AVFM)

As outlined in the end of Section II we propose to neglect quantum-mechanical correction Eq. (17) and to run trajectories on the adiabatic potential surfaces. However to do it one needs the initial conditions for the momenta in the channels which are not populated at the initial moment. Since k_1 is the largest momentum in the system, these momenta can be defined by the expression

$$\hbar k_v = \sqrt{2\mu_R [V_1(R_0, w_0) - V_v(R_0, w_0)] + \hbar^2 k_1^2} \quad (66)$$

where the adiabatic potentials represent cuts through the global potential surface with fixed quasiperiodic coordinates establishing the asymptotic limit. For atom-diatom collisions the different channels correspond to excitation of the atom for fixed internal vibrational coordinate. They may also correspond to different spin-states of the diatomic molecule, as in the case of NO scattered by a silver surface.

We also assume that dependence of the nonadiabatic couplings $\vec{F}_{vv'}$ on the quasi-periodic coordinates Q^1, Q^2, \dots is negligible at large values of the streamline coordinate $R=Q^0$ and only the component $F_{vv'}^0$ along the streamline motion is asymptotically important. As a result of this assumption SME's.(13) become asymptotically separable. This implies that

$$\text{div} \left[\psi_v^2 \vec{P}^{(v)} \right]_{R=\infty} = -\hbar k_v \frac{\partial}{\partial R} (\psi_v^2) \quad (67)$$

and hence

$$\arg[\psi_v(0, w_0)] = -ik_v R_0 + iW^0(w_0)/\hbar + \text{mod}(\pi), \quad (68)$$

$$P_\mu^{(v)}(0, w_0) = P_\mu^{(1)}(0, w_0) \quad \mu > 0. \quad (69)$$

Let us now represent Eqs.(28) as

$$\begin{aligned} i\hbar \dot{R}_{(v-)}[R, w] \left(\frac{\partial \zeta_v^-}{\partial R} \right)_w &= \left[V_v(Q_{(v-)}[R, w]) - E - \frac{1}{2} \left| \vec{P}^{(v-)}[R, w] \right|^2 \right] \zeta_v^-[R, w] \\ &- i\hbar \sum_{v' \neq v} \frac{J_{v-}^{1/2}[R, w]}{J_{v-}^{1/2}[Q_{(v-)}]} F_{vv'}(Q_{(v-)}[R, w]) \cdot \vec{P}^{(v')} [Q_{(v-)}] e^{i\delta W_v[Q_{(v-)}]/\hbar} \zeta_{v'}^-[R, w] \end{aligned} \quad (70)$$

where minus super (sub)-scripts denote the incoming wave. The most essential obstacle in solving these equations in the case of more-than-one channels is that the functions $\zeta_v^-[R, w]$ with $v' \neq v$ in the right-hand side of Eq. (70) are supposed to be evaluated on the trajectory $Q_{(v)}[t_{(v)}, w_0]$.

The components $P_\mu^{(v)}[Q_{(v-)}]$ of the momentum $\vec{P}^{(v)}[Q_{(v-)}]$, Jacobian $J_{v-}[Q_{(v-)}]$ and the phase shift $\delta W_v[Q_{(v-)}]$ are approximated respectively as

$$\sqrt{g^{0\mu}/2} P_0^{(v)}[Q_{(v-)}] = -p_{(v)} - \sqrt{\left[E - V(Q_{(v-)}) - \frac{1}{2} \sum_{\mu, \mu' > 0} g^{\mu\mu'} P_\mu^{(v)} P_{\mu'}^{(v)} \right]^2 + p_{(v)}^2}. \quad (71)$$

$$P_{\mu}^{(\nu)} [Q_{(\nu-)}] \approx P_{\mu}^{(\nu)} [Q_{(\nu'-)}]$$

$$\pm \left[\sqrt{E - V(R, Q^1, \dots, Q^{\mu-1}, Q_{(\nu)}^{\mu}, Q^{\mu+1}, \dots)} \right] - \sqrt{E - V(R, Q^1, \dots, Q^{\mu-1}, Q_{(\nu')}^{\mu}, Q^{\mu+1}, \dots)}$$

$$\mu > 0 \quad (72)$$

with

$$P_{(\nu)} \equiv \frac{1}{2} \sum_{\mu > 0} g^{0\mu} P_{\mu}^{(\nu)} \quad (73)$$

$$Q^{\mu'} [R, w] \equiv \frac{1}{2} \left(Q_{(\nu-)}^{\mu'} [R, w] + Q_{(\nu'-)}^{\mu'} [R, w] \right) \quad (74)$$

$$J_{\nu-} [Q_{(\nu-)}] \approx J_{\nu-} [Q_{(\nu'-)}] \prod_{\mu \geq 0} \frac{P_{\mu}^{(\nu)} [Q_{(\nu-)}]}{P_{\mu}^{(\nu)} [Q_{(\nu'-)}]} \quad (75)$$

$$\delta W_{\nu} [Q_{(\nu-)}] \equiv \sum_{s > 0} \int_{w_{(\nu)}^s}^{w_{(\nu)}^s} dw^s P_s^{(\nu)} [Q_{(\nu-)}] \quad (76)$$

(Sign (+) or (-) in Eq. (72) is chosen depending on the direction of the appropriate one-dimensional motion.) We integrate Eq. (70) by running a set of trajectories on the adiabatic potential surfaces with the initial conditions given by Eqs.(68) and (69) for the momenta and

$$\zeta_{\nu}(0, w_0) = \delta_{\nu 1} [\rho^0(w_0)]^{1/2} \exp \left(-ik_1 R_0 + iW_{\nu}^0(w_0)/\hbar \right) \quad (77)$$

for the wavefunctions themselves.

The most important consequence of the presented mathematical arguments is that the semiclassical multichannel solution sought for does have the eikonal form -- remember that existence theorems have been proved³ only for single-channel processes. The equations for the outgoing wave are similar to Eq. (70) except that they are solved with different initial conditions

formulated using the WKB connection formula at the classical turning point for the streamline motion on the appropriate adiabatic potential surface.

One of the most important advantages of the new theory, compared with SCEM, is that the wavefunctions are propagated by means of the single-channel semiclassical equations in regions where the nonadiabatic couplings vanish. In particular, this automatically excludes population of energetically forbidden states, which is usually observed if wavefunctions are propagated according to the prescriptions of SCEM.

It is worth emphasizing that the most serious approximations are made by us to extrapolate wavefunctions from one trajectory to another in the space of quasi-periodic degrees of freedom. To find a solution of the one-dimensional problem one just needs to propagate SME's (13) along the

streamline coordinate R with $P \rightarrow (v)$ (R) evaluated from the classical trajectory run on the v th adiabatic potential surface, instead of using the exact self-consistent potential Eq. (16).

6. Evaluation of the S-matrix elements from semiclassical wavefunctions

To avoid the singularities at the classical turning points, when evaluating the S-matrix elements:

$$S_{v;v'}^{(v)} = \frac{1}{2} \sqrt{k_{v'}^{(v)}} e^{-ik_{v'}^{(v)} R_f} \sum_{v=\pm 1} \int dw \psi_{vv}(R_f, w; v) u_{v'}(w) . \quad (78)$$

where $u_{v'}(w)$ is an exact quantum-mechanical wave function and v is a set of the appropriate quantum numbers, we first represent Eq. (78) as

$$S_{v;v'}^{(v)} \approx \frac{1}{\Delta R} \int_{R_f}^{R_f + \Delta R} dR S_{v;v'}^{(v)} \quad (79)$$

The relation turns into the identity if we deal with the exact matrix element which is independent of R . We thus find

$$\Delta R \sqrt{k_v^{(v)}} S_{v;v'}^{(v)} \approx \sum_{v=\pm 1} \int d\tau \sqrt{k^{(v)}(w_0, v)} e^{i f^{(w_0, v)}_f} \int_0^{1/2} dt \zeta_{vv}(t, w_0, v) \zeta'_{vv}(t, w_0, v) u_{v'}(w(t; w_0)) , \quad (80)$$

where $d\tau \equiv d\tau^1 d\tau^2 \dots$,

$$\zeta_{vv}(t, w_0^v) \equiv \zeta_{vv}(t, w_0^v) e^{-ik^{(v)}(w_0^v) R(t, w_0^v)} \quad (81)$$

$$\frac{dw^s}{d\tau^s} = p^s(w^s)/m_s \geq 0 \quad (82)$$

(with p^s and m^s used for the momentum and the effective mass of the sth quasi-periodic degree of freedom) and J_v is the absolute value of determinant of the auxiliary matrix with the elements

$$\tilde{Q}_{(v)}^{\mu s} \equiv Q_{(v)}^{\mu s} P_{(v)}^{\mu}(w_0^v) \quad (83)$$

propagated instead of the functions $Q_{(v)}^{\mu s}$ to avoid singularities in the initial conditions for functions Eq. (37). (The function $\rho^0(w_0)$ in Eq. (77) is chosen in such a way that the matrix element $S_{v,v}^{(1)}$ is equal to 1 for elastic collisions.) The crucial advantage of the integral Eq. (80) compared with Eq. (78) is that the Jacobian J_v appears now in the numerator and it is multiplied by function Eq. (81) which is nonsingular, in contrast to the function ψ_{vv} (see Eq.(29)).

7. Conclusions

The analysis presented in this subsection revealed some promising new directions in practical implementation of multichannel multidimensional semiclassical theory. We have developed a self-consistent approach that makes it possible to address (under some reasonable assumptions) the most important issues of semiclassical theory. The following computationally affordable algorithms could be cited as the main results of this subsection:

- (1) well-defined prescriptions for continuation of global (multidimensional) semiclassical wavefunctions through classical turning points,
- (2) a practical numerical algorithm to extract final populations of vibrational levels from the semiclassical outgoing solution,
- (3) implementation of the single-surface developments (1) and (2) in the multichannel theory with valid use of the Ehrenfest effective potential (SCM), and
- (4) development of the new multichannel semiclassical theory referred to as "Self-Consistent Adiabatically-Corrected Eikonal Method" (SCACEM) that goes beyond the

assumptions underlying SCEM and explicitly takes into account specific topology of the adiabatic potential surfaces.

We have obtained some preliminary but very encouraging numerical results²¹ in support of our treatment of the single-surface problem by considering vibrational energy transfer in atom-diatom collisions in the IOS approximation²². Another project which was recently initiated to test the validity of the developed formalism is a study of rotational excitation of the rigid NO molecule scattered by the uncorrugated silver surface. The main attraction of this problem is that exact quantum-mechanical calculations have been performed by Smedley, Corey and Alexander²³, including electronically inelastic scattering due to nonadiabatic couplings between different spin-orbit and Λ -doublet states. Excellent agreement between those calculations and the one-dimensional reduction of SCEM, treating rotations quantum-mechanically has been reported in an earlier publication²⁴; our next step is to construct semiclassical wavefunctions from realistic classical trajectories: this is being done for NO approaching the smooth rigid surface to compare the obtained state-to-state information with the results of the previous studies.

Appendix A

Let us consider nutational motion of a diatomic molecule described by the Schroedinger equation:

$$\left[-\hbar^2 \frac{1}{\sin \theta} \frac{d}{d\theta} \sin \theta \frac{d}{d\theta} + \frac{m^2 \hbar^2}{\sin^2 \theta} + 2I^* (V(\theta) - \epsilon_{|m|}) \right] \psi_m = 0 \quad (84)$$

where the angle θ is restricted to the interval $(0, \pi)$. We consider the general case, allowing the molecule to rotate around the quantization axis. We will need such an extension when considering the rotationally inelastic scattering of diatomics by a corrugated rigid surface, because molecule-surface interactions couple states with different m . In following Langer's suggestion¹⁵, we should now transform the finite interval $(0, \pi)$ onto the whole axis $(-\infty, +\infty)$. As initially emphasized by Fröman and Fröman²⁵ such a transformation does not lead to a unique modification of the Bohr-Sommerfeld quantization rule. To eliminate the ambiguity, Adams and Miller²⁶ suggested choosing the transformation that reproduces the exact quantum spectrum of free motion. This suggestion seems especially appropriate for the scattering problem in question. We show below that the mapping transformation

$$x = \ln \left(\operatorname{tg} \frac{\theta}{2} \right). \quad (85)$$

leads one to the semiclassical energy levels shifted up by the same constant $\hbar^2/(8I^*)$ from the exact rotational levels $j(j+1)\hbar^2/(2I^*)$. The appropriate semiclassical wavefunctions have been discussed in detail by Landau and Lifshitz² who, however, come to this result only after neglecting the singular quantum-mechanical correction, whereas we prove that transformation Eq. (85) mapping the interval $(0, \pi)$ on the whole axis $(-\infty, +\infty)$ simply eliminates it. In fact, taking into account that

$$e^x = \operatorname{tg} \frac{\theta}{2} \quad (86)$$

we find

$$\frac{dx}{d\theta} = \frac{1}{\sin \theta} \quad (87)$$

and hence Eq.(84) takes the form:

$$\left[-\frac{\hbar^2}{2} \frac{d^2}{dx^2} + \frac{1}{2}(m\hbar)^2 + v(x) \right] \Psi_m = 0. \quad (88)$$

with

$$v(x) \equiv -4I^*[V(\theta(x)) - \epsilon] e^{2x} (1 + e^{2x})^{-2}. \quad (89)$$

We thus find that $-(m\hbar)^2/2$ now plays a role of the energy levels in the potential well $v(x)$. In the particular case of free nutational motion $V(\theta) \equiv 0$ and $-I^*\epsilon \leq v(x) \leq 0$, i. e., $-(m\hbar)^2 \geq -2I^*\epsilon$ and hence

$$\epsilon \geq \frac{m^2 \hbar^2}{2I^*}. \quad (90)$$

Applying the usual WKB rules to potential (89):

$$\int_{x_-}^{x_+} dx \sqrt{-(m\hbar)^2 - 2v(x)} = \pi \hbar (n + 1/2) \quad (91)$$

and coming then back to the angle θ we find that the semiclassical energy spectrum for Eq.(84) is given by the relation:

$$\int_{\theta_-}^{\theta_+} d\theta \sqrt{2I^*(\epsilon_{|m|} - V(\theta)) - \frac{m^2 \hbar^2}{\sin^2 \theta}} = \pi \hbar (n + 1/2) . \quad (92)$$

For free nutational motion the change of variables $r = \cos \theta$ leads one to the integral easily evaluated by means of the method of residues, by analogy with a similar derivation given by Sommerfeld for the Coulomb problem (see Ch.9 in Ref. 12). The residues at the points -1, +1 and

infinity are equal to $R_{-1} = i|m|/2$, $R_{+1} = i|m|/2$ and $R_{\infty} = -i \sqrt{2I^* \epsilon_{j,|m|}}$ respectively so that

$$\left(\sqrt{2I^* \epsilon_{j,|m|}} - |m| \hbar \right) = \hbar (n + 1/2) \quad (93)$$

and hence

$$\epsilon_{j,|m|} = \frac{\hbar^2 j(j+1)}{2I^*} + \frac{\hbar^2}{8I^*} . \quad (94)$$

We see that quantization condition Eq. (92) reproduces the exact values for rotational frequencies but the zeroth point energy turns out to be larger by $\hbar^2/(8I^*)$.

Appendix B

Evaluation of the forces F_{μ} according to SCEM recipe Eq. (63) is complicated by the fact that the set of equations

$$\dot{P}_{\mu} = F_{\mu} , \quad (95)$$

$$\dot{Q}^{\mu s} = \frac{\partial \dot{Q}^{\mu}}{\partial w^s} = \sum_{\mu'} \left[g^{\mu \mu'} P_{\mu s} + P_{\mu'} \sum_{\mu''} Q^{\mu'' s} \frac{\partial g^{\mu \mu'}}{\partial Q^{\mu''}} \right] , \quad (96)$$

$$\begin{aligned}
\dot{P}_{\mu s} &= \frac{\partial F_{\mu}}{\partial w^s} \\
&= \sum_{\mu', \mu''} \left[P_{\mu s} P_{\mu''} \frac{\partial g^{\mu' \mu''}}{\partial Q^{\mu}} + P_{\mu'} P_{\mu''} \sum_{\mu'''} Q^{\mu'''} \frac{\partial^2 g^{\mu' \mu''}}{\partial Q^{\mu} \partial Q^{\mu''}} \right] \\
&\quad + \sum_{\mu'} Q^{\mu s} \underline{\beta}^{\dagger} \frac{\partial^2 H}{\partial Q^{\mu} \partial Q^{\mu'}} \underline{\beta} / \bar{\rho} - 2 \left(\bar{\rho}_{,s} \operatorname{Re}(\underline{\beta}^{\dagger} H \underline{\beta}_{,s}) + \bar{\rho}_{,s} \operatorname{Re}(\underline{\beta}^{\dagger} H \underline{\beta}_{,s'}) \right) / \bar{\rho}^2 \\
&\quad + \sum_{s' > 0} \frac{\partial q^{s'}}{\partial Q^{\mu}} \sum_{\mu'} Q^{\mu s'} \left[2 \operatorname{Re} \left(\underline{\beta}^{\dagger} \frac{\partial H}{\partial Q^{\mu'}} \underline{\beta}_{,s'} \right) / \bar{\rho} - \bar{\rho}_{,s'} \underline{\beta}^{\dagger} \frac{\partial H}{\partial Q^{\mu'}} \underline{\beta} / \bar{\rho}^2 \right] \quad (97)
\end{aligned}$$

$$i \hbar \frac{d \underline{\beta}_{,s}}{dt} = \begin{bmatrix} H & -\bar{V} & 1 \\ & & \end{bmatrix} \underline{\beta}_{,s} + \sum_{\mu'} Q^{\mu s} \frac{\partial H}{\partial Q^{\mu'}} \underline{\beta} - \frac{\partial \bar{V}}{\partial q^s} \underline{\beta} \quad (98)$$

with

$$\frac{\partial \bar{V}}{\partial q^s} = \sum_{\mu} Q^{\mu s} \underline{\beta}^{\dagger} \frac{\partial H}{\partial Q^{\mu}} \underline{\beta} / \bar{\rho} + 2 \operatorname{Re} \left(\underline{\beta}^{\dagger} H \underline{\beta}_{,s} \right) / \bar{\rho} - \bar{\rho}_{,s} \underline{\beta}^{\dagger} H \underline{\beta} / \bar{\rho}^2. \quad (99)$$

is unclosed because we need to know the derivatives of the functions $Q^{\mu s}$ with respect to $q^{s'}$:

$$\frac{\partial Q^{\mu s}}{\partial q^{s'}} = \frac{\partial^2 Q^{\mu}}{\partial q^s \partial q^{s'}} \equiv Q_{ss'}^{\mu} \quad (100)$$

as follows from the relation:

$$\frac{\partial}{\partial q^s} \left(\frac{\partial q^{s'}}{\partial Q^{\mu}} \right) = - \sum_{\mu'} \frac{\partial q^{s'}}{\partial Q^{\mu'}} Q_{ss'}^{\mu'} \frac{\partial q^{s''}}{\partial Q^{\mu}} \quad (101)$$

obtained by differentiating the identity

$$\sum_{\mu'} \frac{\partial q^{s'}}{\partial Q^{\mu'}} Q^{\mu' s''} = \delta_{s' s''} \quad (102)$$

with respect to q^s . The situation is completely different from that for the single-channel problem because in the latter case the potential is a known function of the coordinates.

To overcome this difficulty we evaluate the functions $Q_{ss'}^{\mu'}$ in Eq. (100), assuming that the problem is adiabatically separable, namely, differentiating the equation:

$$t - t_1 = m^s \int_{w^s(t_1, w_0^s)}^{w^s(t, w_0^s)} d\tilde{w}^s / p^s(\tilde{w}^s) \quad (103)$$

with respect to w_0^s we find

$$Q^{ss}(t, w_0^s) / P_s(t, w_0^s) \approx Q^{ss}(t_1, w_0^s) / P_s(t_1, w_0^s) \quad (104)$$

and hence

$$\dot{Q}^{\mu s} \approx \delta_{\mu s} \dot{P}_\mu / P_\mu \quad (105)$$

Differentiating Eq. (102) with respect to $w_0^{s''}$ we conclude that propagation of the functions $Q_{ss'}^{\mu}$ in time is governed in the aforementioned approximation by the equations:

$$\dot{Q}_{ss'}^{\mu} = \delta_{\mu s} \left[\dot{P}_{\mu s'} / P_\mu - \dot{P}_\mu P_{\mu s''} / P_\mu^2 \right] \quad (106)$$

REFERENCES

- 1 D. W. Schwenke, D. G. Truhlar, *Theor. Chim. Acta* **72**, 1 (1987); *J. Chem. Phys.* **88**, 4800 (1988).
- 2 L. D. Landau and E. M. Lifshitz, Quantum Mechanics, Pergamon Press, New York (1965).
- 3 V. P. Maslov and M. V. Fedoriuk, Semiclassical Approximation in Quantum Mechanics, D. Reidel, Boston (1981).
- 4 S. K. Knudson, J. B. Delos and B. Bloom, *J. Chem. Phys.* **83**, 5703 (1985)
- 5 P. K. Swaminathan, C. D. Stodden, and D. A. Micha, *J. Chem. Phys.* **90**, 5501 (1989).
- 6 R. A. Marcus, *Chem. Phys. Lett.* **7**, 525 (1970); *J. Chem. Phys.* **54**, 3935 (1971); **56**, 311, 3548 (1972); *Discuss. Faraday Soc.* **55**, 34 (1973).
- 7 W. H. Miller, *J. Chem. Phys.* **53**, 1949, 3578 (1970); **54**, 5386 (1971); *Adv. Chem. Phys.* **25**, 69 (1974); **30**, 77 (1975); *Discuss. Faraday Soc.* **62**, 34 (1976).
- 8 J. B. Delos, *Adv. Chem. Phys.* **65**, 161 (1986).
- 9 D. A. Micha, *J. Chem. Phys.* **78**, 7138 (1983).
- 10 L. A. Schiff, Quantum Mechanics, McGraw-Hill, New York (1955).
- 11 P. A. M. Dirac, The Principles of Quantum Mechanics, Cambridge Press, Oxford (1958).
- 12 H. Goldstein, Classical Mechanics, Addison-Wesley, London (1950).
- 13 A. Kyrala, Theoretical Physics: Applications of Vectors, Matrices, Tensors and Quaternions, W.B. Saunders, Philadelphia (1967).
- 14 B. Podolsky, *Phys. Rev.* **32**, 812 (1928).
- 15 R. E. Langer, *Phys. Rev.* **51**, 669 (1937).
- 16 C. D. Stodden and D. A. Micha, *Int. J. Quantum Chem. Symp.*, **21**, 239 (1987)
- 17 C. D. Stodden, Ph.D. Thesis, University of Florida, Gainesville (1988); C. D. Stodden and D. A. Micha, in preparation.
- 18 (a) J. C. Tully and R. K. Preston, *J. Chem. Phys.* **55**, 562 (1971); (b) J. C. Tully, in: Dynamics of Molecular Collisions, Part B, ed. by W. H. Miller, p.217 (1976); (c) D. G. Truhlar, J. W. Duff, N. C. Blais, J. C. Tully and B. G. Garrett, *J. Chem. Phys.* **77**, 764, (1982).

- 19 (a) K. J. McCann and M. R. Flannery, Chem. Phys. Lett. **35**, 124 (1975); J. Chem. Phys. **63**, 4695 (1975); (b) S. D. Augustin and H. Rabitz, *ibid.* **69**, 3214 (1978).
- 20 H.-D. Meyer and W. H. Miller, J. Chem. Phys., **70**, 3214 (1979).
- 21 P. K. Swaminathan, G. A. Natanson, B. C. Garrett and M. J. Redmon, "Accurate Computations of Energy Transfer in Atom-Diatom Collisions: Comparative Study of Vibrational Excitations Using Semiclassical Wavefunctions and Coupled Quantal States", in preparation.
- 22 See eg. V. Khare, D. J. Kouri, J. Jellinek, and M. Baer, in: Potential Energy Surfaces and Dynamics Calculations, D. G. Truhlar, ed., (Plenum, New York, 1981) p. 475.
- 23 J. C. Smedley, G. C. Corey and M. H. Alexander, J. Chem. Phys. **87**, 3218 (1987).
- 24 B. M. Rice, B. C. Garrett, P. K. Swaminathan and M. H. Alexander, J. Chem. Phys. **90**, 575 (1989).
- 25 N. F. Fröman and P. O. Fröman, Nuovo Cimento **20**, 121 (1974).
- 26 J. E. Adams and W. H. Miller, J. Chem. Phys. **67**, 5775 (1978).

He-He* Scattering Calculations

1. Model Validation Calculations

Quantal Scattering Validation of the SCE Methodology

The validity of the SCEM for describing the quenching of electronically excited atoms in the gas phase has been tested by comparison with quantum mechanical calculations on the He₂ system. This model is based on an analysis of the relevant electronic states of the He₂ system in the Ω basis.

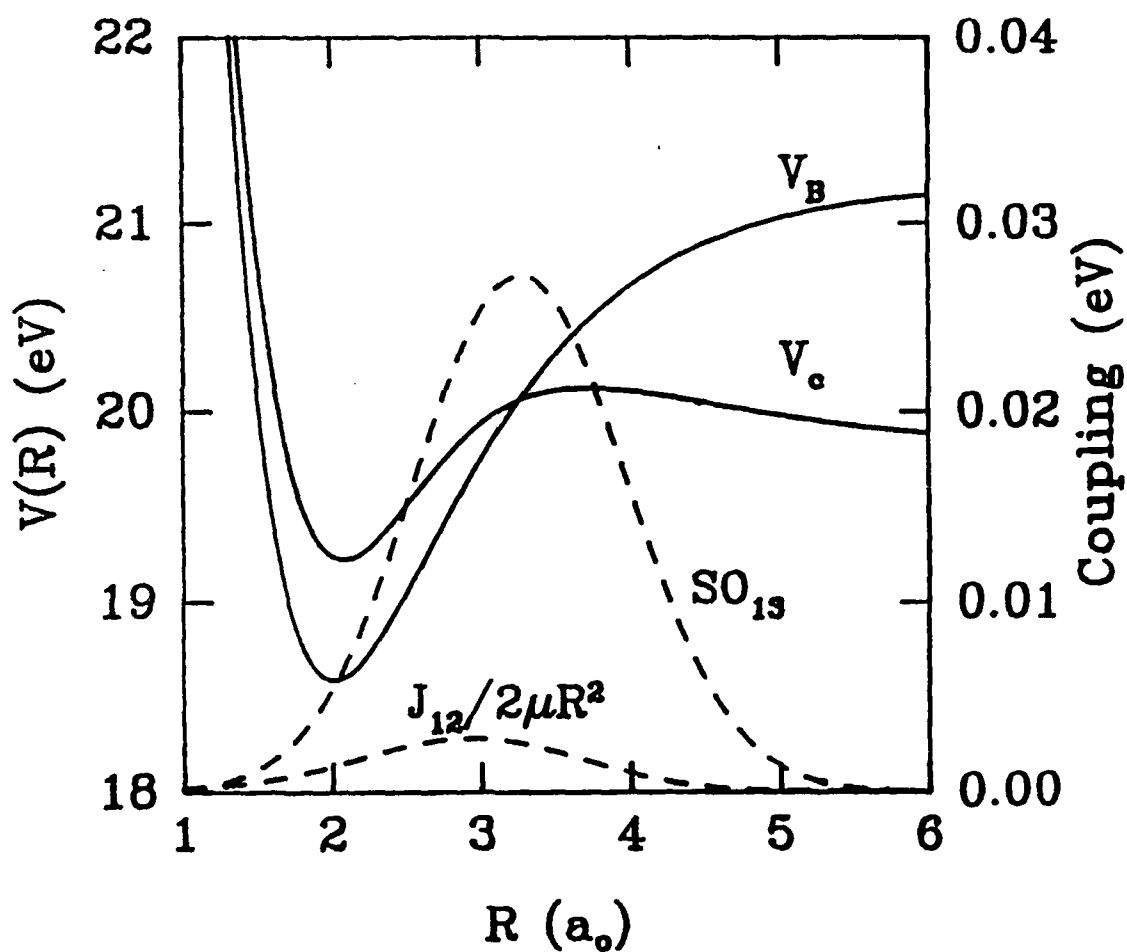


Figure 1. He-He* potential energy curves and couplings for two-state model.

We examined a model which includes only coupling by nonadiabatic processes: the quenching of the $2p^1P$ state of He to the $2s^3S$ state in collisions with a ground state He atom. This model includes the $2-1_g$, $2-0_g^-$ and $3-1_g$ molecular states. The $2-1_g$ state correlates asymptotically with the $2p^1P$ atomic state and has the $B^1\Pi_g$ AS state as the dominant component. The $2-0_g^-$ and $3-1_g$ states are nearly degenerate, correlate asymptotically with the $2s^3S$ atomic state, and have the $c^3\Sigma_g^+$ AS state as the dominant component. Denoting these molecular states 1, 2, and 3, respectively, the electronic Hamiltonian in a diabatic Ω basis is given by

$$H_{el} = \begin{vmatrix} V_1 & \frac{J_{12}}{2\mu R^2} & SO_{13} \\ \frac{J_{12}}{2\mu R^2} & V_2 & \frac{J_{23}}{2\mu R^2} \\ SO_{13} & \frac{J_{23}}{2\mu R^2} & V_3 \end{vmatrix} \quad (107)$$

where V_1 and $V_2 \approx V_3$ are the adiabatic potentials for the B and approximately degenerate c states, respectively, μ is the reduced mass of He_2 , J_{12} and J_{23} are matrix elements of the electronic angular momentum ladder operator between the state pairs 1-2 and 2-3, respectively, and SO_{13} is the matrix element of the spin-orbit operator between states 1 and 3. For the present calculations the adiabatic potentials are approximated from known spectroscopic information. The couplings are approximated as Gaussians centered around the crossing point between the B and c states.

The relevant experimental features to be calculated typically include the shape of the cross sections for electronic transitions as a function of the collision energy. Figure 2 shows a favorable comparison between the SCEM final cross section results for this model with exact quantal scattering results. Keeping in mind that the SCEM is a semiclassical theory of electronic transitions, the excellent agreement of Fig. 3 for detailed opacities (solid line: EXACT; dashed line: SCEM) provides a positive step in the validation of the SCEM technology being employed in this research.

Being a semiclassical description, the SCEM framework is typically employed to describe either a forward process or the reverse process of a quantum mechanical state-to-state transition but not both within the same computation. Achievement of state-to-state time reversal can however be readily checked by making comparisons of the SCEM treatment of excitation and quenching

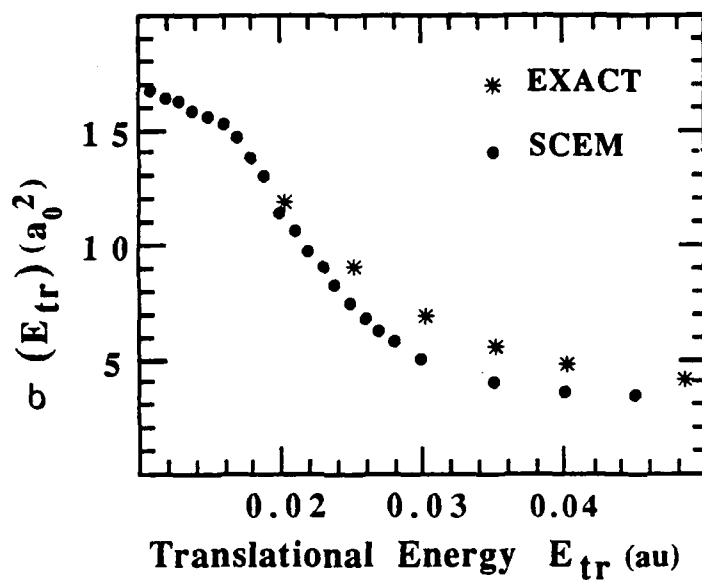


Figure 2. Cross section for $\text{He}(^1\text{P})$ quenching to $\text{He}(^3\text{S})$. The comparison is between exact quantum results and semiclassical SCEM results within the infinite-order-sudden approximation (IOS).

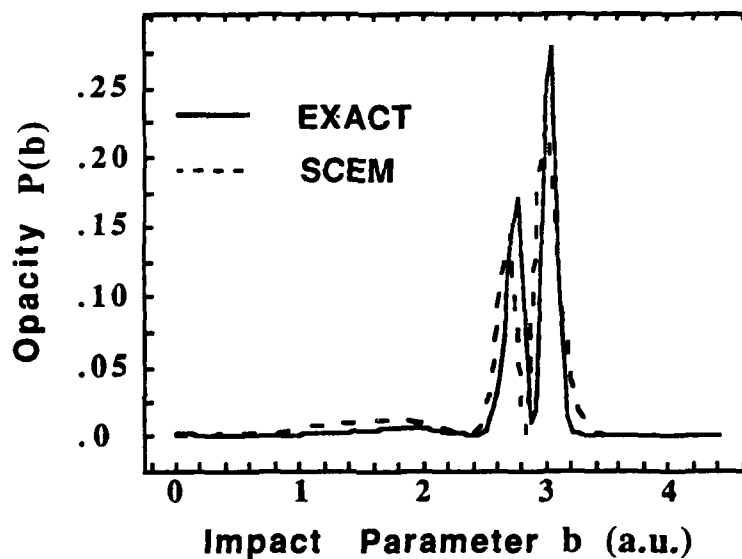


Figure 3. Opacity function for $\text{He}(^1\text{P})$ quenching to $\text{He}(^3\text{S})$. Methods are as in Fig. 2.

dynamics separately. This has been done for the He_2^* system by employing detailed balance as follows:

$$k_i^2 \sigma_{i \rightarrow j} = k_j^2 \sigma_{j \rightarrow i} \quad (108)$$

where

$$k_i^2 = \frac{8\pi^2 \mu E_{\text{tr}, i}}{h^2} = \frac{8\pi^2 \mu}{h^2} (E_{\text{tot}} - W_i) \quad (109)$$

Detailed balance was tested for $E_{\text{tot}}=0.82833H$, $W_1=0.72833H$, $W_2=0.77972H$ and it was found that

$$k_1^2 \sigma_{1 \rightarrow 2} = 1127.7 \text{ and } k_2^2 \sigma_{2 \rightarrow 1} = 1238.5$$

thereby displaying an excellent 10% agreement of detailed balance from these completely distinct SCEM runs.

2. Radiative versus Nonradiative Quenching in the Gas Phase

Theoretical Treatment of the Photon in Radiative Quenching:

We treat the problem of radiative quenching in the same formal framework as used on an earlier occasion to treat photoexcitation in polyatomics. This is feasible in principle because these processes are inversely related to each other and involve the same underlying hamiltonian; also, this is conceptually useful because of the structure of the SCE methodology. We only briefly point out certain essential aspects of this framework to the problems now on hand and the validation requirements of the SCEM.

The radiative quenching hamiltonian within the electron-field representation can be written as:

$$H = -(\hbar^2 / 2\mu) \nabla_{\mathbf{R}}^2 + H_{\text{el}} + H_{\text{rad}} + H_{\text{int}} \quad (110)$$

with

$$H_{\text{el}} = H_{\text{el}}^{(0)} + H_{\text{s.o.}} \quad (111)$$

where $H_{\text{el}}^{(0)}$ contains the electronic kinetic energy as well as the interactions of the electrons and the nuclei among themselves whereas $H_{\text{s.o.}}$ denotes the spin-orbit interaction which often plays

an important role in the stability and collision dynamics of HEDM's. We will employ a second quantized form of the framework with

$$H_{el} = \sum_{\alpha} C_{\alpha}^{\dagger} C_{\alpha} E_{\alpha}(\mathbf{R}) \quad (112)$$

denoting the diagonalized operator H_{el} , and $E_{\alpha}(\mathbf{R})$ the energies of the kets $|\alpha\rangle, |\alpha'\rangle, \dots$ representing the resulting adiabatic electronic states. C_{α} and C_{α}^{\dagger} therefore denote state annihilation and creation operators. The other terms in the hamiltonian are the multidimensional Laplacian for the collisional and internal nuclear state (projectile and target) nuclear kinetic energies, the radiation field hamiltonian

$$H_{rad} = \sum_{\mathbf{k}, \sigma} \hbar \omega_{\mathbf{k}\sigma} a_{\mathbf{k}\sigma}^{\dagger} a_{\mathbf{k}\sigma} \quad (113)$$

and the radiation-matter coupling term

$$H_{int} = ie \sum_{\mathbf{k}, \sigma} \sum_{\alpha, \alpha'} \left(\frac{\hbar \omega_{\mathbf{k}\sigma}}{2\epsilon_0 V} \right)^{\frac{1}{2}} \hat{\epsilon}_{\mathbf{k}\sigma} \cdot \mathbf{D}_{\alpha\alpha'}(\mathbf{R}) (a_{\mathbf{k}\sigma} - a_{\mathbf{k}\sigma}^{\dagger}) (C_{\alpha}^{\dagger} C_{\alpha'} + C_{\alpha'}^{\dagger} C_{\alpha}) \quad (114)$$

written within the electric dipole approximation. It is seen that H_{int} is controlled by the magnitude of the electronic matrix elements of the molecular total dipole operator:

$$-e \mathbf{D}_{\alpha\alpha'}(\mathbf{R}) = \langle \alpha | \mu_d | \alpha' \rangle \quad (115)$$

with $\mu_d = -e \sum_i \mathbf{r}_i + \sum_I Z_I \mathbf{R}_I$, where \mathbf{r}_i denotes all electron coordinates, \mathbf{R}_I all nuclear ones, e is the absolute value of one electronic charge and Z_I represents the nuclear charge. $a_{\mathbf{k}\sigma}$ and $a_{\mathbf{k}\sigma}^{\dagger}$ are photon annihilation and creation operators respectively for second quantized radiation field modes in a volume V . ϵ_0 denotes the vacuum electric permittivity and $\hat{\epsilon}_{\mathbf{k}\sigma}$ is a unit vector of the polarization of the radiation (electric) field. With these definitions, the time-independent Schrodinger equation for the radiative quenching from an electronically excited polyatomic molecule that is isolated or in a collisional process is given by,

$$H |\psi(\mathbf{R})\rangle_{e,f} = E(\mathbf{R}) |\psi(\mathbf{R})\rangle_{e,f} \quad (116)$$

$E(\mathbf{R})$ denoting the total energy of the electron-field wavefunction, $|\psi(\mathbf{R})\rangle_{e,f}$ for nuclear configuration \mathbf{R} , which is in turn readily expanded as

$$|\psi(\mathbf{R})\rangle_{e,f} = \sum_{\alpha, N_{k\sigma}} f_{\alpha, N_{k\sigma}}(\mathbf{R}) |\alpha\rangle |N_{k\sigma}\rangle \quad (117)$$

in terms of products of the adiabatic spin-orbit states $|\alpha\rangle$ with photon number states $|N_{k\sigma}\rangle$

yielding the infinite set of coupled equations for the nuclear wavefunctions $f_{\alpha, N_{k\sigma}}(\mathbf{R})$:

$$\sum_{\alpha', N_{k'\sigma'}} \left(-\frac{\hbar}{4\pi\mu} \delta_{\alpha\alpha'} \delta_{N_{k\sigma} N_{k'\sigma'}} \nabla_{\mathbf{R}}^2 + H_{\alpha N_{k\sigma} \alpha' N_{k'\sigma'}}^{(ef)} \right) f_{\alpha', N_{k'\sigma'}}(\mathbf{R}) = E(\mathbf{R}) f_{\alpha, N_{k\sigma}}(\mathbf{R}) \quad (118)$$

where the hamiltonian matrix $H_{\alpha N_{k\sigma} \alpha' N_{k'\sigma'}}^{(ef)}$ includes the various intra and inter- electronic state dipole couplings and momentum (i.e., radial derivative and rotational) couplings. The problems to be treated below are now readily perceived as simple cases of this general radiative quenching hamiltonian that are pertinent for the subtask. A finite set of equations will arise from truncating the hamiltonian matrix to include just the relevant channels for the computations.

Calculations with accurate potentials and couplings:

Based on the recent calculations of accurate potentials and couplings by Yarkony,¹ we have performed several dynamics calculations which are described below.

We examine the pathways of collisional quenching of $\text{He}(2^3\text{S})$ which will become more important at higher gas phase pressures. We assume only binary collisions are important and quenching occurs by nonadiabatic dynamics involving scattering on multiple electronic surfaces, notably the $a(^3\Sigma_u^+)$, $A(^1\Sigma_u^+)$, $b(^3\Pi_g)$, $B(^1\Pi_g)$, $c(^3\Sigma_g^+)$, and $C(^1\Sigma_g^+)$ states of He_2 . Electronically nonadiabatic collisions of $\text{He}(^1\text{S})$ and $\text{He}(2^3\text{S})$ atoms can begin on either the a or c state potentials and ultimately lead to quenching to the X-state. The $a(^3\Sigma_u^+)$ and $c(^3\Sigma_g^+)$ states of He_2 correlate asymptotically with $\text{He}(^1\text{S})$ (ground state) + $\text{He}(2^3\text{S})$. Dynamical studies of the important pathways leading to such an overall spin-forbidden quenching can now be studied employing Yarkony's new *ab initio* results¹ for the relevant potential energy surfaces and nonadiabatic couplings of this metastable system. Since these participating states involve a mixture of singlets and triplets, transitions are to be described in the total angular momentum (Ω)-

Table 2: He₂ electronic states in the Ω basis

Ω state	degeneracy	spectroscopic notation in Λ -S basis	dominant space-spin configuration (M_S)	asymptotic atomic states
$1-0_g^+$	1	X	$^1\Sigma_g^+(0)$	$1s^2\ ^1S, 1s^2\ ^1S$
$1-0_u^-$	1	a	$^3\Sigma_u^+(0)$	$1s2s\ ^3S, 1s^2\ ^1S$
$1-1_u$	2	a	$^3\Sigma_u^+(1), ^3\Sigma_u^+(-1)$	$1s2s\ ^3S, 1s^2\ ^1S$
$1-0_u^+$	1	A	$^1\Sigma_u^+(0)$	$1s2s\ ^1S, 1s^2\ ^1S$
$2-0_g^+$	1	b	$^3\Pi_{g,1}(-1) - ^3\Pi_{g,-1}(1)$	$1s2p\ ^3P, 1s^2\ ^1S$
$1-0_g^-$	1	b	$^3\Pi_{g,1}(-1) + ^3\Pi_{g,-1}(1)$	$1s2p\ ^3P, 1s^2\ ^1S$
$1-1_g$	2	b	$^3\Pi_{g,1}(0), ^3\Pi_{g,-1}(0)$	$1s2p\ ^3P, 1s^2\ ^1S$
$1-2_g$	2	b	$^3\Pi_{g,-1}(-1), ^3\Pi_{g,1}(1)$	$1s2p\ ^3P, 1s^2\ ^1S$
$2-1_g$	2	B	$^1\Pi_{g,-1}(0), ^1\Pi_{g,1}(0)$	$1s2p\ ^1P, 1s^2\ ^1S$
$2-0_g^-$	1	c	$^3\Sigma_g^+(0)$	$1s2s\ ^3S, 1s^2\ ^1S$
$3-1_g$	2	c	$^3\Sigma_g^+(1), ^3\Sigma_g^+(-1)$	$1s2s\ ^3S, 1s^2\ ^1S$
$3-0_g^+$	1	C	$^1\Sigma_g^+(0)$	$1s2s\ ^1S, 1s^2\ ^1S$

Coupling selection rules:

dipole coupling, μ :

radial derivative coupling, $\partial/\partial R$:

angular momentum coupling, J_{\pm} :

$$g \leftrightarrow u, \Delta\Omega = 0, \pm 1$$

$$g \leftrightarrow g, u \leftrightarrow u, \Delta\Omega = 0$$

$$g \leftrightarrow g, u \leftrightarrow u, \Delta\Omega = \pm 1$$

Table 3: Total coupling in the Ω basis

	$1-0_g^+$	$2-0_g^+$	$3-0_g^+$	$1-0_g^-$	$2-0_g^-$	$1-0_u^-$	$1-0_u^+$	$1-1_u$	$1-1_g$	$2-1_g$	$3-1_g$	$1-2_g$
	(X) ^a	(b)	(C)	(b)	(c)	(a)	(A)	(a)	(b)	(B)	(c)	(b)
$1-0_g^+$ (X)	0^b											
$2-0_g^+$ (b)	R	0										
$3-0_g^+$ (C)	R	R	0									
$1-0_g^-$ (b)	0	0	0	0								
$2-0_g^-$ (c)	0	0	0	R	0							
$1-0_u^-$ (a)	μ	μ	μ	μ	μ	0						
$1-0_u^+$ (A)	μ	μ	μ	μ	μ	0	0					
$1-1_u$ (a)	μ	μ	μ	μ	μ	J	J	0				
$1-1_g$ (b)	J	J	J	J	J	μ	μ	μ	0			

Table 3 (continued) : Total coupling in the Ω basis

	$1-0_g^+$ (X) ^a	$2-0_g^+$ (b)	$3-0_g^+$ (C)	$1-0_g^-$ (b)	$2-0_g^-$ (c)	$1-0_u^-$ (a)	$1-0_u^+$ (A)	$1-1_u$ (a)	$1-1_g$ (b)	$2-1_g$ (B)	$3-1_g$ (c)	$1-2_g$ (b)
$2-1_g$ (B)	J	J	J	J	J	μ	μ	μ	R	0		
$3-1_g$ (c)	J	J	J	J	J	μ	μ	μ	R	R	0	
$1-2_g$ (b)	0	0	0	0	0	0	0	μ	J	J	J	0

^a Spectroscopic notation for dominant configuration.

^b Zero indicates the coupling vanishes from symmetry constraints. Letters indicate:

μ nonvanishing dipole coupling.

R nonvanishing d/dR coupling.

J nonvanishing angular momentum coupling.

representation. Tables 2 and 3 indicate the resulting states along with the appropriate radiative and nonadiabatic couplings.

Figure 4 illustrates the important triplet-triplet, singlet-triplet and singlet-singlet dynamical pathways for the $a \rightarrow X$ quenching process. (Please note that the singlet-triplet diagram suppresses intramultiplet couplings). The solid arrows indicate transition dipoles and electronically nonadiabatic dynamical couplings known from Yarkony's calculations (H^{SO} : spin-orbit, μ_{sf} : spin-forbidden dipole, and L : rotational couplings) and the dashed arrow is a negligible (due to large energy gap) H^{SO} coupling. The diagrams in Fig. 4 can be employed to identify two key pathways of quenching: (1) a direct spin-forbidden radiative pathway between the a -state and an X -state dressed with a photon² (as seen in the middle diagram of Fig. 4) and (2) a more complex multistate dynamical route involving hops among a variety of triplet states and eventually crossing into the singlet manifold, where strong quenching propensity prevails.

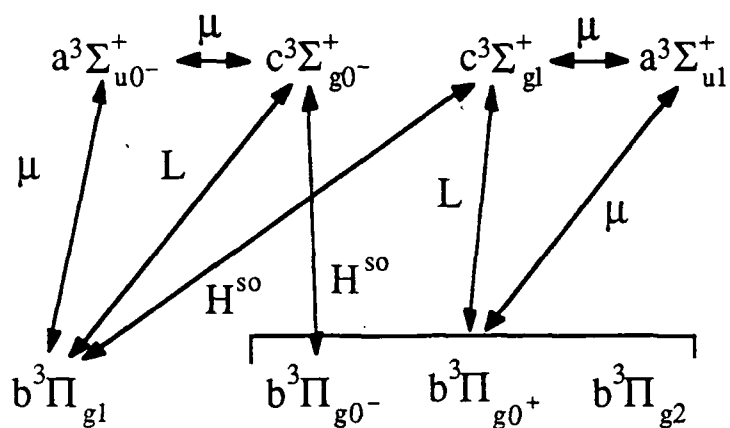
Although the system can in principle quench nonradiatively, it was found that the related probabilities are very low, $\sim 10^{-16}$, compared to $\sim 10^{-8}$ for the radiative routes.

The direct spin-forbidden radiative pathway is studied using a two-state model using the a and X states within the self-consistent eikonal method (SCEM). The relevant potentials and the spin forbidden radiative coupling are shown in Fig. 5 where the X state has been shifted up by the relevant atomic transition energy.² Calculations using SCEM and based on Eq. (118) yielded the following cross sections (in a_0^2) for collision-induced radiative quenching: 1.23×10^{-4} (probability $\sim 1 \times 10^{-6}$), 1.92×10^{-13} (probability $\sim 1 \times 10^{-7}$) at translational energies 5.4 and .27 eV respectively. Probabilities drop down to 1×10^{-8} at .004 eV but climb again to 1×10^{-7} at .002 eV. These numbers are consistent with the experimental³ cross section upper limit of $\sim 1 \times 10^{-9} a_0^2$ which dealt with pressure effects at low translational energies. It is also seen that there is some room for additional quenching contributions while remaining consistent within the experimental upper bound.

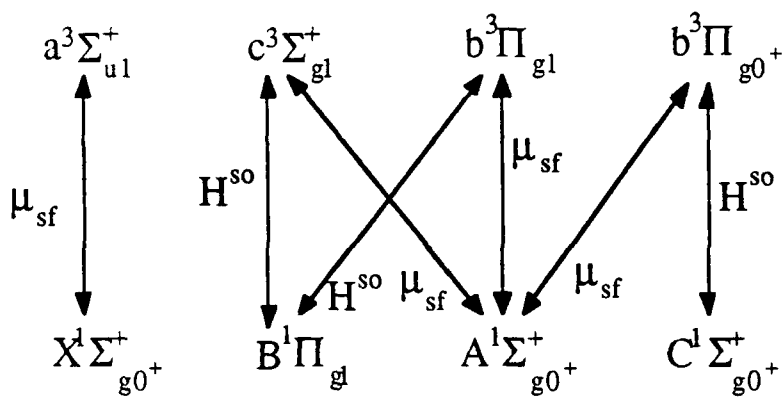
Several different models of the multistate pathways were studied. So far, our results indicate the following notable radiative quenching features. In spite of the many additional radiative and nonradiative pathways available in the many-state model, the nonradiative nonadiabatic route to the singlet manifold is incapable of competing with the propensities of the above two-state radiative route. This is consistent with Yarkony's anticipation¹ of a bottleneck in the multiplet crossover rate. The dynamical problem, however, becomes very complicated when the various photon emitting pathways are included. A full study requires a thorough scan of photon frequency dependence in each dipole coupling: there are 13 dipole couplings, 9 allowed and 4 forbidden. Systematic examination of selected many-state models and trajectories were done to

Figure 4. He₂ Transition Pathways, based on *ab initio* results of Ref. 1.

Triplet-Triplet transition pathways



Singlet-Triplet transition pathways



Singlet-Singlet transition pathways

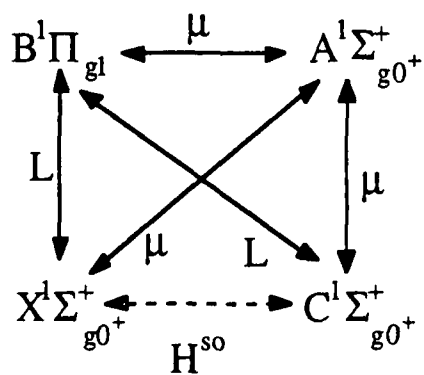
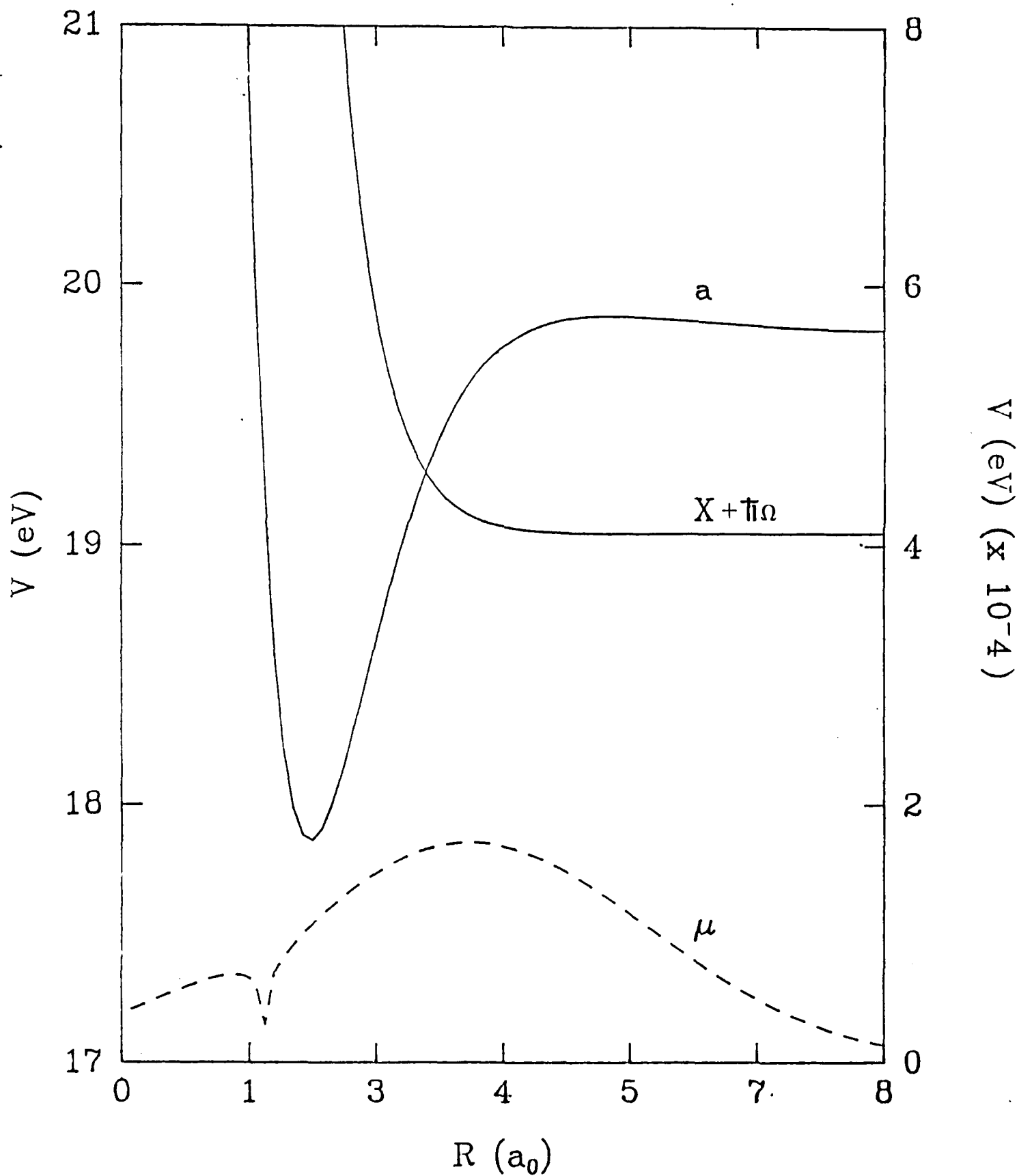


Figure 5. He₂ two-state (a and X) radiative quenching model potentials.



examine the sensitivity to photon frequencies and dependence of results on whether keeping or dropping the radiative couplings. Although dramatic changes have been found in the relative propensities, they remain relatively small compared to the direct route. Hence it is probably safe to *a priori* rule out competition from these pathways at this stage.

REFERENCES

1. D. Yarkony, "On the Quenching of Helium 2^3S : Potential Energy Curves for, and Nonadiabatic, Relativistic and Radiative Couplings between the $a(^3\Sigma_u^+)$, $A(^1\Sigma_u^+)$, $b(^3\Pi_g)$, $B(^1\Pi_g)$, $c(^3\Sigma_g^+)$, and $C(^1\Sigma_g^+)$ states of He_2 .", J. Chem. Phys. (In Press).
2. μ_{sf} is computed in C. Chabalowsky, J. O. Jensen, D. R. Yarkony, and B. H. Lengsfeld III, J. Chem. Phys. **90**, 2504 (1989); the photon energy is chosen to be nearly on resonance with the 2^3S - 1^1S transition.
3. H. W. Moos and J. R. Woodworth, Phys. Rev. Letts. **30**, 775 (1973).

Accurate Computations of Energy Transfer in Atom-Diatom Collisions: Comparative Study of Vibrational Excitations using Semiclassical Wavefunctions and Coupled Quantal States

1. Introduction

Molecular collisional energy transfer presents a computationally challenging problem to the dynamicist even after the global potential energy surface is known. A rich variety of quantum mechanical, semiclassical and classical models may be constructed to solve the problem depending on the behavior of the potential energy surface which controls the collision dynamics. The information from modern laser-based experiments, involving precise microscopically detailed observations of collisions, is in the form of state-resolved cross sections and demand an explanation from theory at that level of detail. Classical mechanics in itself does not offer a long-term solution for obtaining such state-resolved information. Fully quantum mechanical treatments become unwieldy for realistic systems despite recent triumphs that exploit efficient algorithms on supercomputers. Thus there is a present-day need to develop and exploit semiclassical dynamical theories that hold promise. In order to obtain general results, it has to be based on a systematic process involving detailed benchmarks against accurate quantum mechanical results for smaller systems and the development of controlled computational schemes which are careful paths to accomplish the devious transcription from classical trajectories to semiclassical wavefunctions.

The present subsection reports a study of vibrational excitation during atom-diatom collisions in gas phase and is one of many successful numerical experiments in which we have employed the eikonal ansatz for the semiclassical wavefunction. The relevant general formal discussions have been presented in the preceeding section in greater detail. The present section will focus on the formulation for the vibrational excitation problem and its numerical investigation.

In this subsection we consider a two degree of freedom model of atom-diatom collisions ($O+HF$ and $Na+H_2$ collisions are studied) as defined in the rotational infinite order sudden (IOS) approximation. The numerical tests presented here are benchmarked against previously existing quantum IOS (QIOS) results. Two distinct dynamical models are employed in this subsection to describe state-to-state vibrational dynamics: (1) is based on combining a classical treatment of translational motion with a quantal states expansion in target vibrational states (called RSVE: for rotational sudden with vibronic expansion) and (2) is based on employing semiclassical eikonal wavefunctions for all degrees of freedom obtained from their classical trajectories (called SIOS: for semiclassical infinite order sudden).

2. Theory

1. IOS Approximation in the diabatic representation

The rotational IOS approximation¹ for the atom-diatom scattering problem is based on solving the two-dimensional Schroedinger equation with the Hamiltonian:

$$\hat{H}_{\text{IOS}} \equiv \left(-\frac{\hbar^2}{2\mu} \frac{\partial^2}{\partial R^2} - \frac{\hbar^2}{2\mu_{\text{BC}}} \frac{\partial^2}{\partial r^2} + \frac{\hbar^2 l(l+1)}{2\mu R^2} + \frac{\hbar^2 j(j+1)}{2\mu_{\text{BC}} r^2} \right) \mathbf{1} + \underline{\underline{H}}(R, r, \gamma) \quad (119)$$

where $\underline{\underline{H}}(R, r, \gamma)$ is the $n \times n$ matrix of the diabatic potentials and couplings between different electronic states, R is the distance between the center of mass of the diatomic BC and the atom A, r is the bond length in the diatomic BC and γ is the angle between the diatomic and the radius drawn from its center of mass to the atom A.

2. Quantum-mechanical treatment of vibrations.

In following Redmon et. al.² we reduce the problem to the infinite set of the ordinary differential equations of the second order by using the matrix representation for the hamiltonian in the space of the vibrational coordinate r , namely, we use the eigenfunctions of the Schroedinger equation:

$$\left[-\frac{\hbar^2}{2\mu_{\text{BC}}} \frac{d^2}{dr^2} + V_{\text{BC}}(r) + \frac{\hbar^2 j(j+1)}{2\mu_{\text{BC}} r^2} - \epsilon_v^j \right] u_v^j = 0 \quad (120)$$

as the basis set and represent Eq. (120) as

$$-\frac{d^2 \psi_{nv}^{jl}}{dR^2} - k_{jv}^2 \psi_{nv}^{jl} + \sum_{n', v'} h_{nv, n'v'}^{jl}(R, \gamma) \psi_{n'v'}^{jl} = 0, \quad (121)$$

where we put

$$h_{nv, n'v'}^{jl}(R, \gamma) \equiv \delta_{nn'} \delta_{vv'} \frac{l(l+1)}{R^2} + \frac{2\mu}{\hbar^2} \left\{ -\Delta D_\eta + \int dr u_v^j(r) u_{v'}^j(r) [H_{nn}(R, r, \gamma) - \delta_{nn'} V_{\text{BC}}(r)] \right\}, \quad (122)$$

with

$$\hbar k_{jv} \equiv [2\mu(E - \epsilon_v^j)]^{1/2} \quad (123)$$

and

$$\Delta D_\eta \equiv \lim_{R \rightarrow \infty} [H_{\eta\eta}(R, r, \gamma) - H_{11}(R, r, \gamma)] \quad (124)$$

used to evaluate the probabilities of transitions from the η th electronic state.

We solve the set of coupled differential equations Eq. (121) by representing wavefunctions ψ_{nv}^{jl} in the common eikonal form³:

$$\psi_{nv}^{jl}(R; \gamma) = \frac{1}{\sqrt{P^{jl}(R; \gamma)}} \beta_{nv}^{jl}(R; \gamma) \exp [iW^{jl}(R; \gamma)/\hbar] \quad (125)$$

where $W^{jl}(R; \gamma)$ is Hamilton's characteristic function⁴ found from the Hamilton-Jacobi equation⁴:

$$\frac{1}{2\mu} |P^{jl}(R; \gamma)|^2 + \bar{V}^{jl}(R; \gamma) = \frac{1}{2} k_{jv}^2 \quad (126)$$

with

$$P^{jl} = \frac{dW^{jl}}{dR} \quad (127)$$

and $\bar{V}^{jl}(R; \gamma)$ denotes the Ehrenfest potential:

$$\bar{V}^{jl}(R; \gamma) = \sum_{nv, n'v'} h_{nv, n'v'}^{jl} \beta_{nv}^{jl} \beta_{n'v'}^{jl*} / \sum_{nv} |\beta_{nv}^{jl}|^2 \quad (128)$$

The functions β_{nv}^{jl} satisfy the set of coupled equations:

$$i\hbar\beta_{nv}^{jl} = \sum_{nv, n'v'} h_{nv, n'v'}^{jl} \beta_{n'v'}^{jl} - \bar{V}^{jl} \beta_{nv}^{jl} \quad (129)$$

and are solved together with the equation of motion for the potential Eq. (128).

3. Semiclassical treatment of vibrations

A. Equations of Motion

We represent the wavefunction $\psi(R, r; \gamma, lj)$ in the eikonal form:

$$\psi(R, r; \gamma, lj) = A(R, r; \gamma, lj) \exp[iW(R, r; \gamma, lj)/\hbar], \quad (130)$$

where $W(R, r; \gamma, lj)$ is Hamilton's characteristic function

$$\frac{1}{2\mu} \left(\frac{dW}{dR} \right)^2 + \frac{1}{2\mu_r} \left(\frac{dW}{dr} \right)^2 + U(R, r; \gamma, lj) = E \quad (131)$$

for the potential

$$U(R, r; \gamma, lj) \equiv V(R, r; \gamma) + \frac{\hbar^2 l(l+1)}{2\mu R^2} + \frac{\hbar^2 j(j+1)}{2\mu_{BC} r^2} \quad (132)$$

The momenta conjugate to the coordinates R and r are given by the relation:

$$P_0(R, r; \gamma, lj) = \frac{dW}{dR}, \quad P_1(R, r; \gamma, lj) = \frac{dW}{dr} \quad (133)$$

To carry the wavefunction $\psi(R, r; \gamma, lj)$ through turning points we represent it as

$$\psi(t, r_0; \gamma, lj) \equiv J^{-1/2}(t, r_0; \gamma, lj) A(0, r_0; j) \zeta(t, r_0; \gamma, lj) \quad (134)$$

where t is time, r_0 is the initial value of r on the trajectory run on the potential surface U and

$J(t, r_0; \gamma, lj)$ is the Jacobian of the transformation:

$$t, r_0 \rightarrow R(t, r_0; \gamma, lj), r(t, r_0; \gamma, lj), \quad (135)$$

and then assume⁵ that the function $\zeta(t, r_0; \gamma; l_j)$ is continuous everywhere by analogy with the one-dimensional case. We, in following Ref.5, solve the equation:

$$i\hbar \frac{d\zeta}{dt} = \left[U - E - \frac{(P_0)^2}{2\mu} - \frac{(P_1)^2}{2\mu_{BC}} \right] \zeta \quad (136)$$

as if the function $\zeta(t, r_0; \gamma; l_j)$ itself were continuous, finally shifting its phase by $\pi/4$ times the total number of the turning points passed.

B. Initial conditons

Let us put $Q^0 \equiv R$, $Q^1 \equiv r$, $w^1 \equiv r_0$,

$$V_j(r) \equiv V_{BC}(r) + \frac{\hbar^2 j(j+1)}{2\mu_{BC} r^2} \quad (137)$$

Then the initial conditions take the form

$$Q^0(0, r_0, \pm 1) \equiv R_0, \quad Q^1(t_0, r_0, \pm 1) = r_0 \quad (138)$$

$$P^0(t_0, r_0, \pm 1) = -p_{vj}, \quad P^1(t_0, r_0, \pm 1) = \pm p_r(r_0) \quad (139)$$

with

$$p_{vj} = \hbar k_{vj} = \sqrt{2\mu(E - \epsilon_{vj})} \quad (140)$$

and

$$p_r(r) \equiv \sqrt{2\mu_{BC}[\epsilon_{vj} - V_j(r)]}, \quad (141)$$

$$Q_1^0(0, r_0, \pm 1) \equiv 0, \quad Q_1^1(0, r_0, \pm 1) \equiv 1 \quad (142)$$

$$P_1^0(t_0, r_0, \pm 1) \equiv 0, \quad P_1^1(0, r_0, \pm 1) = - \frac{\mu_{BC}}{P_1^1(0, r_0, \pm 1)} \left. \frac{dV_j}{dr} \right|_{r=r_0}, \quad (143)$$

$$W_0(r_0, \pm 1) = \pm \left[\int_{r_-}^{r_0} dr' p_r(r') - \frac{\pi}{4} \right], \quad (144)$$

$$J(0, r_0, \pm 1) \equiv - p_{vj} / \mu, \quad (145)$$

$$\psi(0, r_0, \pm 1) = \frac{1}{2} [k_{vj} |p_r(r_0)|]^{-1/2} e^{iW_0(r_0, \pm 1) - ik_{vj} R_0}, \quad (146)$$

$$\zeta(0, r_0, \pm 1) = \frac{1}{2} |J(0, r_0, \pm 1)|^{1/2} e^{iW_0(r_0, \pm 1) - ik_{vj} R_0}. \quad (147)$$

C. Connection formulae

If the interaction between vibrational and collisional motions is negligible the derivative of r with respect of its initial value r_0 can be evaluated by differentiating the equation:

$$t = \mu_{BC} \int_{r_0}^{r(t, r_0)} dr' / p_r(r') \quad (148)$$

with respect to r_0 at the fixed moment t . We find

$$p_r^{-1}(r) \left(\frac{\partial r}{\partial r_0} \right)_t - p_r^{-1}(r_0) = 0 \quad (149)$$

and hence

$$Q_1^1 = \left(\frac{\partial Q_1}{\partial r_0} \right)_t = p_r(r) / p_r(r_0) \quad (150)$$

Therefore if the off-diagonal element Q_1^0 can be also neglected the Jacobian J factors as

$$\mu J(t, r_0, \pm 1) \approx P^0(t, r_0 \pm 1) P^1(t, r_0 \pm 1) / P^1(t_0, r_0 \pm 1), \quad (151)$$

and its zeros approximately coincide with zeros of the momenta P^0 and P^1 . We thus assume that jumps of the Jacobian on the caustics are governed for adiabatically separable motions by the standard WKB rules, namely, that the function $|\zeta(Q)|$ is continuous there, whereas the phase of the function $\zeta(Q)$ decreases by $\pi/2$:

$$W(Q) \rightarrow W(Q) - \pi/2 \quad (152)$$

if the Jacobian changes its sign, and by π , if both momenta change their sign during the same time step.

D. Average of the final amplitudes over the initial conditions

The exact quantum mechanical wave function has the asymptotics:

$$\psi_{vj}(R_f, r) = \frac{u_{vj}(r)}{k_{vj}^{1/2}} e^{-ik_{vj} R_f} + \sum_{v', j'} S_{vj; v' j'} \frac{u_{v' j'}(r)}{k_{v' j'}^{1/2}} e^{ik_{v' j'} R_f}, \quad (153)$$

where the S-matrix elements $S_{vj; v' j'}$ for $v j \neq v' j'$ are given by the relation:

$$S_{vj; v' j'} = \sqrt{k_{v' j'}} e^{-ik_{v' j'} R_f} \int_0^\infty dr \psi_{vj}(R_f, r) u_{v' j'}(r). \quad (154)$$

By analogy with Eq. (154) we evaluate the semiclassical S-matrix elements by means of the relation:

$$S_{vj; v' j'} = \frac{1}{2} \sqrt{k_{v' j'}} e^{-ik_{v' j'} R_f} \sum_{v=\pm 1} \int_0^\infty dr \psi_{vj}(R_f, r; v) u_{v' j'}(r). \quad (155)$$

To avoid of the singularities in the turning points we first represent this matrix element as the two-dimensional integral using the relation:

$$S_{vj; v' j'} \approx \frac{1}{\Delta R} \int_{R_f}^{R_f + \Delta R} dR S_{vj; v' j'}. \quad (156)$$

(The relation turns into the identity if we deal with the exact matrix element which is independent of R.) Substituting Eq. (155) into Eq. (156) we find

$$\begin{aligned}
 & \Delta R \left(k_{vj} \mu_{BC} C_{vj} \right)^{1/2} S_{vj;v'j'} \\
 &= \sum_{v=\pm 1} \int_{r_-}^{r_+} dr_0 \left[\frac{k(r_0, v)}{p_r(r_0, v)} \right]^{1/2} \int_0^{t_f(r_0, v)} dt J^{1/2}(t, r_0, v) \zeta'_{vj}(t, r_0, v) u_{vj}(r(t); r_0) \\
 &= \frac{1}{\mu_{BC}^{3/4}} \sum_{v=\pm 1} \int_0^{T/2} d\tau k^{1/2}[\tau, v] \int_0^{t_f[\tau, v]} dt J^{1/2}[t, \tau, v] \zeta'_{vj}[t, \tau, v] u_{vj}(r(t); r_0(\tau)),
 \end{aligned} \tag{157}$$

where

$$\zeta'_{vj}(t, r_0, v) \equiv \zeta_{vj}(t, r_0, v) e^{-ik(r_0, v)R(t, r_0, v)} \tag{158}$$

$$J(t, r_0, v) \equiv P^1(t_0, r_0, v) J(t, r_0, v) = \begin{vmatrix} P^0 & P^1 \\ \tilde{Q}_1^0 & \tilde{Q}_1^1 \end{vmatrix} \tag{159}$$

with

$$\tilde{Q}_1^0(t, r_0, v) \equiv P^1(t_0, r_0, v) Q_1^0(t, r_0, v), \quad \tilde{Q}_1^1(t, r_0, v) \equiv P^1(t_0, r_0, v) Q_1^1(t, r_0, v). \tag{160}$$

and the notations $[\tau, v]$ and $[t, \tau, v]$ stand for $(r_0(\tau), v)$ and $(t, r_0(\tau), v)$. We directly propagate

\tilde{Q}_1^0 and \tilde{Q}_1^1 along the trajectory to avoid possible complications coming from the singularities in Eq. (143) which appear if the trajectory starts from the turning point.

3. Potential Energy Surfaces

Two candidates of collisional excitation of vibrational levels were studied, (1) in $O(^3P) + HF(v=0, j=0)$ collisions and, (2) in $Na(3s^2S) + H_2(v=0, j=0)$ collisions, both of which have previously existing potential energy surface information. The potential energy surface for the OHF

system is based on an earlier UHF calculation² consisting of a sum over pairs plus three-body correcting analytical fit (surface 1 of Ref. 2) whereas the NaH_2 collisions were studied on a DIM potential energy surface.⁶ A LEPS fit to MCSCF results for OHF were also generated in Ref. 2 to enable the dynamical study of the H abstraction reaction, but this needs to be employed only at higher energies than presently reported. We refrain from including the analytical and numerical details regarding the potential surfaces for brevity since they are available elsewhere.

A central feature of the OHF potential surface that is relevant for vibrational excitation dynamics is the expected concentration of most of the excitation (at lower energies) to a narrow range of IOS-angles, close to the approach of O atom from the H-atom end of the HF molecule; in this direction, the potential surface allows a reactive encounter to occur at higher energies. This will be borne out by the dynamics results below. In the case of NaH_2 collisions, only the electronically adiabatic ground surface (obtained from diagonalizing the eight diabatic DIM surfaces of Ref. 6) is employed in the electronically elastic results to be presented below for comparing QIOS and RSVE results.

4. Computational Details

The RSVE dynamical calculations using Eqs. (129) are straightforward once the potential matrix in the vibronic basis is set up. This is done by diagonalizing the asymptotic vibrational Schrodinger equation in a harmonic basis set or employing one of many standard numerical algorithms¹ to obtain the target states. The atom-diatom potential matrix is readily computed along the trajectory since it is expanded in these target states which have amplitudes that vary with time according to Eq. (129), thereby leading to a time-dependent potential obeying Eq. (128). The amplitude initial conditions are chosen to correspond to unit probability in the diatomic $v=0$ state. The separation R is chosen large and the asymptotic negative relative momentum is defined by the channel potential in the $v=0$ channel and collision energy. The final amplitudes in other state channels resulting from solving the dynamical equations yield the inelastic transition probabilities. The computation of cross sections involves integration over many trajectories that represent varying IOS-angles and impact parameters for each given initial rovibrational state. All the preliminary computations reported here are for initial $v=j=0$ for the diatomic and the study examines dependence on collision energy and total angular momentum (semiclassically defined by the impact parameter).

The SIOS calculations start with the generation of a bundle of classical trajectories determined by the collision energy and total angular momentum. Only 20 trajectories are employed in the present results. The main task involves building the semiclassical eikonal wavefunction along these trajectories giving special attention to the semiclassical phase changes at caustics (such as classical turning points). The latter are determined by the semiclassical Born Oppenheimer

approximation (see previous section and Appendix 2) applied to the present problem. The post-collision eikonal wavefunction is then projected onto selected final states to directly determine the S-matrix elements for inelastic transitions. The projection process employs interpolation of the asymptotic eikonal wavefunction to result in a finely grided numerical quadrature for S-matrix amplitudes since the inelastic trajectories end in a nonuniform grid even when the initial conditions start from a uniform grid. Cross section computations involve integration of these amplitudes over IOS-angles and impact parameters and introduce further quantal interference effects.

5. Results and Discussion

Figure 6 shows that excellent agreement with an exact limit QIOS benchmark is obtainable from the RSVE computations. This success of RSVE in gas phase is consistent with the similar success that the coupled states ansatz has had in treating rotationally-electronically inelastic gas/surface encounters involving up to 282 channels.⁷ The most exciting aspect of Fig. 6 is however the promise shown there by the SIOS method, which is seen to capture the essential physics of this collision; the results shown are from SIOS calculations that employ semiclassical wavefunctions based on a meager 20 trajectories and are not yet numerically the best they can be.

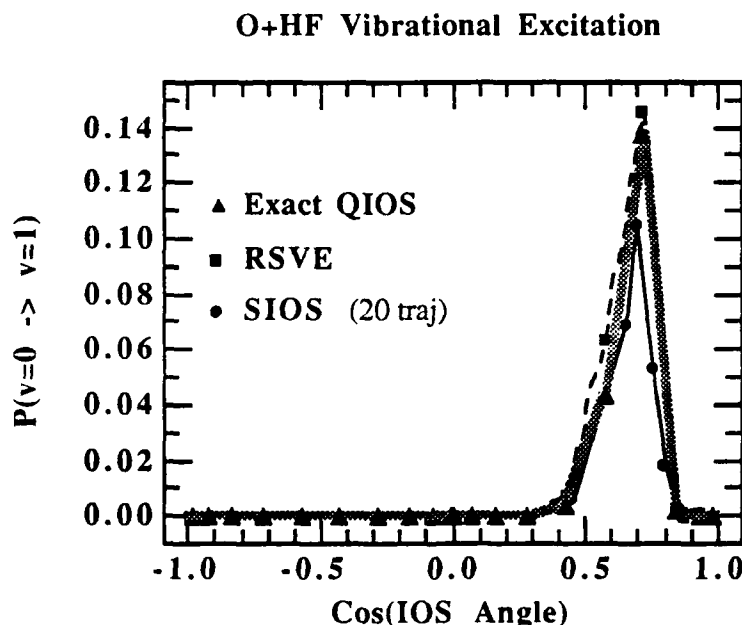


Figure 6. Comparison of angle-dependent accurate quantum-IOS probabilities with those obtained with the new semiclassical method for $v=0 \rightarrow v=1$ vibrational excitation in collisions between $O(^3P)$ atoms and HF molecules at a translational energy of 3 eV. Both total and internal angular momenta are zero.

Figures 7 and 8 show dependence on total angular momentum for the two examples of vibrational excitation studied here. Fig. 7 contains all the data available at the time of this report. (Detailed calculations are in progress to make a full assessment of the methodologies in different L and E_{tr} regimes.) The NaH_2 computations were done to see if the quality of agreement is maintained for a completely different molecular system and Fig. 8 is encouraging (note that H_2 being a homonuclear diatomic molecule is fully studied by sampling half the IOS-angle space compared to HF).

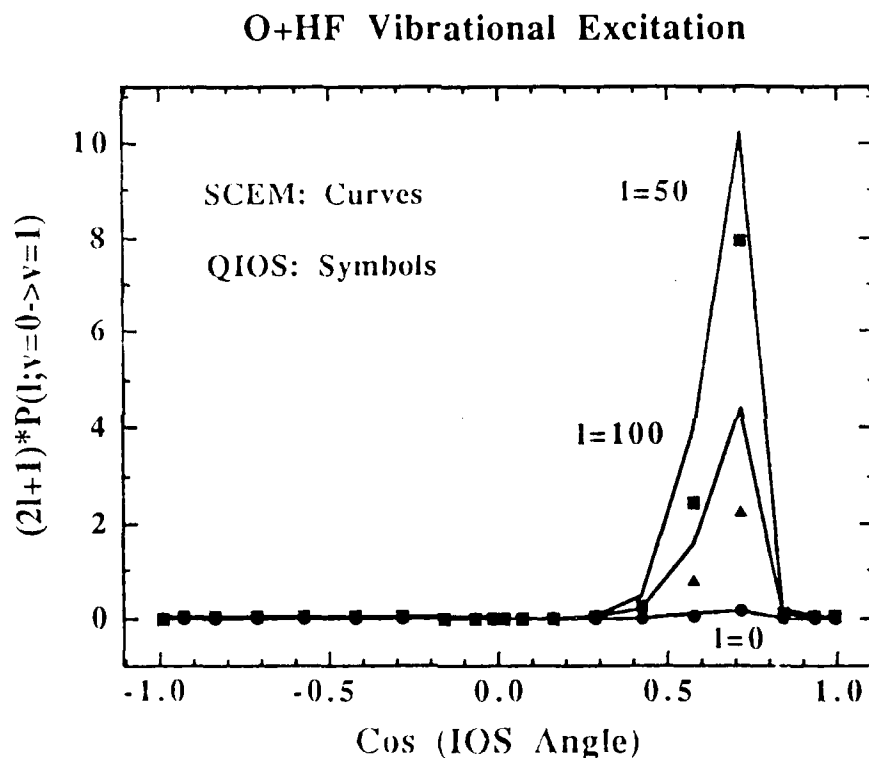


Figure 7. Comparison of angle-dependence of accurate quantum-IOS opacities with those obtained with the new semiclassical method for $\text{O}(^3\text{P})$ atoms colliding with ground-state HF molecules. Curves correspond to different values of orbital angular momentum. Translational energy is 3.0 eV.

Na+H₂ Vibrational Excitation

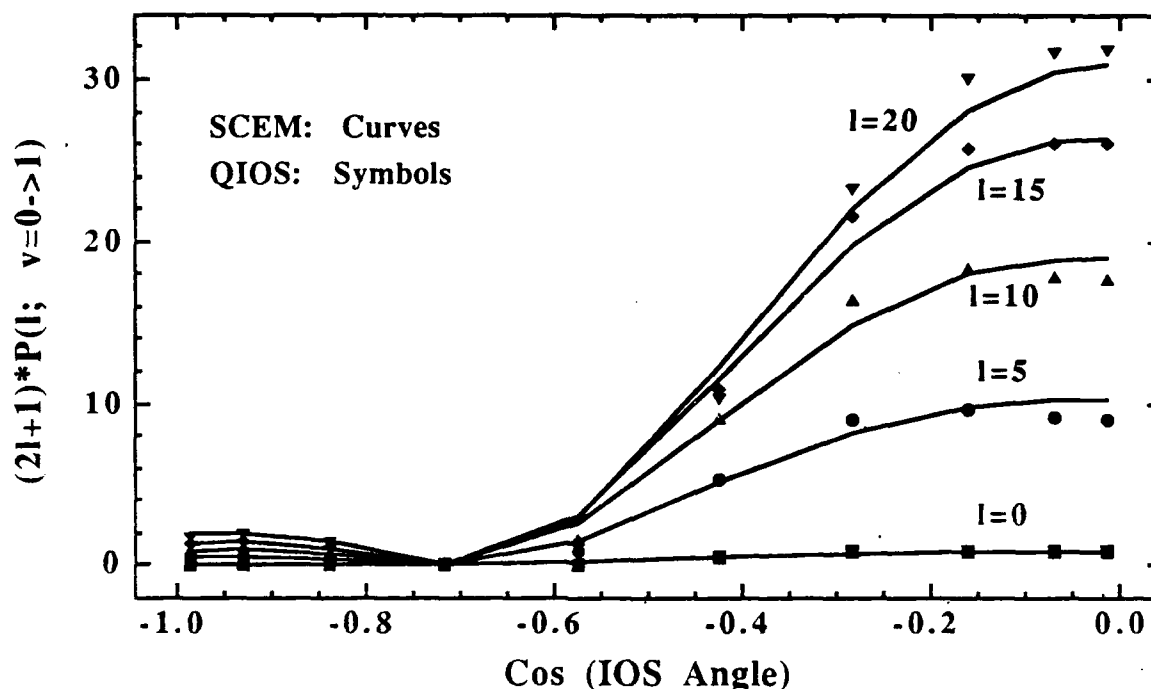


Figure 8. Comparison of angle-dependent opacities from IOS quantum calculations with those obtained with the new semiclassical method for (3s²S) Na atoms colliding with ground-state H₂ molecules. Curves correspond to different values of orbital angular momentum. Total energy is 2.04 eV.

6. Concluding Remarks

We have produced a systematic numerical benchmark for collisional excitation of vibrational levels employing semiclassical methods. Two semiclassical computational routes, (1) using a coupled quantal states ansatz to describe vibrational states quantum mechanically and translational motion classically, within the SCЕМ framework, and (2) using semiclassical wavefunctions generated from classical trajectory results using a newly developed (semiclassical Born-Oppenheimer approximation) procedure were tested against exact quantum limit results. Both the semiclassical methods were successful in obtaining reliable numbers for state-to-state vibrational excitation probabilities. The use of method (2), termed SIOS herein, is indicated as an exciting prospect: such a technique is to be welcomed as a computational route allowing the transformation of information from classical trajectories to state-to-state transition amplitudes at the semiclassical level. The novel feature of the SIOS scheme employed here compared to rigorous S-matrix theory of Miller⁸ (which was difficult to apply in practical problems and soon went out of

use) is that there are no nonlinear root trajectory searches to be performed here; instead, amplitudes are obtained by projecting the eikonal scattering wavefunction on to specific final states. The promise of such a method was demonstrated earlier in the Franck-Condon region for photodissociation,⁹ but the present validation for vibrational excitation processes significantly extends the validity regime, by demonstrating that useful quality persists in outgoing eikonal wavefunctions in the asymptotic region provided valid connection formulae are employed.

REFERENCES

- 1 See eg. V. Khare, D. J. Kouri, J. Jellinek, and M. Baer, in: Potential Energy Surfaces and Dynamics Calculations, D. C. Truhlar, ed., (Plenum, New York, 1981) p. 475.
- 2 M. J. Redmon, L. T. Redmon, and B. C. Garrett, in AFRPL Final Report AFRPL TR-84-030, "Collisional Excitation Cross Sections", Sec. 3. (1984).
- 3 D. A. Micha, J. Chem. Phys. **78**, 7138 (1983).
- 4 H. Goldstein, "Classical Mechanics", Addison-Wesley, London (1950).
- 5 G. Natanson and P. K. Swaminathan, "Semiclassical Methodology for Computing Multichannel Eikonal Wavefunctions in Molecular Collisions: A Reformulation and Extension", unpublished manuscript (1989).
- 6 D. G. Truhlar, J. W. Duff, N. C. Blais, J. C. Tully, and B. C. Garrett, J. Chem. Phys. **77**, 764 (1982); N. C. Blais, D. G. Truhlar and B. C. Garrett, J. Chem. Phys. **78**, 2956 (1983).
- 7 B. M. Rice, B. C. Garrett, P. K. Swaminathan, and M. H. Alexander, J. Chem. Phys. **90**, 575 (1989).
- 8 See W. H. Miller, Adv. Chem. Phys. **25**, 69 (1974) for a review.
- 9 P. K. Swaminathan, C. L. Stodden, and D. A. Micha, J. Chem. Phys. **90**, 5501 (1989).

The Quenching of Na(3^2P) by H_2 : A Quantal IOS Calculation of Electronic-to-Vibrational Energy Transfer

1. Introduction

The quenching of electronically excited Na by H_2 is a prototype for electronic-to-vibrational (E-V) energy transfer in molecular collisions. E-V energy transfer involving alkali atoms has been widely studied both experimentally and theoretically.¹⁻¹⁴ The theoretical interpretation of the Na- H_2 quenching process has focused upon the two lowest states of $^2A'$ symmetry;^{6,10,13,15-17} for C_{2v} geometries these are the 1^2A_1 and 1^2B_2 states. The 1^2B_2 state has a well; it dissociates to $Na(3p^2P) + H_2$, and it exhibits a conical intersection with the 1^2A_1 surface that dissociates to ground-electronic-state reagents. For less symmetric geometries, both these states become $^2A'$. Previous dynamical studies indicate that these two electronic states can qualitatively describe the quenching process.^{5,10,13} A quantitative description of this process requires both potential energy surfaces for the electronic states of importance and the nonadiabatic coupling terms between these electronic states. *Ab initio* restricted Hartree-Fock calculations have been reported for the potential energies for the two lowest $^2A'$ states for about 100 nuclear arrangements; however, no *ab initio* calculations of the nonadiabatic coupling terms have been reported, and the potential energy calculations including electron correlation (by the coupled-electron-pairs approximation -- CEPA) have been performed only for C_{2v} geometries.^{6,10}

Recently the diatomics-in-molecules (DIM) method^{18,19} has been applied to calculate the three lowest-energy $^2A'$ potential energy surfaces of NaH_2 .^{13,17} The two lowest-energy surfaces agree well with the available *ab initio* calculations of Botschwina and Meyer.^{6,10} A major advantage of using the DIM formalism is that it provides a global representation of the potential energy surfaces and the couplings between them.

There has been a large amount of work on developing methods for the quantum mechanical treatment of electronic transitions in atom-molecule collisions.²⁰⁻³² Zimmermann and George²¹ compared the use of diabatic and adiabatic representations for atom-vibrator collisions. In the adiabatic representation coupling between different electronic states introduces first-derivative terms in the coupled-channel equations. Zimmermann and George solved the adiabatic coupled-channel equations by transforming the N second-order differential equations into a set of $2N$ first-order differential equations. Another alternative, employed by Baer and coworkers,²³⁻²⁵ is to obtain coupled-channel equations that could be solved using the efficient computational algorithms developed for second-order differential equations without first-derivative terms. In Baer's approach a transformation is made from the adiabatic representation to a diabatic representation in which all coupling arises through off-diagonal elements of the potential matrix. In general such a transformation does not exist,³³ but it does exist if the nonadiabatic couplings are approximated by

the Preston-Tully^{19,34} approximation, as used in the DIM method. Baer's approach has been applied to collinear atom-diatomic collisions, and more recently Rebentrost and Lester^{26,27} have used a similar diabatic transformation to treat the nonreactive F + H₂ problem in three dimensions.

The previous quantum mechanical calculation on Na + H₂ by McGuire and Bellum⁵ used the two lowest-energy adiabatic potential energy surfaces as an approximation to the diagonal diabatic potential energy surfaces. The off-diagonal terms of the diabatic potential were modelled as gaussian terms centered on the location of the minimum of the energy difference of the adiabatic surfaces. Cross sections were calculated within the rotational infinite-order-sudden (IOS) approximation;^{35,36} however, the integral over the IOS angle was approximated using only the perpendicular-bisector approach of the Na to the H₂ molecule.

In the present calculation we describe a new method for calculating electronic transition cross sections using adiabatic potential energy surfaces and the nonadiabatic coupling terms as input. In this approach we use a mixed adiabatic-diabatic representation in which the motion in the diatomic internuclear distance is treated diabatically and the motion in the Na to center-of-mass of H₂ distance is treated adiabatically. We use the rotational IOS approximation to decouple the scattering dynamics in the orientation angle. The R matrix propagation method^{30-32,37-42} is used to solve the coupled equations describing the scattering process in the mixed representation for each value of the orientation angle, and the calculations are converged with respect to the numerical integral over the orientation angle.

In Subsection 2 we present the details of the new theoretical method, and in Subsection 3 we present details of the computational procedure. Subsection 4 contains results of the calculations, and Subsection 5 presents a discussion.

2. Theory

We consider the collision of an atom A with a diatomic molecule BC, where R is the distance from A to the center of mass of BC, r is the BC internuclear distance, and γ is the angle between the **R** and **r** vectors. Within the rotational IOS approximation the total Hamiltonian is given by³⁶

$$H_{\text{IOS}}^{j,l} = -\frac{\hbar^2}{2\mu R} \frac{\partial^2}{\partial R^2} R + \frac{\hbar^2 l(l+1)}{2\mu R^2} + H_{\text{int}}^j \quad (161)$$

where μ is the reduced mass for the R motion, l and j are particular values of the orbital and rotational quantum numbers, respectively, and the Hamiltonian for vibronic coordinates (**x** and **r** where **x** is the collection of electronic coordinates) H_{int}^j is given by

$$H_{\text{int}}^j = -\frac{\hbar^2}{2\mu_{\text{BC}}r} \frac{\partial^2}{\partial r^2} r + \frac{\hbar^2 j(j+1)}{2\mu_{\text{BC}}r^2} + H_{\text{el}} \quad (162)$$

Here μ_{BC} is the reduced mass for the r motion and H_{el} is the electronic Hamiltonian. The approximate Born-Oppenheimer electronically adiabatic eigenfunctions ϕ_n^{aA} for electronic state n satisfy the matrix eigenvalue equations

$$\left\langle \phi_{n'}^{\text{aA}}(\tau) \left| H_{\text{el}} \right| \phi_n^{\text{aA}}(\tau) \right\rangle_x = V_n^{\text{aA}}(r, R, \gamma) \delta_{n'n}, \quad n, n' = 1, \dots, N_{\text{max}} \quad (163)$$

and

$$\left\langle \phi_{n'}^{\text{aA}}(\tau) \left| \phi_n^{\text{aA}}(\tau) \right\rangle_x = \delta_{n'n}, \quad n, n' = 1, \dots, N_{\text{max}} \quad (164)$$

where $V_n^{\text{aA}}(r, R, \gamma)$ is the electronically adiabatic potential energy surface for electronic state n , (τ) denotes dependence on all coordinates (x, r, R, γ) , and we use a bra-ket notation to denote integrals - the subscript denotes the variables integrated out. Within the rotational IOS formalism the orbital angular momenta is conserved and the rotational angular momentum is not coupled with the electronic angular momenta.

A mixed basis for the electronic degrees of freedom is obtained as follows. For fixed R and γ a transformation is made to a representation $\{\phi_n^{\text{dA}}\}$ which is P-diabatic^{31,43} with respect to the r motion but adiabatic with respect to R :

$$\phi_{n'}^{\text{dA}}(\tau) = \sum_{n=1}^{n_{\text{max}}} u_{nn'}(r, R, \gamma) \phi_n^{\text{aA}}(\tau) \quad n' = 1, \dots, n_{\text{max}} \quad (165)$$

where $n_{\text{max}} \leq N_{\text{max}}$. Note that unless n_{max} is infinite, $\phi_{n'}^{\text{dA}}$ is actually a function of r as well as x , R , and γ . This dependence is, however, effectively removed in the n_{max} -fold subspace of retained adiabatic functions by the condition of P-diabaticity, namely,

$$\left\langle \phi_{n'}^{\text{dA}}(\tau) \left| \frac{\partial}{\partial r} \right| \phi_n^{\text{dA}}(\tau) \right\rangle_x = 0 \quad n, n' = 1, \dots, n_{\text{max}} \quad (166)$$

The transformation from the adiabatic to the mixed basis is given by

$$\frac{\partial}{\partial r} u_{n'n}(r, R, \gamma) = - \sum_{n''=1}^{n_{\text{max}}} f_{n'n''}^{\text{aA}}(r, R, \gamma) u_{n''n}(r, R, \gamma) \quad (167)$$

where

$$f_{n'n}^{aA}(r, R, \gamma) = \left\langle \phi_{n'}^{aA}(\tau) \left| \frac{\partial}{\partial r} \right| \phi_n^{aA}(\tau) \right\rangle_x \quad (168)$$

We require u to be an orthogonal matrix so that

$$\langle \phi_{n'}^{dA}(\tau) | \phi_n^{dA}(\tau) \rangle_x = \delta_{n'n} \quad (169)$$

Note that Eq. (167) is analogous to a well known equation used to define P-diabatic bases in atom-atom collisions.^{31-33,44}

The internal wavefunctions $\psi_m^j(\tau)$ are expanded in the mixed basis

$$\psi_m^j(\tau) = r^{-1} \sum_{n=1}^{n_{\max}} \sum_{v_n=0}^{M_n} \phi_n^{dA}(\tau) \rho_{nv_n}^j(r) C_{nv_n, m}^j(R, \gamma) \quad m=1, \dots, M \quad (170)$$

where the total number of channel is given by

$$M = \sum_{n=1}^{n_{\max}} (M_n + 1) \quad (171)$$

and $\rho_{nv}^j(r)$ is a vibrational basis function for electronic state n satisfying

$$\langle r^{-1} \rho_{n'v'}^j(r) | r^{-1} \rho_{nv}^j(r) \rangle_x = S_{n'v'nv} \quad (172)$$

where $S_{n'v'nv} = \delta_{v'v}$ for $n'=n$. Note that integration over r includes an r^2 volume factor. The internal eigenvectors are defined by

$$\langle \psi_m^j(\tau) | H_{\text{int}}^j | \psi_{m'}^j(\tau) \rangle_{x, r} = E_m^j(R, \gamma) \delta_{m'm} \quad m, m'=1, \dots, M \quad (173)$$

and

$$\langle \psi_m^j(\tau) | \psi_{m'}^j(\tau) \rangle_{x, r} = \delta_{m'm} \quad m, m'=1, \dots, M \quad (174)$$

which yields the eigenvalue equation

$$H^j(R, \gamma) C^j(R, \gamma) = C^j(R, \gamma) E^j(R, \gamma) \quad (175)$$

where E^j is a diagonal matrix, the matrix elements of the internal Hamiltonian are given by

$$H_{n'v_n, nv_n}^j(R, \gamma) = \int_0^\infty dr \rho_{n'v_n}^j(r) \left\{ \left[-\frac{\hbar^2}{2\mu_{BC}} \frac{\partial^2}{\partial r^2} + \frac{\hbar^2 j(j+1)}{2\mu_{BC} r^2} \right] \delta_{n'n} + V_{n'n}^{dA}(r, R, \gamma) \right\} \rho_{nv_n}^j(r) \quad (176)$$

and the potential matrix V_{nn}^{dA} is given by

$$V^{dA}(r, R, \gamma) = u^T(r, R, \gamma) V^{aA}(r, R, \gamma) u(r, R, \gamma) \quad (177)$$

The total scattering wavefunction for an initial state m_0 , a fixed value of the conserved quantity l , and a typical or average value j of the rotational quantum number is expanded in eigenvectors of the internal Hamiltonian

$$\Psi_{m_0}^{jl}(\tau) = R^{-1} \sum_m^M \psi_m^j(\tau) \chi_{mm_0}^{jl}(R, \gamma) \quad (178)$$

The rotational-IOS close-coupling equations for a fixed γ are given by

$$\int dx \int_0^\infty dr r^2 \psi_{m'}^j(\tau)^* \left[H_{IOS}^j - E \right] \Psi_{m_0}^{jl}(\tau) = 0 \quad (179)$$

Substituting Eqs (161) and (178) into Eq. (179) gives

$$\sum_{m=1}^M \left\{ \left[-\frac{\hbar^2}{2\mu} \frac{\partial^2}{\partial R^2} + \frac{\hbar^2 l(l+1)}{2\mu R^2} + E_{m'}^j(R, \gamma) \right] \delta_{m'm} - \frac{\hbar^2}{\mu} F_{m'm}^j(R, \gamma) \frac{\partial}{\partial r} - \frac{\hbar^2}{2\mu} G_{m'm}^j(R, \gamma) \right\} \chi_{mm_0}^{jl}(R, \gamma) = 0 \quad (180)$$

The coupling terms are defined by

$$F_{m'm}^j(R, \gamma) = \left\langle \psi_{m'}^j(\tau) \left| \frac{\partial}{\partial R} \right| \psi_m^j(\tau) \right\rangle_{x, r} \quad (181)$$

$$G_{m'm}^j(R, \gamma) = \left\langle \psi_{m'}^j(\tau) \left| \frac{\partial^2}{\partial R^2} \right| \psi_m^j(\tau) \right\rangle_{x, r} \quad (182)$$

These expression can be evaluated by using Eq. (170); however, this requires calculations of derivatives of $C_{mv}^j(R, \gamma)$ and matrix elements of the derivative operators in the ϕ^{dA} basis.

The radial wavefunctions $\chi_{mm_0}^{jl}(R, \gamma)$ are subject to the standard boundary conditions³⁶

$$\chi_{mm_0}^{jl}(R, \gamma) \xrightarrow{R \rightarrow 0} 0 \quad (183)$$

and

$$\begin{aligned} \chi_{mm_0}^{jl}(R, \gamma) \xrightarrow{R \rightarrow \infty} k_{jm}^{-1/2} \left\{ \delta_{mm_0} \exp[-i(k_{jm}R - l\pi/2)] \right. \\ \left. - S_{mm_0}^{jl}(\gamma) \exp[i(k_{jm}R - l\pi/2)] \right\} \end{aligned} \quad (184)$$

where the asymptotic wavenumber is defined by

$$k_{jm}^2 = \lim_{R \rightarrow \infty} \frac{2\mu}{\hbar^2} [E - E_m^j(R, \gamma)] \quad (185)$$

Opacity functions can be defined for each value of j and l

$$P_{m_0 \rightarrow m'}^{jl} = \frac{1}{2} \int_0^\pi d\gamma \sin \gamma \left| \delta_{m'm_0} - S_{m'm_0}^{jl}(\gamma) \right|^2 \quad (186)$$

and the total cross section for transition from initial state j_0, m_0 to final level m' summed over all final rotational quantum numbers j' is

$$\sigma_{m_0 \rightarrow m'}^j = \frac{\pi}{k_{jm_0}^2} \sum_l (2l+1) P_{m_0 \rightarrow m'}^{jl} \quad (187)$$

Notice that this result is independent of j_0 in the rotational IOS, but it does depend slightly on j , which is a parameter of the approximation scheme.

3. Computational details

A. Vibrational basis functions

For the Na + H₂ system, the electronic states considered here should correlate with H₂ in its ground electronic state when the Na to H₂ distance is large. However, within the DIM model used here the second electronic state corresponds to Na (3p²P) + H₂(¹Σ_g) for r less than about 3.1 a_0 , but for r greater than this value it crosses with Na(3s²S) + H₂(³Σ_u). At the crossing point the energy is about 5eV above the zero of energy at Na(3s²S) + H₂(¹Σ_g) with $r = r_{eq}$, but the potential then drops to about 4.74 eV as r increases. Therefore, the vibrational states are computed individually for the two electronic states. Within the DIM formalism, all electronic coupling vanishes for Na infinitely separated from H₂ and the asymptotic diatomic potential are simply the adiabatic potentials for the vibrating, rotating diatomic molecule. The vibrational basis function are defined by

$$\left[-\frac{\hbar^2}{2\mu_{BC}} \frac{\partial^2}{\partial r^2} + \frac{\hbar^2 j(j+1)}{2\mu_{BC} r^2} + V_{HH,n}(r) \right] \rho_{nv}^j(r) = \epsilon_{nv}^j \rho_{nv}^j(r) \quad (188)$$

where $V_{HH,n}(r)$ is the asymptotic H₂ vibrational potential for the electronic state n . The energy levels ϵ_{nv}^j are obtained numerically by the Cooley-Cashion method.⁴⁵ All integrals over r are done by Gauss-Hermite quadrature using 50-100 points. The quadrature points are defined by $r_i = r_{eq} + x_i/\alpha$ where x_i are the Gauss-Hermite quadrature nodes, and α is the range parameter for the ground state H₂ vibrational potential taken to be 4.57082 a_0^{-1} . The numerical values of the vibrational basis functions are stored on the grid of quadrature points $\{r_k\}_{k=1}^K$ to be used in subsequent numerical integrals, e.g. Eq. (176).

B. P-diabatic transformation

Equation (167) for the transformation matrix u is solved by the Magnus method.³² The transformation matrix is only needed at the Gaussian quadrature points and the Magnus approximation yields

$$u(r_{k+1}, R, \gamma) = \exp \left\{ - (r_{k+1} - r_k) f^{aA} \left[\frac{1}{2}(r_{k+1} + r_k), R, \gamma \right] \right\} u(r_k, R, \gamma) \quad (189)$$

The choice of u at the first grid point is arbitrary, and if no further approximations are made the final results of the calculations are independent of this choice. For convenience we set $u_{nn}(r_0, R, \gamma) = \delta_{nn}$ for all R, γ and find u for $r < r_0$ and $r > r_0$ by inward and outward application of Eq.

(185), respectively. r_0 is chosen to be a grid point near r_e . The exponential of a matrix is evaluated by the method of ref. 46.

C. R-matrix propagation

Equation (180) is not solved directly for the radial wavefunctions; instead we use the R-matrix propagation method^{30-32,37-42} to obtain a global R matrix for relating the ratio of the radial wavefunction and its derivative at large R values to the ratio at small R values. The S matrix is then obtained from the R matrix. The method for treating electronic transitions in systems with one internuclear degree of freedom by the R-matrix propagation method when the input is in an adiabatic representation has been presented previously.^{31,32} This method is extended here to treat the case of several nuclear degrees of freedom where the representation is adiabatic in the propagation coordinate and diabatic in other coordinates, as in Subsection 2. In the R-matrix propagation method we use internal basis functions $\psi_m^j(\mathbf{x}, r, R^i, \gamma)$ that are independent of the radial coordinate R within each sector (i) centered at R^i . Propagation of the global R matrix across a sector is accomplished in terms of the eigenvalues $E_m^j(R^i, \gamma)$ of the internal Hamiltonian. The coupling between the internal states arises at the sector boundaries in transforming from the internal basis functions in one sector to those in the adjacent sector. It is the definition of this sector transformation matrix which is the essential aspect of the scheme.

We will consider two ways to calculate the sector transformation matrix with no further approximations, i.e., so that the results are independent of the initial condition used in integrating Eq. (189) and are equivalent to what would be obtained by numerical integration of the Eqs. (180). Then we will consider a fixed-diabatic-states approximation in which the P-diabaticity in the r coordinate of the basis functions of Subsection 2 is interpreted as if

$$\frac{\partial}{\partial r} \phi_n^{dA}(\tau) = 0 \quad (190)$$

Assuming Eq. (190) is mathematically equivalent to assuming that the electronic states included in the expansion are a complete set since Eq. (166) shows that the derivative of Eq. (190) is orthogonal to the other electronic functions included in the electronic basis. The fixed-diabatic-states approximation greatly simplifies the numerical work; we shall test its accuracy by comparing the final cross sections to those computed without this approximation.

First consider the accurate calculation of the sector transformation matrix. The transformation matrix from sector i to sector i+1 is defined by

$$T_{m'm}^{i,i+1}(\gamma) = \langle \psi_m^j(\mathbf{x}, r, R^i, \gamma) | \psi_m^j(\mathbf{x}, r, R^{i+1}, \gamma) \rangle_{\mathbf{x}, r} \quad (191)$$

This can be approximated by^{31,32}

$$T_{m'm}^{i,i+1}(\gamma) \equiv \exp \left\{ (R^{i+1} - R^i) F_{m'm}^j \left[\frac{1}{2} (R^i + R^{i+1}), \gamma \right] \right\} \quad (192)$$

where $F_{m'm}^j(R, \gamma)$ is defined in Eq. (181). This expression requires the evaluation of numerical first derivatives and to avoid having to compute the numerical derivatives of $u(r, R, \gamma)$ and $C(R, \gamma)$ we use an alternative method to obtain the sector transformation matrix. Substituting Eq. (170) into Eq. (192) yields

$$T_{m'm}^{i,i+1}(\gamma) = \sum_{n'=1}^{n_{\max}} \sum_{v_{n'}=0}^{M_{n'}} \sum_{n=1}^{n_{\max}} \sum_{v_n=0}^{M_n} C_{n'v_{n'},m'}^j(R^i, \gamma) O_{n'v_{n'},nv_n}^{i,i+1}(\gamma) C_{nv_n,m}^j(R^i, \gamma) \quad (193)$$

where the overlap matrix is defined by

$$O_{n'v_{n'},nv_n}^{i,i+1}(\gamma) = \int_0^\infty dr \rho_{v_{n'}}^j(r) \langle \phi_{n'}^{dA}(x, r, R^i, \gamma) | \phi_n^{dA}(x, r, R^{i+1}, \gamma) \rangle_x \rho_{v_n}^j(r) \quad (194)$$

Using Eq. (165) gives our final expression for the overlap matrix

$$O_{n'v_{n'},nv_n}^{i,i+1}(\gamma) = \int_0^\infty dr \rho_{v_{n'}}^j(r) \sum_{n''n'''}^{n_{\max}} u_{n''n'''}(r, R^i, \gamma) t_{n''n'''}^{i,i+1}(r, \gamma) u_{n''n'''}(r, R^{i+1}, \gamma) \rho_{v_n}^j(r) \quad (195)$$

where

$$t_{n''n'''}^{i,i+1}(r, \gamma) = \langle \phi_{n''}^{aA}(x, r, R^i, \gamma) | \phi_{n'''}^{aA}(x, r, R^{i+1}, \gamma) \rangle_x \quad (196)$$

$$\equiv \exp \left\{ (R^{i+1} - R^i) F_{n''n'''}^{aA} \left[r, \frac{1}{2} (R^i + R^{i+1}), \gamma \right] \right\} \quad (197)$$

and

$$F_{n''n'''}^{aA}(R, \gamma) = \left\langle \phi_{n''}^{aA}(\tau) \left| \frac{\partial}{\partial R} \right| \phi_{n'''}^{aA}(\tau) \right\rangle_x \quad (198)$$

It is important to note that the overlap matrix in Eq. (195) is not necessarily orthogonal. Orthogonal overlap matrices are guaranteed only when the primitive basis functions (ψ^j in this case)

do not change from sector to sector. However, because of the diabatic transformation in each sector the overlap matrix is orthogonal only under special conditions. Consider the matrix product

$$\begin{aligned}
 & \sum_{n''=1}^{n_{\max}} \sum_{v_{n''}=0}^{N_{n''}} O_{n''v_{n''}n''v_{n'}}^{i,i+1}(\gamma) O_{n''v_{n''}n''v_n}^{i,i+1}(\gamma) \\
 &= \sum_{n''=1}^{n_{\max}} \int_0^\infty dr \int_0^\infty dr' \rho_{v_{n'}}^j(r) \rho_{v_n}^j(r') \sum_{v_{n''}=0}^{M_{n''}} \rho_{v_{n''}}^j(r) \rho_{v_{n''}}^j(r') \\
 & \langle \phi_{n'}^{dA}(i+1) | \phi_{n''}^{dA}(i) \rangle_x \langle \phi_{n''}^{dA}(i) | \phi_n^{dA}(i+1) \rangle_x \quad (199)
 \end{aligned}$$

where $\phi_n^{dA}(i)$ denotes $\phi_n^{dA}(\mathbf{x}, r, R^i, \gamma)$. The overlap matrix is orthogonal only if the matrix defined in Eq. (199) is the unit matrix. This can happen only if the vibrational states within each electronic manifold are a complete set, i.e.,

$$\sum_{v_{n''}=0}^{N_{n''}} \rho_{v_{n''}}^j(r) \rho_{v_{n''}}^j(r') = \delta(r - r') \quad (200)$$

and the electronic states are also a complete set, i.e.,

$$\sum_{n=1}^{n_{\max}} | \phi_n^{dA}(i) \rangle \langle \phi_n^{dA}(i) | = 1 \quad (201)$$

For the calculations performed here these conditions are not generally valid, and we therefore use the correct equations for propagation of the sector R matrices.^{31,47}

If the fixed-diabatic-states approximation is employed, Eq. (190), the matrix elements $t_{n'n}^{i,i+1}(r, \gamma)$ become independent of r and can be evaluated at one arbitrary value of r . For the chose of $r=r_0$, the expression for the sector transformation matrix simplifies to

$$\begin{aligned}
 T_{m'm}^{i,i+1}(\gamma) &\approx \sum_{p',p}^M C_{p'm}^j(R^i, \gamma) \delta_{v(p')v(p)} \sum_{n''=1}^{n_{\max}} u_{n'n(p')} (r_0 R^i, \gamma) \\
 & t_{n'n''}^{i,i+1}(r_0, \gamma) u_{n''n(p)} (r_0 R^{i+1}, \gamma) C_{pm}^j(R^{i+1}, \gamma) \quad (202)
 \end{aligned}$$

$$= \sum_{p',p}^M C_{p'm}^j(R^i, \gamma) \delta_{v(p')v(p)} t_{n(p')n(p)}^{i,i+1}(r, \gamma) C_{pm}^j(R^{i+1}, \gamma) \quad (203)$$

4. Results

In Fig. 9, contours of the energy for the two lowest adiabatic potentials $V_n^{aA}(r, R, \gamma)$ are shown as a function of the H-H internuclear distance r and the distance R from the Na atom to the center of mass of H_2 , at three values of the angle γ . In Fig. 10, the two lowest adiabatic potential energies along cuts in r are shown at three different values of R and for the same three values of γ . Evidence of an avoided crossing between the second state and third state are evident for the potentials at $R=5 a_0$. The nonadiabatic coupling element in r between these two lowest states $f_{12}^{aA}(r, R, \gamma)$ is shown in Fig. 11 for the three values of R at the three values of γ . The coupling exhibits one major peak which shifts to higher values of r for increasing values of R . The mixed adiabatic-diabatic potential matrix $V_{nn}^{dA}(r, R, \gamma)$ obtained from the P-diabatic transformation is displayed in Fig. 12. The diagonal elements are close to the adiabatic curves shown in Fig. 20 especially near the minima in the potentials. The two diagonal curves tend to cross near values of r which displayed maximum in the nonadiabatic coupling. Figure 13 shows the eigenvalues of the internal Hamiltonian $E_m^j(R, \gamma)$ as a function of the Na to H_2 distance for a fixed value of γ . These curves exhibit multiple avoided crossing indicative of a system with strong coupling. Figure 14 shows the first preliminary results for scattering of $Na(3p^2P)$ from H_2 in its ground vibrational state at a total energy of 3 eV. Probabilities are shown for only the 4 final states with the largest probabilities. The elastic channel is dominant, but the $v=2$ state is shown to be much larger than all other states except for $v=0$ and 4 at angles near 30° . This is qualitatively in agreement with the experimental results of Hertel et. al.^{8,9}

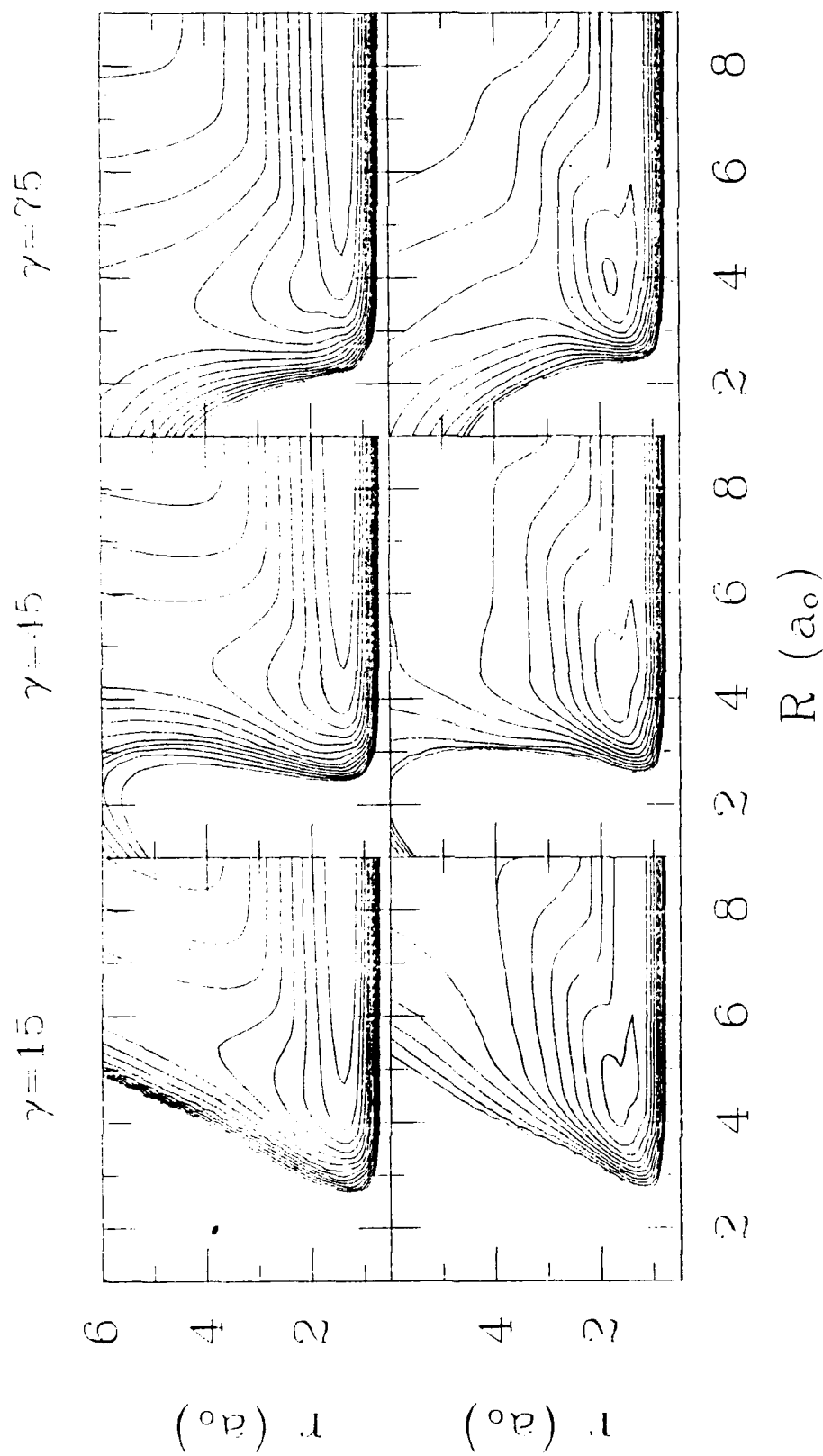


Figure 9. Potential energy contours for the two lowest adiabatic potential energy surface $V_n^{aA}(r, R, \gamma)$ of NaH_2 as functions of the H_2 distance r and Na-to- H_2 distance R , for fixed angle γ between the \mathbf{r} and \mathbf{R} vectors. The left, center, and right columns of plots are for $\gamma = 15, 45$, and 75 degrees, respectively (90 degrees corresponds to perpendicular approach of Na to H_2). The top row displays the lowest adiabatic potential. The contours are evenly spaced at 0.5 eV; the zero of energy is $\text{Na}(3^2\text{S})$ infinitely separated from H_2 at its equilibrium geometry.

Figure 10. Adiabatic potential energy curves $V_n^{aA}(r, R, \gamma)$ for the two lowest energy states of NaH_2 . The curves are plotted as a function of the H_2 distance r for fixed Na-to- H_2 distance R and for fixed angle γ between the r and R vectors. The top, middle, and bottom rows of plots are for $R = 3, 4$, and $5 a_0$, respectively. The left, center, and right columns of plots are for $\gamma = 15, 45$, and 75 degrees, respectively (90 degrees corresponds to perpendicular approach of Na to H_2).

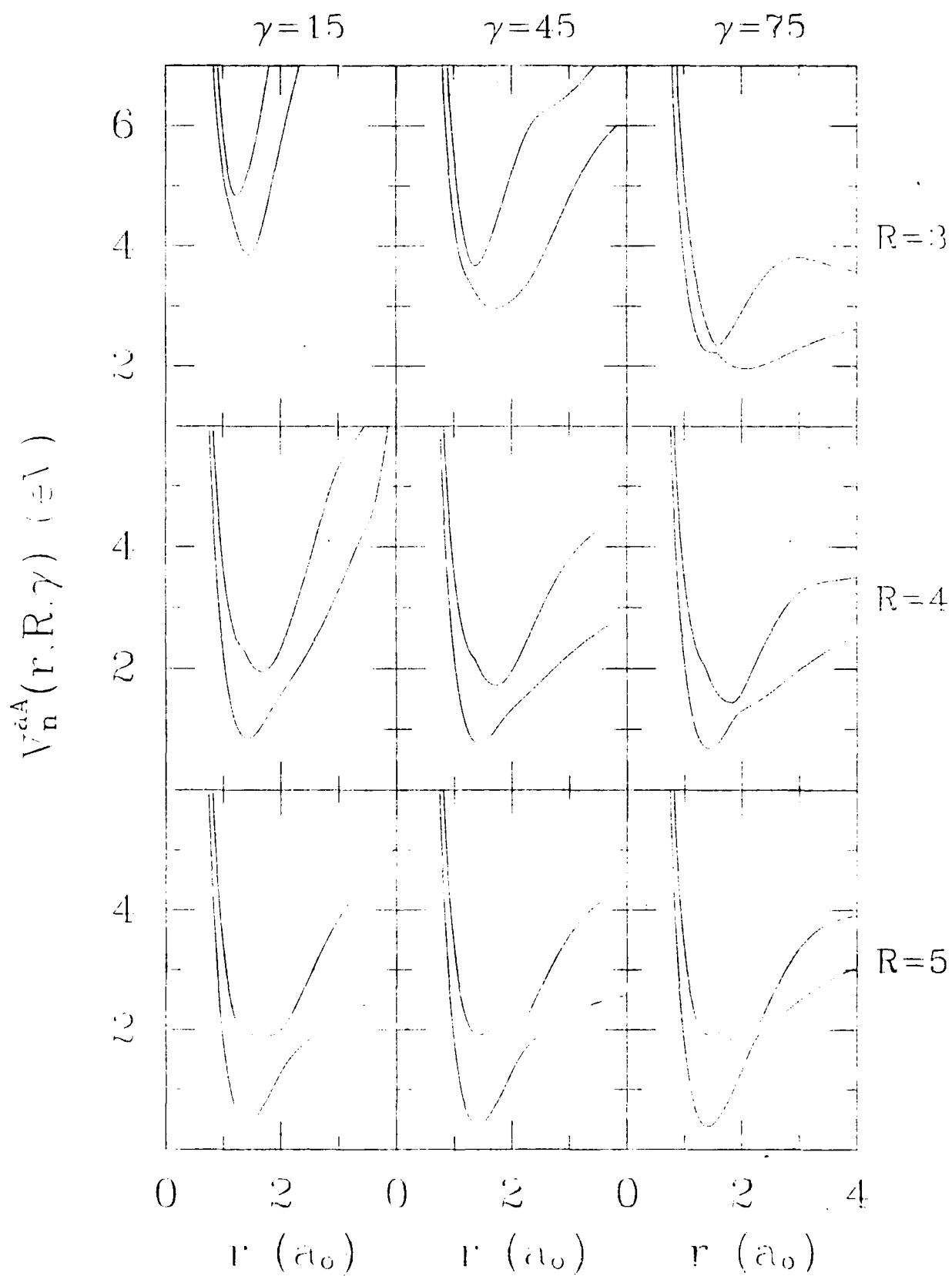


Figure 11. Same as figure 10, expect for the nonadiabatic coupling terms $f_{12}^{aA}(r,R,\gamma)$ between the two lowest energy states of NaH_2 .

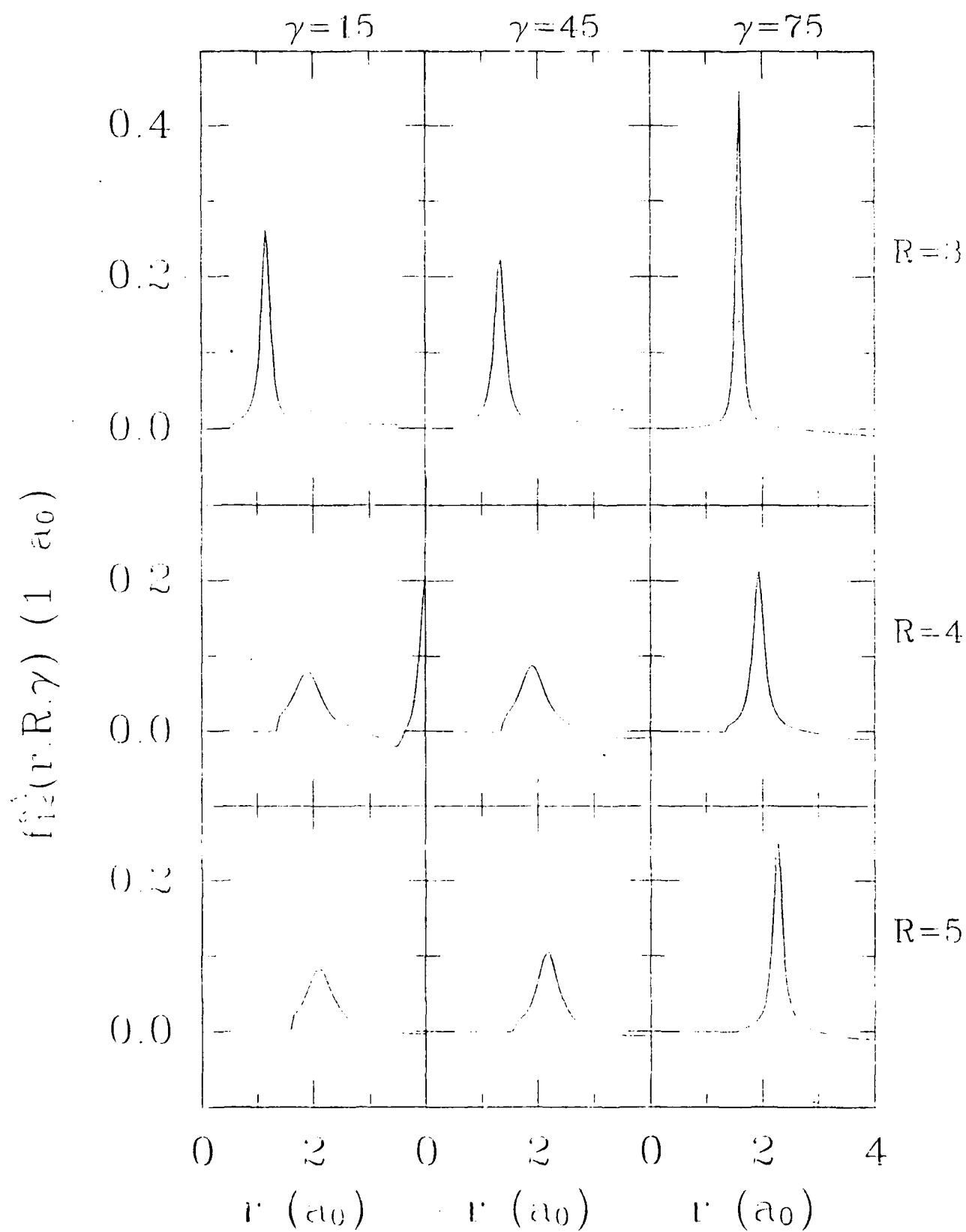


Figure 12. Same as figure 12, expect for the mixed adiabatic-diabatic potential curves $V_{nn}^{dA}(r,R,\gamma)$ obtained from the two lowest adiabatic states of NaH_2 and their nonadiabatic coupling elements. The transformation matrix from the adiabatic to diabatic representation is arbitrarily chosen to be the unit matrix at $r=1.4 a_0$.

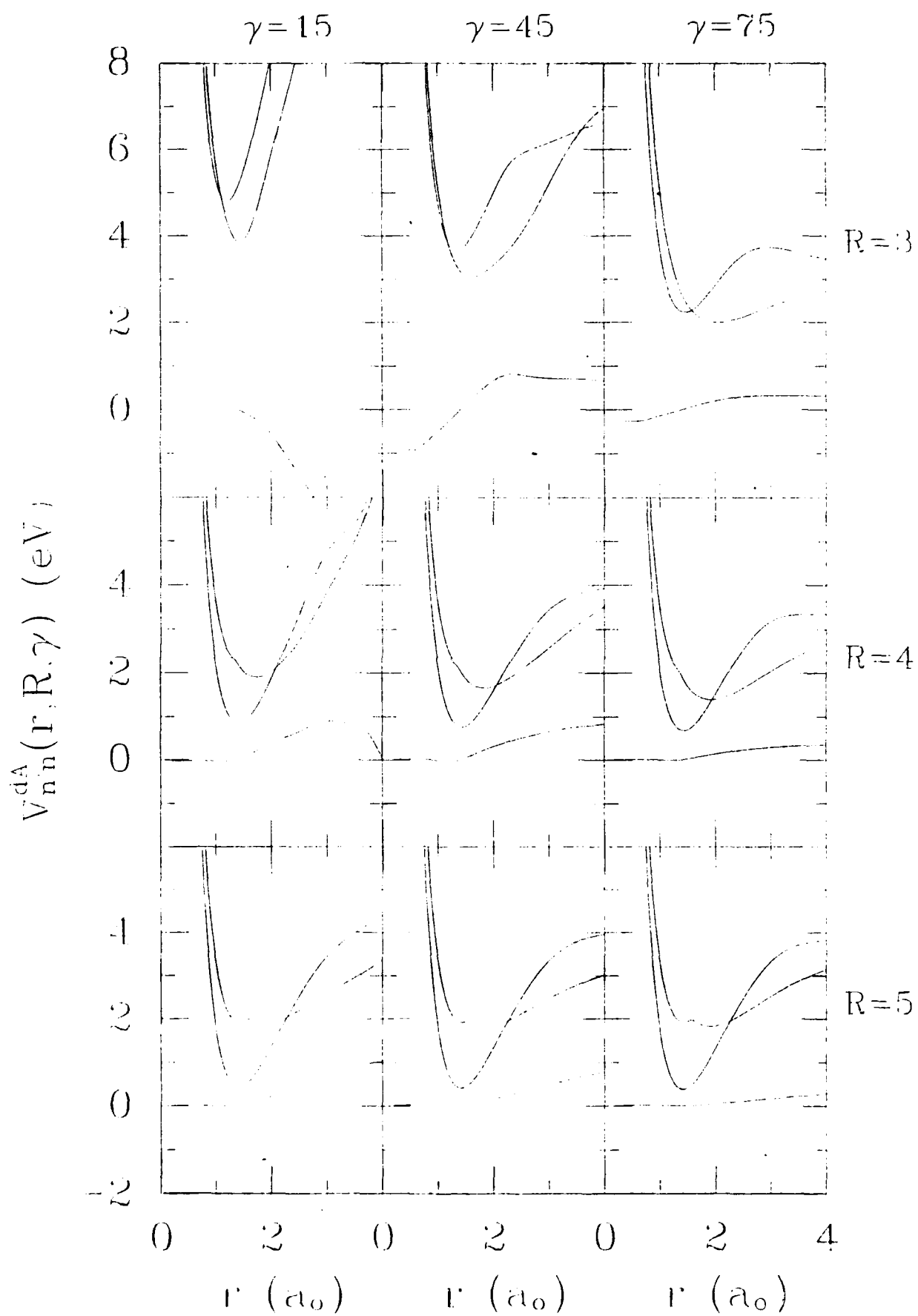


Figure 13. Eigenvalues $E_m^j(R, \gamma)$ of the internal Hamiltonian in the mixed adiabatic-diabatic electronic representation for $\gamma = 2.7^\circ$.

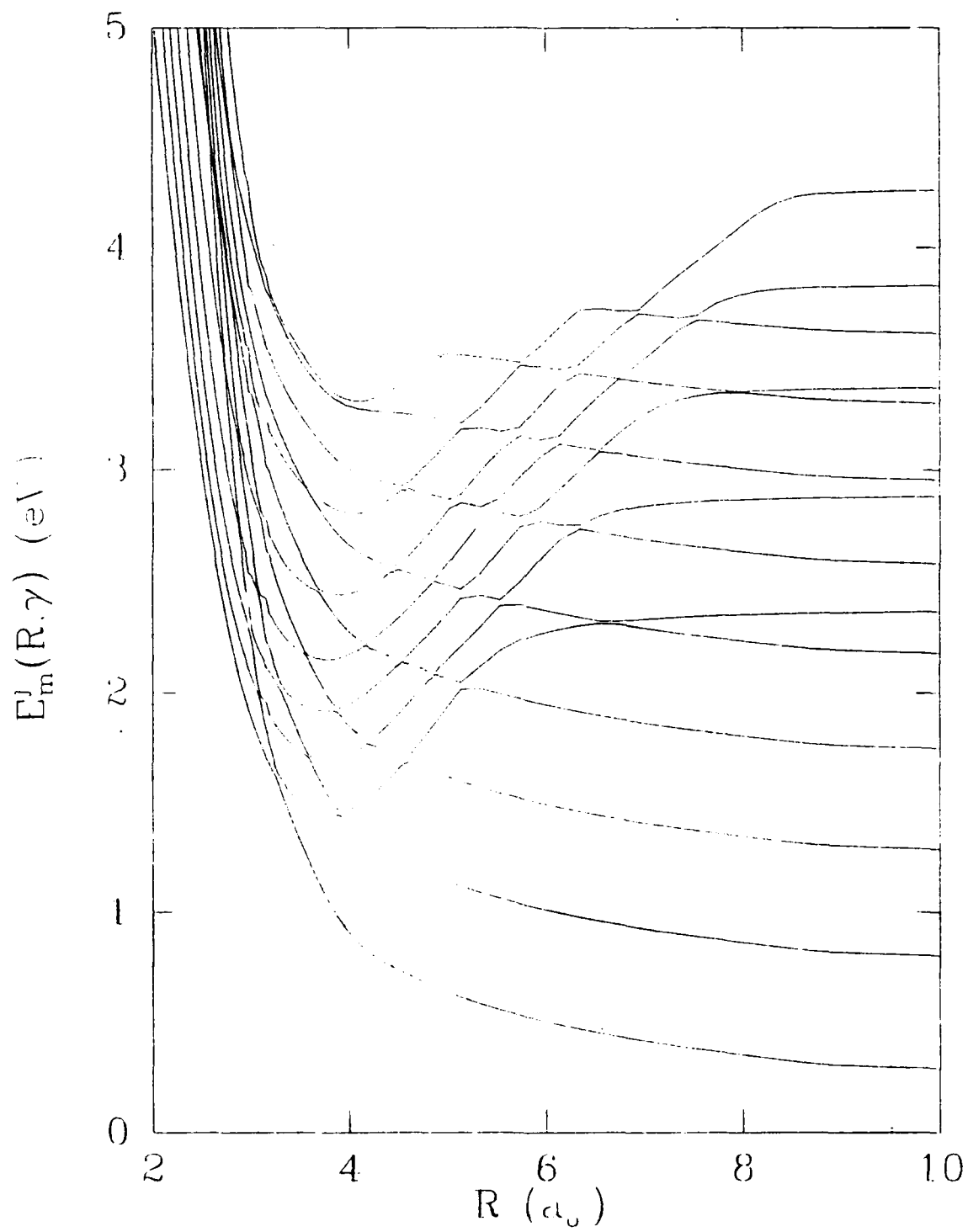
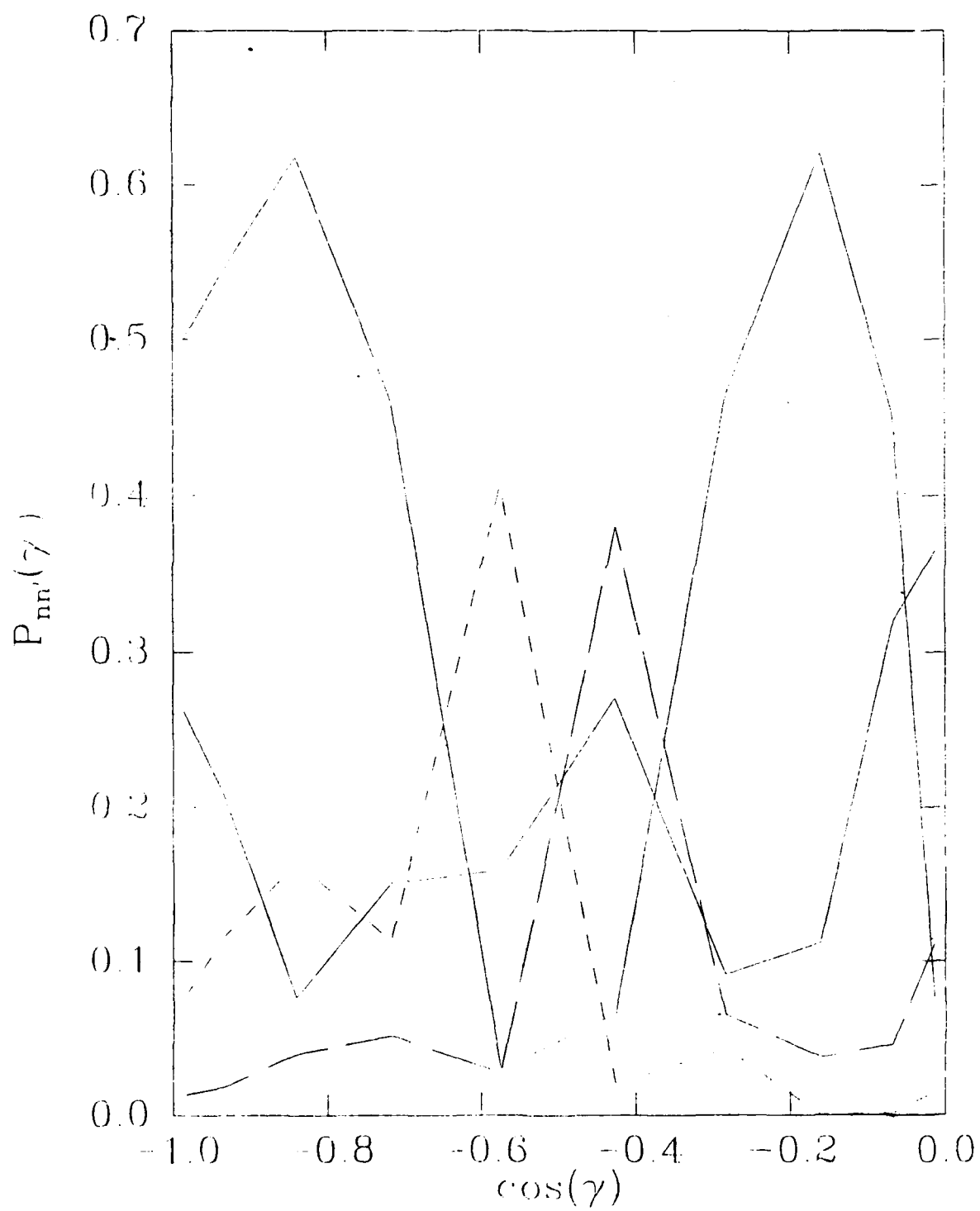


Figure 14. Transition probabilities $S_{mm}^{jl}(\gamma)^2$ as a function of the IOS angle γ for collisions of Na($3p^2P$) with H_2 in its ground vibrational state at a total energy of 3 eV. The solid curve with the largest magnitude is for the elastic channel -- production of Na($3p^2P$) and H_2 in its ground vibrational state. The long dashed, the other solid, the short dashed curve are for quenching of Na to the $3s^2S$ state to form H_2 $v=0$, 2, and 4, respectively.



REFERENCES

1. S. Lemont and G. W. Flynn, *Annu. Rev. Phys. Chem.* **28**, 261 (1977).
2. J. A. Silver, N. C. Blais, and G. H. Kwei, *J. Chem. Phys.* **71**, 3412 (1979).
3. E. A. Gislason, A. W. Kleyn, and J. Los, *Chem. Phys.* **59**, 91 (1981).
4. A. W. Kleyn, J. Los, and E. A. Gislason, *Phys. Reports* **90**, 1 (1982).
5. P. McGuire and J. C. Bellum, *J. Chem. Phys.* **71**, 1975 (1979).
6. P. Botschwina, Ph.D. thesis, University of Kaiserslautern, 1980 (unpublished).
7. P. Habitz, *Chem. Phys.* **54**, 131 (1980).
8. I. V. Hertel, *Advan. Chem. Phys.* **45**, 341 (1981).
9. I. V. Hertel, *Advan. Chem. Phys.* **46**, 472 (1982).
10. P. Botschwina, W. Meyer, I. V. Hertel, and W. Reiland, *J. Chem. Phys.* **75**, 5438 (1981).
11. W. Reiland, Ph.D. thesis, Free University of Berlin, 1982 (unpublished); W. Reiland, U. Tittes, I. V. Hertel, *Phys. Rev. Lett.* **48**, 1389 (1982).
12. P. Archirel and P. Habitz, *Chem. Phys.* (1982).
13. D. G. Truhlar, J. W. Duff, N. C. Blais, J. C. Tully, and B. C. Garrett, *J. Chem. Phys.*, **77**, 764 (1982).
14. W. H. Breckenridge and H. Umemoto, *Advan. Chem. Phys.* **46**, 325 (1982).
15. J. L. Magee and T. Ri, *J. Chem. Phys.* **9**, 639 (1941)
16. K. J. Laidler, *J. Chem. Phys.* **10**, 34 (1942).
17. N. C. Blais, D. G. Truhlar, and B. C. Garrett, *J. Chem. Phys.* **78**, 2956 (1983).
18. J. C. Tully, *J. Chem. Phys.* **58**, 1396 (1973).
19. J. C. Tully, *J. Chem. Phys.* **59**, 5122 (1973).

20. B. R. Johnson and R. D. Levine, Chem. Phys. Lett. **13**, 168 (1972).
21. I. H. Zimmermann and T. F. George, Chem. Phys. **7**, 323 (1975); J. Chem. Phys. **63**, 2109 (1975).
22. P. L. DeVries and T. F. George, J. Chem. Phys. **67**, 1293 (1977).
23. M. Baer, Chem. Phys. Lett. **35**, 112 (1975); Chem. Phys. **15**, 49 (1976); Mol. Phys. **35**, 1637 (1978), **40**, 1011 (1980).
24. Z. H. Top and M. Baer, Chem. Phys. **25**, 1 (1977); J. Chem. Phys. **66**, 1363 (1977).
25. M. Baer and J. A. Beswick, Chem. Phys. Lett. **51**, 360 (1977); Phys. Rev. A **19**, 1559 (1979).
26. F. Rebentrost and W. A. Lester, Jr., J. Chem. Phys. **63**, 3737 (1975); **64**, 3879, 4223 (1976); **67**, 3367 (1977).
27. F. Rebentrost, Theor. Chem. Adv. Perspectives **6B**,1 (1981).
28. D. L. Miller and R. E. Wyatt, J. Chem. Phys. **67**, 1302 (1977).
29. V. K. Babamov, J. Chem. Phys. **69**, 3414 (1978).
30. E. B. Stechel, T. G. Schmalz, and J. C. Light, J. Chem. Phys. **74**, 412 (1981).
31. B. C. Garrett and D. G. Truhlar, Theor. Chem. Adv. Perspectives **6A**, 215 (1981).
32. B. C. Garrett, M. J. Redmon, D. G. Truhlar, and C. F. Melius, J. Chem. Phys. **74**, 412 (1981).
33. C. A. Mead and D. G. Truhlar, J. Chem. Phys. **77**, 6090 (1982).
34. R. K. Preston and J. C. Tully, J. Chem. Phys. **54**, 4297 (1971).
35. There are many references for the rotational IOS approximation, see, e.g., M. A. Brandt and D. G. Truhlar, Chem. Phys. Lett. **23**, 48 (1973); R. T Pack, J. Chem. Phys. **60**, 633 (1974); D. Secrest, J. Chem. Phys. **62**, 710 (1975); J. M. Bowman and S. C. Leasure, J. Chem. Phys. **66**, 288, 4724(E) (1977); R. Goldflam, S. Green, and D. J. Kouri, J. Chem. Phys. **67**, 4149 (1977); Ref. 36; V. Khare, D. J. Kouri, J. Jellinek, and M. Baer, in

Potential Energy Surfaces and Dynamics Calculations, edited by D. G. Truhlar (Plenum, New York, 1981), p. 475; J. Jellinek and M. Baer, *J. Chem. Phys.* **76**, 4883 (1982); and references therein.

36. G. A. Parker and R. T. Pack, *J. Chem. Phys.* **68**, 1585 (1978).
37. J. C. Light and R. B. Walker, *J. Chem. Phys.* **65**, 4272 (1976).
38. D. G. Truhlar and N. A. Mullaney, *J. Chem. Phys.* **68**, 1574 (1978).
39. N. A. Mullaney and D. G. Truhlar, *Chem. Phys. Lett.* **58**, 512 (1978); *Chem. Phys.* **39**, 91 (1979).
40. N. M. Harvey, Ph.D. Thesis, University of Minnesota, Minneapolis, MN, 1979 (unpublished).
41. D. G. Truhlar, N. M. Harvey, K. Onda, M. A. Brandt, in *Algorithms and Computer Codes for Atomic and Molecular Quantum Scattering Theory*, Vol. I, edited by L. D. Thomas (National Resource for Computation in Chemistry, Lawrence Berkeley Laboratory, Berkeley, CA, 1979), p. 220.
42. N. M. Harvey and D. G. Truhlar, *Chem. Phys. Lett.* **74**, 252 (1980).
43. J. B. Delos and W. R. Thorson, *J. Chem. Phys.* **70**, 1774 (1979).
44. T. G. Heil and A. Dalgarno, *J. Phys. B* **12**, L557 (1979).
45. J. W. Cooley, *Math. Computation* **15**, 363 (1961); J. K. Cashion, *J. Chem. Phys.* **39**, 1872 (1963).
46. E. Dalgaard and P. Jorgensen, *J. Chem. Phys.* **69**, 3833 (1978).
47. E. B. Stechel, T. G. Schmalz, and J. C. Light, *J. Chem. Phys.* **70**, 5640 (1979).

Condensed Phase Modelling and Computer Experiments

Introduction

Condensed phase modelling and simulations are essential to HEDM research. The condensed phase will be the relevant phase for storage and initial processing of HEDM's. Our focus is on treating those chemical processes involving energetic species that are local centers of energy storage in the medium (in contrast to an extended storage in an overall metastable solid matrix). The key role of condensed phase modelling and simulations in our research can be appreciated if the system is imagined to be divided into a few atoms constituting the energetic species and the rest of the bulk phase material. The few atoms constitute a primary region, while the bulk phase material constitutes a heat bath.

The present three year program employed a new capability involving semiclassical methods. The new method treated the fully correlated dynamics of the chemistry in the primary zone region. If this region is only subject to electronically adiabatic dynamics, and did not involve energy transfer between quantized nuclear (rovibrational, phonon) states, it could be readily treated by electronically adiabatic classical dynamics, that was well-established prior to our research program. When the key to energy leakage or transfer away from the primary zone lies in quantum mechanical effects, involving multidimensional quantized vibrations or possible electronic inelasticity, it is known that a simple classical description is not sufficient. The present new semiclassical methods could be employed to treat these many-atom energy transfer and dynamics problems since quantum mechanical dynamical techniques are not computationally feasible.

One role of our simulation work is to define parameters to describe the heatbath dynamics properly and efficiently via few-body heatbath models; the latter improve the efficiency of performing repeated dynamics calculations, once a heatbath is characterized. Another important role of simulations is to reveal the truth about what happens in a given model; since simulations are "computer experiments", they often reveal unanticipated phenomena. Our computer experiments have been restricted to the proposed classical Monte Carlo (MC) and Molecular Dynamics (MD) simulation methods from the outset since quantal bath effects constitute an extensive problem by themselves. Thus the studies presented in this report employ the systems helium and hydrogen at high pressures so that they are well described by classical simulations.

The following subsection presents results of our simulations on storing excited metastable helium atoms in high pressure (GPa) bulk helium liquid. This is followed by a subsection on heatbath modelling based on the methods employed in this research.

Monte Carlo Simulations of Helium Bubble States

1. Introduction

It is known from studies on excited helium species¹ produced by keV electron bombardment of liquid He that there are excited atomic and molecular species trapped in physical bubbles, the latter essentially involving a vacuum embedded in the liquid bulk. The nature of these bubble states have been discussed² and the species that exist within them have been identified by spectroscopic methods and subsequently subjected to simple model-based interpretations. The bubbles are stabilized by the repulsive interaction of the Rydberg-like excited electron with bath He atoms. They have radii in the range 5-20 Å depending on the excited species and the thermodynamic state. The mechanism that supports the excited species in a bubble is closely related to that for the case of electron-containing bubbles in liquid Helium. The repulsion of the solvating He atoms of the liquid by the excited electron of the atomic or molecular species is considerably less than that of a free electron since the nuclear or molecular core compensates by holding on to the excited electron. Thus the radii of the bubbles in the electron case are almost twice larger than the above. A related phenomenon of recent interest has been that of noble gas bubbles in metals³ where there have been a few atomistic simulations.⁴ Atomistic calculations of He* bubbles in liquid He, unlike the studies of noble-gas bubbles in metals, are quite limited.⁵

The previous structural analysis of the bubble⁵ has been at a thermodynamic state point where quantum mechanical effects are important. The calculations were carried out in the zero-temperature limit, from first principles, using a variational Jastrow wave function and the integral equations approach for fluid mixtures. It may be asked whether these quantal liquid effects are always necessary for the bubble formation. When the thermodynamic state is changed by raising the temperature or pressure or varying the density, regimes will appear where classical dynamics is appropriate and it may be anticipated from simple models² of the classical energetics for the bubble formation that a stable bubble will be formed even classically. If this is realistic, it means that a computer simulation methodology based on classical molecular dynamics and Monte Carlo techniques will provide the necessary structural and dynamical information for this classical regime.

The classical regime occurs at room temperature in a very high pressure range (GPa regime). In this regime we assess the influence of the liquid in affecting the metastability of the electronically excited He-species. Due to the large size of the bubble (of diameter 5-10 Å), the trapped excited species can undergo collisions reminiscent of gas-surface processes, with the inner surface of the bubble, that are then responsible for nonradiative quenching. Computer simulations such as the ones explored here can provide the data (frequency moments of the heatbath spectral density) necessary to parameterize a Generalized Langevin Equation (GLE) model⁶ of the

condensed phase dynamics influencing the metastable's quenching process. Our plan is to study the electronically inelastic dynamics of the trapped metastable species by the Self-Consistent Eikonal Method (SCEM)⁷ in a merged (SCEM+GLE) stochastic semiclassical framework⁸.

The computer simulations also help explore the possible phenomena that can occur. In the present system, solvent He atoms can cluster with the solute He* to form n-mers depending on pressure. We explore the n-values of the He_n clusters occurring in the bubble states under the simulation conditions and find the observed average <n> as the pressure is increased. At very low pressures such as the ones corresponding to the past experiments on these metastables, primarily dimers (n=2) have been reported. At the pressures studied here, we find <n> as high as 5-6 while the bubble state character of the (model) system is still in tact. The <n> value is also dependent on the electronic state (a or c) involved and thus could reveal the possible importance of any electronic nonadiabaticities of the solute-solvent interaction.

Subsection 2 describes the interaction model employed in our simulations, and Subsection 3 gives the simulation details of the investigation. The concluding Subsection 4 contains the main results and discussion.

2. Interaction Potentials

In order to characterize the He* bubble in liquid He for various pressures, one needs the energetics of cluster formation within the bubble in the form of an interaction potential function. Due to the unavailability of estimates of many-body interaction energies between electronically excited stable clusters of He atoms with solvent He atoms, the present model essentially employs a sum of the two-body potentials: it is based on using the diatomic sets a, X or c, X depending on the g/u state of He-He* potential energy; thus it effectively ignores certain many-body effects. It is hoped that the qualitative description of bubble states of high pressure liquid Helium should be reasonable with this model although the quantitative nature of the present results may be changed by such many-body energetics.

Our Monte Carlo (MC) simulations are based on the recently developed He₂* (a ³Σ_u⁺ and c ³Σ_g⁺) potentials⁹ in a system consisting of one excited He* (³S) atom situated in bulk liquid He environment, the atoms of the latter interacting with each other via the effective (labelled X-state here for convenience) Aziz potential.¹⁰

$$\varphi(r) = \varepsilon [b e^{-\alpha R} - \{ C_6 R^{-6} + C_8 R^{-8} + C_{10} R^{-10} \} f(R)] \quad (204)$$

$$f(R) = \begin{cases} \exp [-(d/R - 1)^2], & R < d \\ 1, & R > d \end{cases} \quad (205)$$

where $R = r/r_m$, $r_m = 2.9673 \text{ \AA}$, $b = 544850.4$, $\alpha = 13.353384$, $C_6 = 1.3732412$, $C_8 = 0.4253785$, $C_{10} = 0.1781$, $d = 1.241314$, $\epsilon/k_B = 10.8 \text{ K}$, and k_B is the Boltzmann constant.

The above potential parameters were obtained¹⁰ by fitting to the He_2 dimer electronic and vibrational energy levels, second-virial coefficients, thermal-conductivity, high-temperature viscosity, and differential cross-section measurements. The Aziz pair potential has recently been used in a variety of condensed phase simulation studies¹¹ and found to reproduce adequately a sizable number of experimental data particularly the equation of state¹², appropriate to our moderately high pressure studies¹³.

Jordan, Siddiqui and Siska⁹ have recently developed interaction potential models for the $a^3\Sigma_u^+$ and $c^3\Sigma_g^+$ states of He_2 on the basis of generalized Morse-Hulburt-Hirschfelder functions to describe both the well regions (Region A) and barriers (Region B) and of improved Tang-Toennies form for the long-range van der Waals interaction (Region C). We refer the reader to their work for the functional forms in each region. The 17-parameter (see table II of ref. 4a except that due to a misprint, the sign of the c parameter entering Region B interaction must be changed for the a -state potential fit) models have been obtained by using the data from crossed beam scattering experiments, *ab initio* results and low-temperature exchange rates. The a -state potential has an attractive well for separations of about 1 \AA , followed by a high repulsive barrier around 2.7 \AA . The excited a -state potential has a hump in the region of 2.7 \AA below which is located the bound $\text{He}_2^*(^3\Sigma_u^+)$ species having an equilibrium separation of close to 1 \AA . Similar behavior is also found for the c -state potential corresponding to $\text{He}_2^*(^3\Sigma_g^+)$ the main difference from the a -state being the larger barrier. The minima for the c - and a -states are very close. Figure 15 shows a comparison of the intermediate range parts of the He-He interactions as well as the Siska a - and c -states which control the nature of the Helium bubble which surrounds the excited atomic He^* species. In order to test the effect of interaction potential on the structure of the formed bubble, the available new *ab initio* potential for the long range part of the a -state devised by Konowalow and Lengsfeld¹⁴ (denoted here as the KL potential) has also been employed in one set of simulation runs¹³ (see sec. IV). The well depth of the KL potential is almost a factor of 4 larger than the small van der Waals well of the Siska a -state and the KL hump is slightly higher than the Siska hump. Except for this test¹³ the potentials of ref. 9 were exclusively employed in this work.

3. Simulation Details

The MC simulations were done on a He^*/He solution employing the above described interaction potentials in a system consisting of one excited $\text{He}^*(^3S)$ atom situated in a bath of many He -atoms with periodic boundary conditions representing bulk liquid He . These simulations

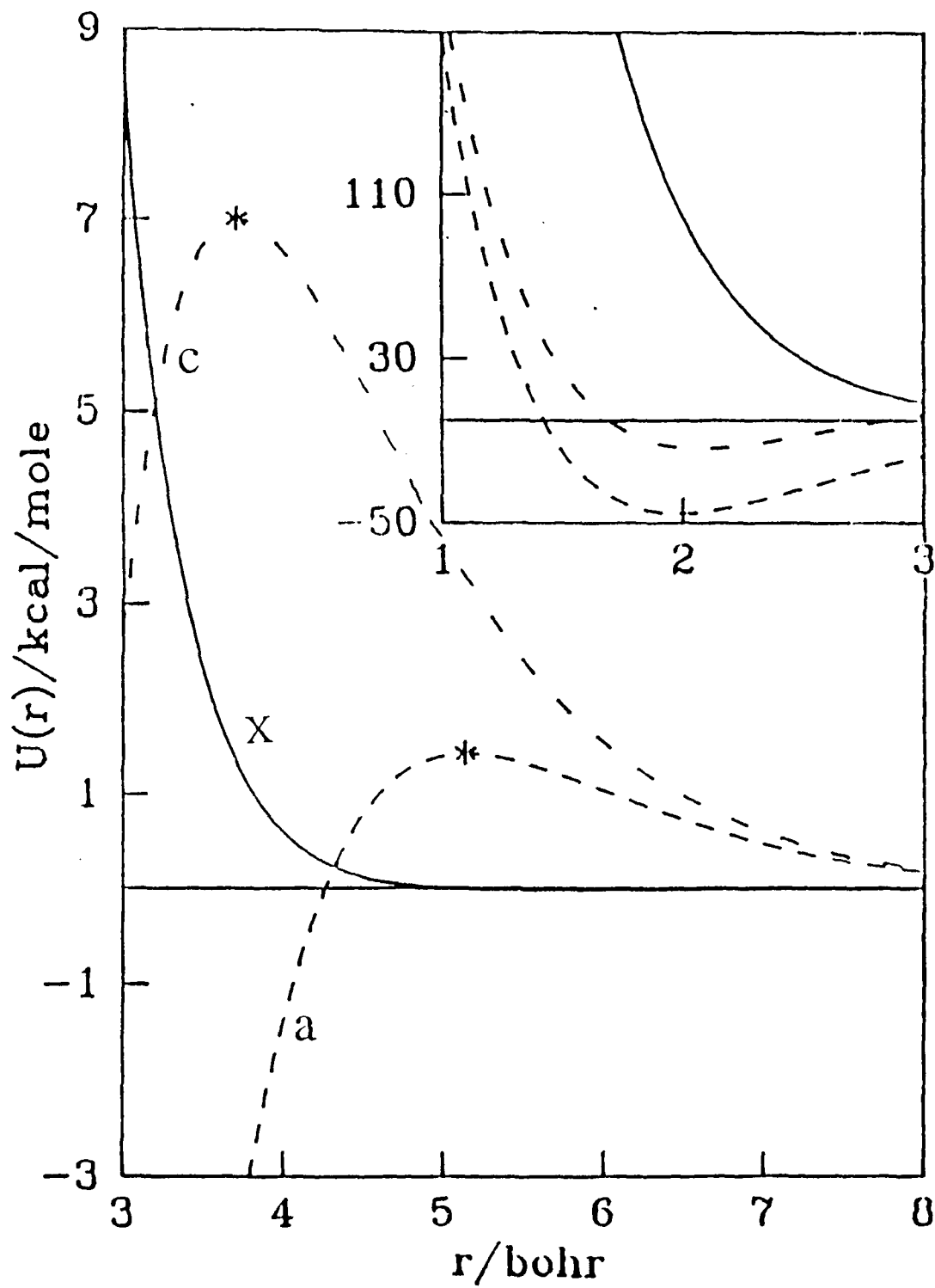
basically pose two problems: (1) convergence of the results because of the infinite dilution studies, and (2) trapping of He atoms (due to the absorbing-sphere nature of the a- and c-state potentials that allow a barrier crossing to occur resulting in a temporary absorption of solvent atoms) and formation of compact clusters of He atoms (that result upon several solvent atoms crossing over to the region below the barrier, that is to the left of the * marked in Fig. 15). The former problem has been addressed by performing very long and large scale simulations for better statistics. The number of particles needed for production runs depends on the number of solvation shells to be included in the simulation box. In order to study the structure of the second solvation shell at high pressures (which is not expected to be completely determined by the 256 particle simulations) as well as to eliminate simulation box-edge effects on the structure of the bubble, we performed 500 particle simulations where necessary. The bubble structure has been obtained from an average of three MC runs at each pressure with appropriate MC move step-size; each run consisted of one million MC moves. We then adapted a nine-point moving polynomial smoother algorithm¹⁵ on the mean radial distribution function so as to eliminate numerical noise which can obscure relevant features in the distribution.

The solvent atom's access, on passing over the a- or c-state barrier, to the attractive region below the barrier adds to the complexity of simulations due to trapping of solvent He atoms and formation of an He_n^* complex in the inner region of the bubble. This may cause simulation problems not only in the formation of the bubble but also in characterizing the realistic structural features of the pertinent bubble states. Further, it is expected that dynamical simulations, necessary to obtain reliable GLE parameters, cannot be easily carried out with such barrier-crossing (see Fig. 15 for comparison of energetics) and reaction problems involving the solvent. In order to examine these effects on the structure, we concentrated on MC simulations. Towards the goal of assessing these barrier crossing effects on the bubble state, we experimented with different ways of eliminating the trapping of He atoms to form the He_n^* species. As a result, the problem of characterization of the He^* bubble in liquid He is examined here based on two types (see below) of MC simulations of an excited He^* species (a and c states) in the condensed phase He environment (solution).

A. Straight Simulation:

In this study, we mostly performed a standard or natural (straight) simulation of the solution system allowing the uninterrupted formation of He_n^* complexes. This was done to explore the effect of a nonequilibrium reactive flux being allowed to naturally influence the solvation structure. The simulation procedure used was standard except that He^* is placed at the centre of the simulation cell in the beginning of the run.

Figure 15. Pairwise-additive potentials, $U(r)$, for the ground (X) state of He_2 , and for the excited a- and c-states of He_2^* . The inset figure shows the r -dependence of the potentials for small values of r .



B. Prevention of clustering:

Simulation of solvent structure around a specified metastable species, He_n^* , requires that the species be somehow kept from transforming (by barrier crossing reaction with the solvent) to other possible species during simulation. We have explored the effects of the following two simple schemes of preventing such a clustering.

In the simulations described below, we simplify the algorithm by fixing the He^* atom at the centre of our simulation cell and keeping it fixed there (clamped) during the MC run. This was done after testing such a procedure in comparison to an unclamped one. Clamping also helps economize prevention of the possible disruption of the formed bubble, the possible disruption being due to the He^* moving to the edge of the simulation cell during the simulation.

1. Simple Rejection:

In order to restrict the trapping of He atoms below the barrier region by the simple rejection method, we opted to reject any attempted MC move if the distance between the He^* and He is less than that of the corresponding barrier location (5.1 and 3.7 bohrs for a- and c- states respectively). The number of such rejected moves is monitored along with various thermodynamic quantities such as energy, and pressure. In order to assess the effect of such rejected moves, a series of MC simulations were performed for both a- and c-states at two pressures. All the simulation results are obtained by averaging over 2 to 3 million moves for 256 particles. Where necessary, we have performed 500 particle simulations as are mentioned below.

2. Flow Instead of Rejection:

Though the MC moves are being rejected in the above simple rejection procedure if the atoms go inside the barrier location, the solvent atoms being left at or near the barrier location is expected to contribute some additional features in the structure. In order to eliminate such effects due to the simple rejection of reaction around the barrier location, in the flow type of solvation model, atoms trying to enter the bubble (i.e., either dimerize or form higher clusters) are instead displaced across to the respective octant corners of the cubic simulation cell. It can be visualized that this results in a flow system.

4. Results & Discussion

To date, experimental studies on helium metastables and the theoretical models employed for them have been in the low pressure and temperature regime. The occurrence of Helium atoms and He_2^* species have been documented in this regime. Higher order clusters of He atoms such as might be expected at higher pressures are being explored here for the first time. The studies performed by us so far are largely in the nature of an exploration of the technology required to

characterize these highly excited species in condensed phases. We summarize the salient points that have arisen in the course of our computer experiments while presenting a discussion of the relevant structural and dynamical issues many of which are accessible to observation by modern experiments not yet performed for the present systems.

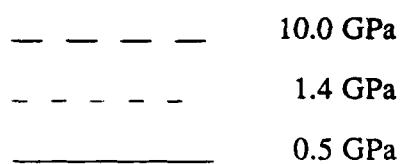
A. Bubble Structure

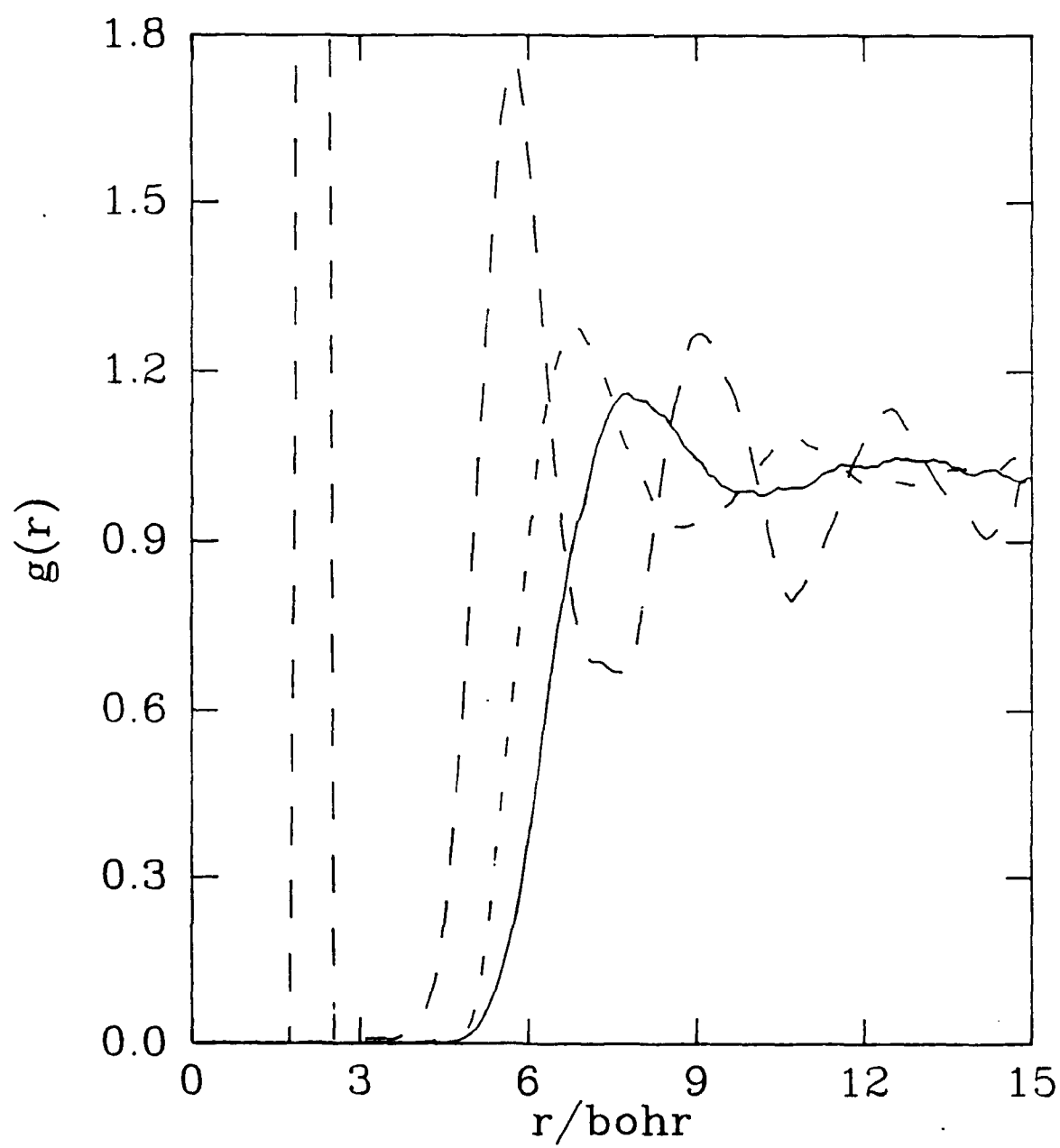
The existence of a bubble-like structure in solution is clearly seen upon examining the radial distribution function (RDF) for the solute-solvent pairs (computed by averaging over the MC runs made). We discuss differences among the RDF's in terms of the potential function employed for the solute-solvent interaction (a- or c-state) and other parameters of the simulation (eg. pressure, imposed boundary conditions (cf: sec. III) etc.).

To begin with, we tested the effect of clamping the He^* atom on the RDF's. Essentially identical results were obtained for the c-state bubbles at pressures of 0.5 and 1.4 GPa by constraining or not constraining the He^* (but, in the latter case, ensuring that the box is large enough for the entire bubble to stay inside it for the whole simulation run). Secondly, The KL a-state bubble was simulated to see if the differences in the two a-state potentials (of ref. 9 and 14) are detectable in the bubble structure and hence judge the adequacy of the long-range potential being employed. Although minor quantitative differences in peak heights were noticeable,¹³ the peak positions were found to be essentially the same. These changes in peak heights were qualitatively consistent with the difference in the potentials employed: these are a shorter first peak attributable to the higher barrier of KL and a minor shift of probability to larger distances (closer to the van der Waals minimum), but not significant accumulation to reflect any important role due to the deeper well there. Thus the a-state potential of Ref. 9 was retained for the rest of the work.

Figure 16 presents our results for the He^* -He radial distribution functions (RDF) of c-state at 0.5, 1.4, and 10 GPa obtained using the Straight model simulations. The RDF's for 0.5 and 1.4 GPa show no density of He atoms below the peak structure located at $5-6a_0$. It is seen by comparing to the distance scale of the potential functions in Fig. 15 that the structured RDF for these two pressures represent the density distribution of the first few solvation shells of the "bubble" within which the atomic He^* species is located. The large RDF peak for 10 GPa near $2a_0$ can be understood to reveal the formation of a possible cluster, He_n^* , and the remaining outer structure as due to the formation of the bubble. The clear demarkation between the two (inner versus outer peaks) seen in the fact that the probability becomes zero near about 4 bohrs and rises slowly from then onwards indicates that it makes sense to call the object responsible for the short range structure a "bubble state" just as was done for the atomic and dimer cases at lower pressures based on experiments. It may be asked if the structure of the bubble solvation shells will be

Figure 16. The structure of the He*(c) bubble as a function of pressure:





influenced due to the additional interactions of the solvent with the absorbed solvent atoms present in the cluster species within the bubble. If these interactions are important, the solvation structure at these pressures would correspond to a different bubble state for different cluster species. We have found that (see below) in two of the lower pressures studied here (0.5 and 1.4 GPa), this is probably not a significant effect although this effect could be present at 10 GPa. The average number, $\langle n \rangle$, of atoms present in the bubble have been monitored during the simulations and are included in Table 4.

Figure 17 contains, for the same pressures, the corresponding RDFs from simulations based on the a-state interaction. Comparison of Figs. 17 and 18 indicate the following: (1) there is a shift in peak positions for both a- and c-states towards smaller radii for higher pressures. The shift in the peak positions as well as the appearance of a second solvation shell at higher pressure can be readily understood in terms of packing effects based on available volume; (2) the bubble peak positions do not depend on the g/u electronic state characters of the He^*-He interactions and could be because they basically lie close in energy; (3) the difference in peak heights (higher for the c-state bubble at 10 GPa) could be due to a combination of the higher slope of the c-state barrier near $5.7a_0$ as well as excluded volume forces from additional atoms ($\langle n \rangle = 3.6$ for c-state in Table 4) of the cluster within the bubble. Clearly, at 10 GPa, the a-state has more particles within the bubble (see $\langle n \rangle = 6.1$ for a-state in Table 4) at this pressure but they are found unable to contribute enough additional repulsion to compensate also for the higher slope of c-state potential near $5.7a_0$; and (4) There is significant cluster formation, revealed by short-range structures in the a-bubble RDF, at the two lower pressures, in contrast to the c-bubble. The fact that the outer part of the RDF's for the two states at these lower pressures (0.5 and 1.4 GPa) coincide, just as expected from the almost degenerate nature of the g/u potentials for distances beyond $6a_0$, confirms that the potential energy contribution of the additional atoms from the cluster located within the bubble to solvation structure modification is negligible at least when $\langle n \rangle$ is as high as around 6 (Note that although the $\langle n \rangle$ value for c-state cluster at 10 GPa in relation to point 3 above is only between 3 and 4, the peak position in question is of shorter range at 10 GPa).

B. Clustering Propensity

The value of $\langle n \rangle$ is seen to depend on which electronic state is involved so that electronic nonadiabaticities would have an effect on this simple quantity. The propensity for the formation of He_n^* complexes was found more pronounced in the a-state compared to the c-state and is attributable to their barrier height difference. In this work we found high pressure values of $\langle n \rangle$ (see Table 4) significantly larger than the value of 2 that presumably occurs at ordinary low pressures (as in reports based on previous experiments). Table 4 also presents additional simulation data for a and c states, such as the average He^*-He bond separation in the cluster that is

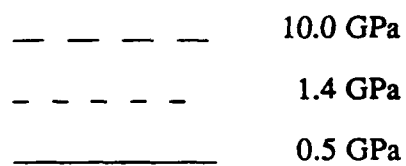
trapped within the bubble. A unit value for RDF corresponds to the uncorrelated limit of average liquid bulk pair probability. The pair probability for the inner part (i.e., within the bubble) of the RDF is found to be an order of magnitude larger (with peak heights, seen for e.g., as in the inset of Fig. 17 shown, of around 10-30) than the average long-range bulk pair probability. These relative RDF magnitudes reflect the much more compact nature of the cluster located within the bubble when compared to the liquid bulk. This compact nature leads us to a physical picture akin to gas/surface type collision dynamics between the species in the bubble and the concave inner surface of the bubble.

The $\langle n \rangle$ values for a-bubble appear to have saturated to a value around 6 at the highest pressures studied here, and an order of magnitude increase in the pressure beyond the saturation point is seen to maintain the bubble structure intact. What $\langle n \rangle$ reveals is the relative change in the free energy of cluster formation within the bubble. The variation of $\langle n \rangle$ may be termed a static solvent effect. It must be noted here that MC simulations do not yield the n -value dynamical fluctuations which may affect the observability conditions for the n -mers.

The questions of how much these clustering reactions influence the bubble and the dynamics of a given n -mer in solution are not addressed by these MC simulations within the Straight model. In attempting to develop some insight into these processes, we have developed the other two models described in Subection 3 that prevent further clustering of a specified n -mer with a solvent atom to form an $(n+1)$ -mer. Results for RDF's from the Flow model, the Simple Rejection model, and the Straight model for the a-state at 1.4 GPa are compared in Fig. 18. The first two types of simulations (termed Monomer'1 and Monomer'2 in Fig. 18) constrain the bubble species to be solely He^* atoms by preventing the formation of even He_2^* . Clearly, neither the peak positions nor the peak structural features are in good agreement with each other in Fig. 18, thereby displaying tremendous sensitivity to the simulation model choice and the important role of reaction in bubble structure maintenance, at least for this $n=1$ case. This $\langle n \rangle$ is quite low compared to the average $\langle n \rangle = 6.3$ value of Table 4 for this pressure. Thus the atomic species examined is probably an unstable one under the conditions of 1.4 GPa. Naturally, no rejection scheme makes physical sense unless the level n , at which He_n^* is fixed, is a stable (albeit metastable) species in the condensed phase matrix.

We conclude the discussion of the nonclustering model studies with a few remarks on the technology used to do the simulations. It was found that the 256-particle Flow model simulation resulted in RDF values greater than 1.0 around the boundary of the simulation cell. In order to avoid this spurious effect as well as to reduce any possible effect on the main peak of the bubble, we performed 500-particle simulations and this is the one included in Fig. 18. The first peak position and height are reproducible in both sets (256 and 500 particle runs) of simulations. The

Figure 17. The structure of the He*(a) bubble as a function of pressure:



The inset shows the short-range structure.

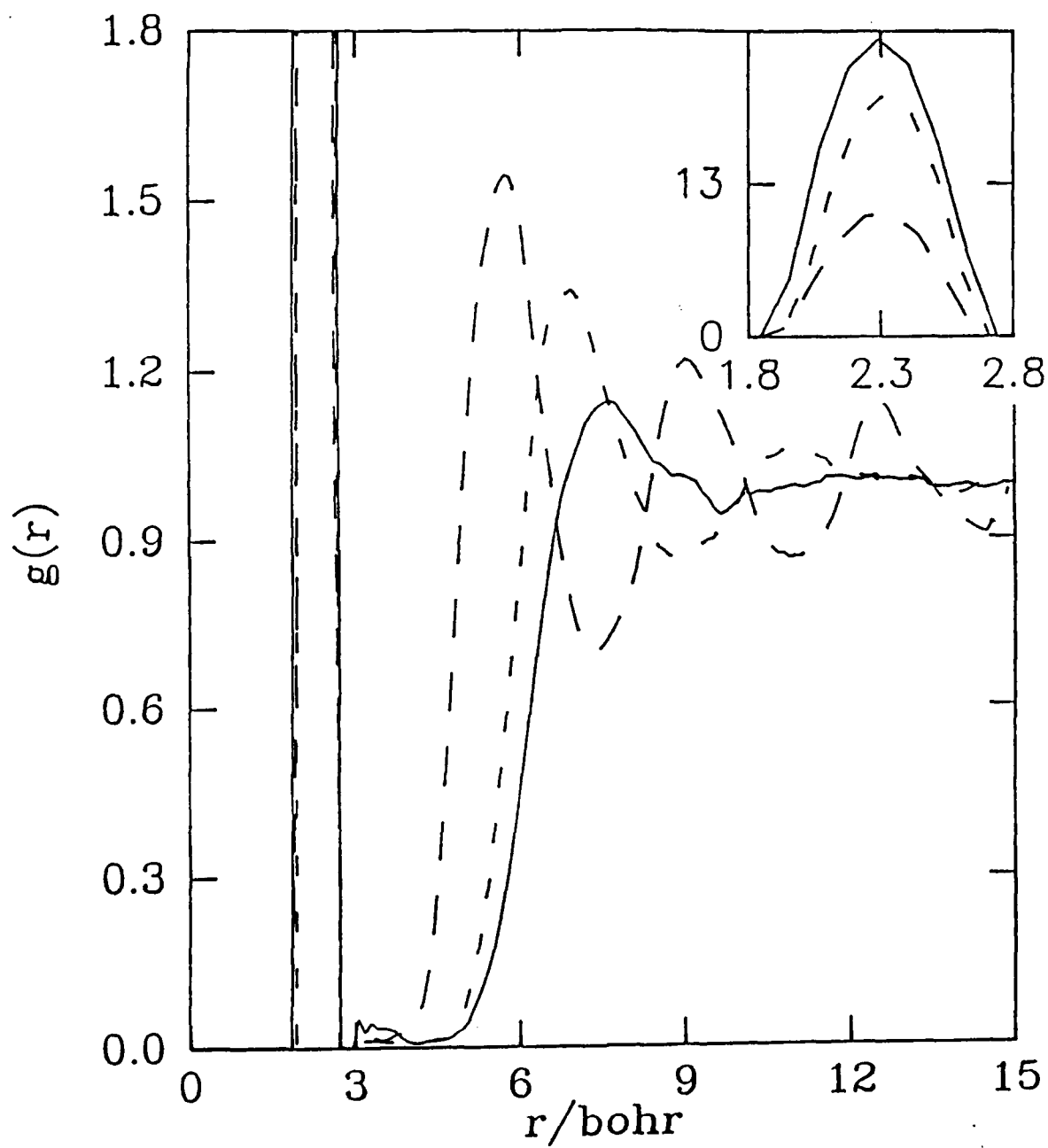
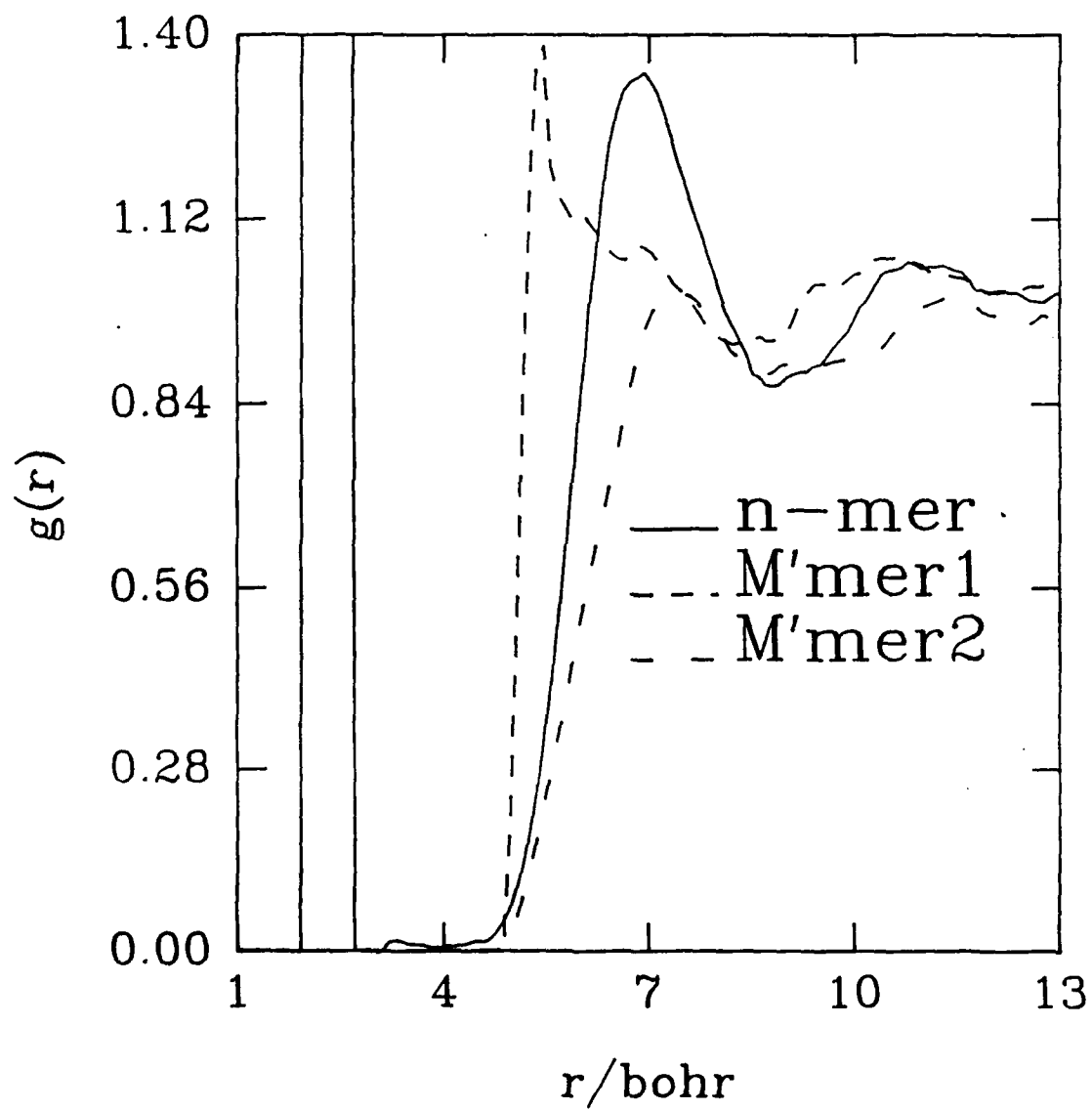


Figure 18. The structure of the $\text{He}^*(a)$ bubble for different simulation strategies that prevent clustering with the solvent (as discussed in Subsections 3 and 4 of this section).



Flow model RDF in Fig. 18 may imply that although the bubble may have been formed it is disrupted or diffused out because the particles responsible for its formation are being taken out to the corners of the cell. Clearly, the simple prescriptions of the nonclustering models employed here are insufficient for achieving the purpose of realistic characterization of n -mers when n is very different from $\langle n \rangle$. It is hoped that improved simulation schemes can be devised, but (we feel) perhaps only for situations when n is closer to $\langle n \rangle$ so as to study pertinent species (which should not have n that is too different from $\langle n \rangle$).

5. Conclusion

We have presented results of a thermodynamic state dependent MC study of the Helium bubble states arising from electronically excited He^* metastables being trapped in a condensed phase He environment. Even in this classical regime, bubbles were found to exist and house the excited species, although the bubble contents are a sensitive function of pressure. Various RDF's were presented to analyze and interpret the bubble changes with pressure, electronic state features etc..

This type of simulation is also highly pertinent to materials problems such as embrittlement in fusion reactor materials associated with generation of He that have attracted considerable interest in recent years. Bombardment with heavy noble-gas ions is widely used in various modern preparation processes¹⁶ for metal surfaces and films. It has been shown that the He embrittlement observed in metals was due to the trapping and subsequent bubble formation at radiation induced defects as well as in the absence of radiation damage¹⁷. To evaluate the effects of noble gases on physical or material properties of metals, it is therefore important to be able to characterize noble-gas bubbles and to develop an understanding of their behavior. There have been a number of atomistic calculations⁴ to explain the bubble formation and the involved self-trapping mechanism of He in metals. We have revealed certain technically feasible aspects as well as raised some pertinent issues relating to characterizing the role of a reactive species being present within bubbles.

Table 4^a: MC Results of He^{*}(2³S) in He (1¹S) bath at 300K

$v_m/\text{Cm}^3 \text{ mol}^{-1}$	$\langle P \rangle/\text{GPa}$	$\langle U \rangle/\text{kJ mol}^{-1}$	'n-mer' Structure	
			$\langle r_{\text{He}^*-\text{He}} \rangle/a_0$	$\langle n \rangle$
17.95	0.29	0.36	2.29	5.6
13.17	0.55	-2.0	2.29	5.9
	0.57	0.85	--	0
9.02	1.4	-0.9	2.32	6.3
	1.5	2.2	--	0
4.76	10.1	10.4	2.24	6.1
	10.3	11.9	2.14	3.6
4.35	13.8	14.2	2.27	6.1
	13.9	15.6		4.2

(a) First and second row values for each volume correspond to a- and c-states of He-He^{*} interaction.

REFERENCES

- 1 (a) W. S. Dennis, E. Durbin, Jr., W.A. Fitzsimmons, O. Heybey, and G. K. Walters, Phys. Rev. Letts. **23**, 1083 (1969); (b) J. C. Hill, O. Heybey, and G. K. Walters, *ibid.* **26**, 1213 (1971); (c) John L. Watkins, Jonas S. Zmuidzinas, and Gary A. Williams Physica **108B**, 1313 (1981).
- 2 (a) See (1a); (b) A. P. Hickman and N. F. Lane, Phys. Rev. Letts. **26**, 1216 (1971); (c) A. P. Hickman, W. Steets, and N. F. Lane, Phys. Rev. **B12**, 3705 (1975); Y. M. Shih and C-W. Woo Phys. Rev. **A8**, 1437 (1973).
- 3 (a) E. V. Kornelsen, Can. J. Phys. **48**, 2812 (1970); (b) W. D. Wilson and C. L. Bisson Radiad. Eff. **22**, 63 (1974).
- 4 (a) W. D. Wilson, C. L. Bisson, and M. I. Baskes Phys. Rev. **B 24**, 5616 (1981); (b) Refs. in Advances in the Mechanics and Physics of Surfaces, ed. R. M. Latanision and T. E. Fisher, Harwood Academic Publishers, (1983); (c) K. O. Jensen and R. M. Nieminen, Phys. Rev. **B 35**, 2087 (1987); *Ibid.* **36**, 8219 (1987).
- 5 J. P. Hansen and E. L. Pollock, Phys. Rev. **A5**, 2214 (1972).
- 6 ω_{e0} and ω_{c1} are related to the second and fourth frequency moments of the system spectral density and are defined for eg. by S. A. Adelman J. Chem. Phys. **73**, 3145 (1980); (b) For definition of GLE parameters in a partial clamping approximation scheme, see S. A. Adelman J. Chem. Phys. **81**, 2776 (1984).
- 7 D. A. Micha, J. Chem. Phys. **78**, 7138 (1983).
- 8 P. K. Swaminathan, B. C. Garrett, and C. S. Murthy J. Chem. Phys. **88**, 2822 (1988); B. C. Garrett, P. K. Swaminathan, C. S. Murthy, and M. J. Redmon J. Chem. Phys. **87**, 3207 (1987).
- 9 (a) R. M. Jordan, H. R. Siddiqui, and P. E. Siska J. Chem. Phys. **84**, 6719 (1986); (b) R. M. Jordan and P. E. Siska J. Chem. Phys. **80**, 5027 (1984).
- 10 R. Aziz, V. P. S. Nain, J. S. Carley, W. L. Taylor, and G. T. McConville, J. Chem. Phys. **70**, 4330 (1979).
- 11 (a) D. Levesque, J. J. Weis, and M. L. Klein, Phys. Rev. Lett. **51**, 670 (1983); (b) D. Levesque, J. J. Weis, and P. Loubeyre, Phys. Rev. **B 34**, 178 (1986); (c) D. Frenkel, Phys. Rev. Lett. **56**, 858 (1986); (d) D. M. Ceperly and H. Partridge, J. Chem. Phys. **84**, 820 (1986); (e) P. Loubeyre, Physica **139&140 B**, 224 (1986); (f) P. Loubeyre, Phys. Rev. Lett. **58**, 1857 (1987); (g) M. Takahashi, J. Phys. Soc. Japan, **55**, 1952 (1986); (h) W. B. Smith and K. Singer Molec. Phys. (in press).
- 12 R. L. Mills, D. H. Liebermberg, and J. C. Bronson, Phys. Rev. **B 21**, 5137 (1980).
- 13 P. K. Swaminathan and C. S. Murthy (unpublished results).
- 14 D. Konowalow and B. Lengsfeld, J. Chem. Phys. **87**, 4000 (1987).

- 15 A. Savitsky and M. J. E. Golay, *Anal. Chem.* **36**, 1627 (1964).
- 16 (a) R. G. Musket, W. McLean, C. A. Colmenares, D. M. Makowiecki, and W. J. Siekhaus, *Appl. Surf. Sci.* **10**, 143 (1982); (b) S. Matteson and M. A. Nicolet, *Annu. Rev. Mater. Sci.* **13**, 339 (1983).
- 17 (a) G. J. Thomas, W. A. Swansiger, and M. I. Baskes, *J. Appl. Phys.* **50**, 1942 (1979); (b) G. J. Thomas and R. Bastasz, *J. Appl. Phys.* **52**, 6426 (1981).

Heatbath Models for Helium Bubble States

1. Introduction

Production of ^4He , the identification of (metastable) excited states of ^4He atoms, and exploration of associated problems in fusion reactors¹ have all been active areas of experimental study for some time. On the theoretical front, in the use of *ab initio*, lattice dynamical, and statistical mechanical approaches, helium has long attracted many researchers because it constitutes a fundamental system that is challenging for technique developments involving quantum effects in various contexts.²

The indications, obtained in recent high-pressure experiments³ using the diamond-anvil-cell technique, of a possible new solid phase around 300 K along the melting curve, have resulted in extensive theoretical research⁴ effort on solid He. This is largely because of the availability of a reasonably accurate pair potential^{2c} and the recent advances in the computer simulation techniques for studying phase transitions⁵ and estimating free-energies.⁶ There have also been a few studies in the fluid phase,⁷ dealing with the thermodynamic properties and equilibrium structure.

Our goal is to theoretically treat the dynamics of electronically excited species and the condensed phase influence on such species. We have chosen ^4He for the benchmark studies necessary for computational method developments. In the present work, we performed classical Monte Carlo (MC) and classical molecular dynamics (MD) (where appropriate) simulations on liquid He as well as solution systems consisting of one excited $\text{He}^*(^3\text{S})$ atom situated in bulk liquid He environment. Our work is focused on state points near 300 K in the high pressure (GPa) regime. We have not addressed the quantum translational aspect and the three-body force-effects on the structure and dynamics of liquid He, although they deserve a special and large effort in order to accurately quantify such effects. Although these effects are at the outset expected to be important for He, it is anticipated from the existing investigations on He⁸ that quantum effects have only a minor role to play at high densities (high-pressure 10-20 GPa). Our work here is based on classical simulations using the recently developed Aziz potential.^{2c}

We now turn to the question of the degree of suitability of the Aziz effective pair potential for realistic simulations of ^4He and effects of three-body forces. Although the Aziz pair potential has been widely used in the recent high density studies on ^4He which are referred to above, there remain only two recorded deficiencies⁹ of the model: it is (1) too repulsive for distances less than 1.8 Å and (2) fails to explain the thermodynamic stability of the bcc phase around 300 K. The former weakness of the model will matter only at very high densities (pressures above 60 GPa). The latter may well be due to the neglect of three-body forces. It has in fact been recently shown¹⁰ that self-consistent phonon and MC calculations, involving Aziz's pair potential with three-body interactions, produce results in excellent agreement with the experimental equation of state at high

pressures.¹¹ It should however be noted that such refinements are only necessary for resolving the stability of equally competing solid phases such as fcc and hcp and perhaps for detailed description of dynamical properties.

The present simulations of liquid solvation structure can yield the associated heat-bath modelling MTGLE parameters for realistic quenching studies (e.g., in He-He* matrix studies). This involves certain approximate statistical mechanical relations between structural properties and the frequency moments of the GLE heatbath spectral density. Such prescriptions for determination of parameters for stochastic dynamical treatments are delineated in a series of papers by Adelman and coworkers,¹² in particular, within the partial clamping formalism developed for solvated polyatomic entities. A dynamical simulation of solvation is essential for the exact characterization of the dynamics of a heatbath since the real time-dependent friction kernels are dynamical quantities. In this report, following Adelman and coworkers, we examine the validity of a gaussian model for the time dependent solvent friction, and having obtained some MD-based information for the degree of validity of the gaussian model for the solvent, we apply the gaussian model to the MC-based structural (radial distribution functions) data from a solution of He* in He (reported earlier).¹³ This kind of approach is necessary especially because heatbath parameterization via MD simulations is difficult for the solution problem due to the possibility of a reaction between He* and the solvent He. From our present calculations, we obtain evidence for a decrease in pressure sensitivity upon electronic excitation in the high pressure He-matrix, for a modelled excited He* state (specifically, we employed the c-state for He-He* interaction) compared to ground state He (leading to the Aziz potential of He-He interaction).

Subsection 2 describes the adopted interaction potential models and simulation details along with a brief description of how the MTGLE parameters have been estimated in the present work. Subsection 3 contains the main results and discussion.

2. Methodology

A. Potential Models and Simulations

We employed the recently developed multiparameter Aziz model^{2c} of effective pair interactions in condensed phase Helium in our studies of the structure and dynamics of liquid He. This effective pairwise-additive potential has recently been employed in a variety of condensed phase simulation studies,⁴ as discussed in the introduction. It not only reproduces adequately a sizable number of experimental data but also we find that it accounts particularly well for the equation of state¹¹ appropriate to our present moderately high pressure studies. The functional form of the model used can be written as

$$\phi(r) = \epsilon [b e^{-\alpha R} - \{ C_6 R^{-6} + C_8 R^{-8} + C_{10} R^{-10} \} f(R)]$$

$$f(R) = \begin{cases} \exp[-(d/R - 1)^2], & R < d \\ 1, & R > d \end{cases} \quad (206)$$

where $R = r/r_m$, $r_m = 2.9673 \text{ \AA}$, $b = 544850.4$, $\alpha = 13.353384$, $C_6 = 1.3732412$, $C_8 = 0.4253785$, $C_{10} = 0.1781$, $d = 1.241314$, $\epsilon/k_B = 10.8 \text{ K}$, and k_B is the Boltzmann constant. The corresponding potential parameters were determined^{2c} by fitting to the differential cross-section measurements, second-virial coefficients of the gaseous He, thermal-conductivity, high-temperature viscosity, and He₂ dimer electronic and vibrational energy levels.

The solution simulations involve a system consisting of one excited He* atom situated in bulk liquid He environment, the atoms of the latter interacting with each other via the effective Aziz potential, whereas, for the He*-He interactions, we adopted the recently developed He₂* (a ³Σ_u⁺ and c ³Σ_g⁺) potentials of Jordan, Siddiqui and Siska.¹⁴ They employed generalized Morse-Hulburt-Hirschfelder functions to describe both the well regions (Region A) and barriers (Region B) and Tang-Toennies form for the long-range van der Waals interaction (Region C). We refer the reader to their papers for the detailed functional forms in each region. The 17-parameter¹⁵ models have been obtained by using the data from crossed beam scattering experiments, *ab initio* results and low-temperature exchange rates.

B. MTGLE Parameters

The MTGLE parameters needed for the stochastic dynamical modelling in liquid state include the characteristic Einstein frequency, denoted ω_{e0} , the coupling constant, denoted ω_{c1} , and the friction kernel, denoted $\beta(t)$. ω_{e0} enters the stochastic equations of motion and governs the initial energy transfer between the solute species and (approximately) the first solvation shell species of the solvent degrees of freedom. ω_{e0} determines the encounter frequency for solute-solvent collisions that are responsible for maintaining or quenching the metastable species trapped in bulk. ω_{c1} controls the overall efficiency of energy transfer from the reagents to the heatbath.

The detailed theory of MTGLE and expressions for the basic MTGLE parameters, ω_{e0} and ω_{c1} , in various regimes (exact as well as for both isolated and interacting solute atoms) are discussed at length by Adelman and coworkers.¹² For completeness, here we give the appropriate (isotropic liquid satisfying virial theorem) formulae used:

$$\omega_{e0}^2 = -\frac{1}{3m} \left\langle \frac{\partial}{\partial \mathbf{r}} \cdot \mathbf{f} \right\rangle \quad (207)$$

$$\omega_{c_1}^4 = \frac{1}{mM} \left\langle \frac{\partial f}{\partial r} : \frac{\partial f}{\partial r} \right\rangle \quad (208)$$

For pairwise-additive potentials between the atom-solvent species, $\omega_{e_0}^2$ and $\omega_{c_1}^4$, in the linear response approximation, can be expressed¹² in terms of the corresponding radial distribution function (RDF), $g(r)$:

$$\omega_{e_0}^2 = \frac{4\pi\rho}{3m} \int_0^\infty r^2 g(r) [\varphi''(r) + 2\varphi'(r)/r] dr \quad (209)$$

$$\omega_{c_1}^4 = \frac{4\pi\rho}{mM} \int_0^\infty r^2 g(r) [\{\varphi''(r)\}^2 + \{2\varphi'(r)/r\}^2] dr \quad (210)$$

where m and M are the masses of the solute and solvent species, ρ is the solvent number density, $g(r)$ is the solute-solvent radial distribution function, $\varphi(r)$ is the interaction potential between the solute and solvent species.

The time-dependent friction, $\beta(t)$, determines the frictional drag on the various different frequencies participating in the dynamics. If one examines the frequency dependent function $\beta(\omega)$, obtained by fourier transforming $\beta(t)$, the values of $\beta(\omega)$ at the frequencies corresponding to critical dynamical regions on the potentials play a key role in describing important solvent effects. It is possible to compute $\beta(t)$ from the present MD runs by employing the Volterra integral equation¹⁶ relating various time correlation functions obtainable from the MD simulation trajectories. In addition to the VACF, these correlation functions include position autocorrelation as well as position-velocity cross-correlation functions.¹⁷

3. Results and Discussion

Certain features of condensed phase Helium are unique and noteworthy in the simulation results. First of all, the classical MC/MD simulation procedures yield reasonably converged results for the liquid state condensed Helium only when the number of particles in the system is near 256 for lower pressures, and 500 for the higher pressures (>10 GPa). This is because there are three significant peaks in the radial distribution function (see below) and that means two solvation shells around each He atom, which requires the larger number of atoms than the 108 particles usually employed for the Argon system. Further, the behavior of He in the condensed phase is quite different from the case of Argon. The most striking aspect of this is the predominant role of entropy effects in the liquid free energy of binding (this is reflected in the fact that the internal energy of binding is an excess positive quantity as actually seen in the simulations as well as in the configurational integral, which may be readily computed from the known radial distribution

functions). In Table 5, we report the molar volumes at which simulations have been performed, the configurational internal energies, observed pressures, and the factor PV/RT .

The computed trends in liquid structure, dynamics, and the MTGLE heatbath parameters for pure liquid Helium as a function of pressure are presented in Figs. 19 through 21 respectively. Liquid Helium may be treated classically in the examples shown, all of which correspond to a temperature of around 300 K. As pressure is increased quantum effects become less, and may possibly become relatively important for the present pressures of 0.3, 0.5 and 1.4 GPa. This may be borne out from the factor PV/RT , reported in the last column of table 5. On the basis of an oscillator model obeying the Gruneisen equation of state for the solid and using estimated Gruneisen parameter and the Debye temperature at room temperature and high pressures, Levesque et al,^{4a} estimated $\Delta P_Q V / RT \approx 1$, where ΔP_Q is the leading quantum contribution to the pressure. As our temperature and pressure range is analogous to their studies along the melting curve, one may assume a value similar to theirs for the quantum contribution to the pressure. Such a value for the quantum contribution to the pressure may be compared with the PV/RT values reported in table 5.

Figure 19 displays the RDFs for six different pressures, three of which (0.3, 0.5 and 1.4 GPa) are close to the gaseous fluid and three (10.4, 12.7, and 14.4 GPa) are close to a liquid under high pressure. The RDFs reflect the decreasing nearest neighbor distances with increasing pressure and the more diffuse distributions of neighbors in the gaseous fluid phase. The 10GPa and 14 GPa results were obtained from 500 particle simulations and are more accurate than the 256 particle 12.7 GPa result. The He atom's velocity autocorrelation functions (VACF) shown in Fig. 20 display a dramatic change in dynamical character as a function of pressure. In fact, the low pressure VACFs indicate gas-like behavior with a long hydrodynamic positive tail whereas the high pressure ones show the oscillatory structure characterizing a liquid-like condensed phase correlation.¹⁸

Although the quantum effects are expected to contribute to the structure and dynamics of liquid ^4He at 0.3, 0.5 and 1.4 GPa on the basis of the discussions above, recent semiclassical and path-integral simulation studies¹⁹ on modelled rare gas atoms indicate that the effect of semiclassical/quantum corrections to the RDF is not significant. The first peak of RDF gets slightly broadened resulting in reduction of the peak height and closer contact radius value. Such a detailed comparison for the VACFs from classical vs semiclassical/quantum simulations has not been made to our knowledge. The self diffusion constants obtained from the area of the VACFs given by semiclassical (Gaussian wave packet simulations)^{18a} calculations are lower than are obtained by classical MD simulations. Thus further work is needed to establish the quantum effects on the initial decay and the behavior of VACF at intermediate times. We can then assess the

corresponding effects on MTGLE parameters. As the quantum contributions have modest influence on the RDF as discussed above, we may expect that the quantum effects on ω_{e0} would be less severe than on ω_{c1} (see below) and higher moments.

The MTGLE parameters have been obtained for the tagged solute He in liquid He both by direct ensemble average during the simulation run itself using Eqs. (206) and (207) (at the expense of more CPU time for the additional computation in the forces loop) and from the $\phi(r)$ and $g(r)$ in Eqs. 3 and 4. For a pressure of 0.3 GPa, the ω_{e0} and ω_{c1} values are 18 and 28 THz from ensemble averages compared to 16 and 33 THz estimated from Eqs. (208) and (209). Similar comparison can be seen from the results in table 6. Figure 21 shows values for the moments²⁰ of the spectral density, ω_{e0} and ω_{c1} , as a function of pressure obtained as ensemble averages. It is seen that these bulk liquid values are quite sensitive to (and exponentially dependent on) the pressure. The sensitivity of the dynamics shown by the velocity autocorrelation functions in Fig. 20 reflect the basis for the MTGLE parameter variations as well.

Table 6 gives the values of the MTGLE parameters ω_{e0} and ω_{c1} to be used if the He* atom is treated as if it were a diffusing particle in the liquid state with a- and c- state solute-solvent interactions assumed. The table also contains for comparison the corresponding parameters for the ground level He atoms (with X-state interaction) in liquid Helium. The solution values were all obtained from RDFs from MC whereas the X-state parameters have been verified via direct computation of moments in molecular dynamics (Eqs. 207-208) as well as using RDFs (Eqs. 209-210) as discussed above. Since dynamical simulations for the He* in He solution are difficult due to a possible reaction between He* and He, such a comparison (via Eqs. 207-208) is not available for the solution at the present time. However, the pure liquid results based on RDFs give credence to the solution results at the respective pressures. It is seen that the parameters are very sensitive to the electronic states, which simply reveals that the primary zone must ideally include more than the He* atom. The table also contains high frequency parameters for RDFs from each given electronic state being combined with potentials for different electronic states. This sort of comparison reveals the change in the condensed phase dynamics occurring as a result of a sudden electronic transition to which the solvation structure has not adjusted.

Figure 22 displays a comparison of pressure dependent VACFs obtained from a gaussian $\beta(t)$ model with MD-based VACF results for the pure liquid helium. The gaussian model is based on the high frequency parameters of Table 5 and, for a liquid ($\omega_{e0}^2 = \beta(0)$, since, in a liquid, one has zero adiabatic frequency for a tagged particle), is given by,

Figure 19. Variation of fluid structure of model helium with pressure.

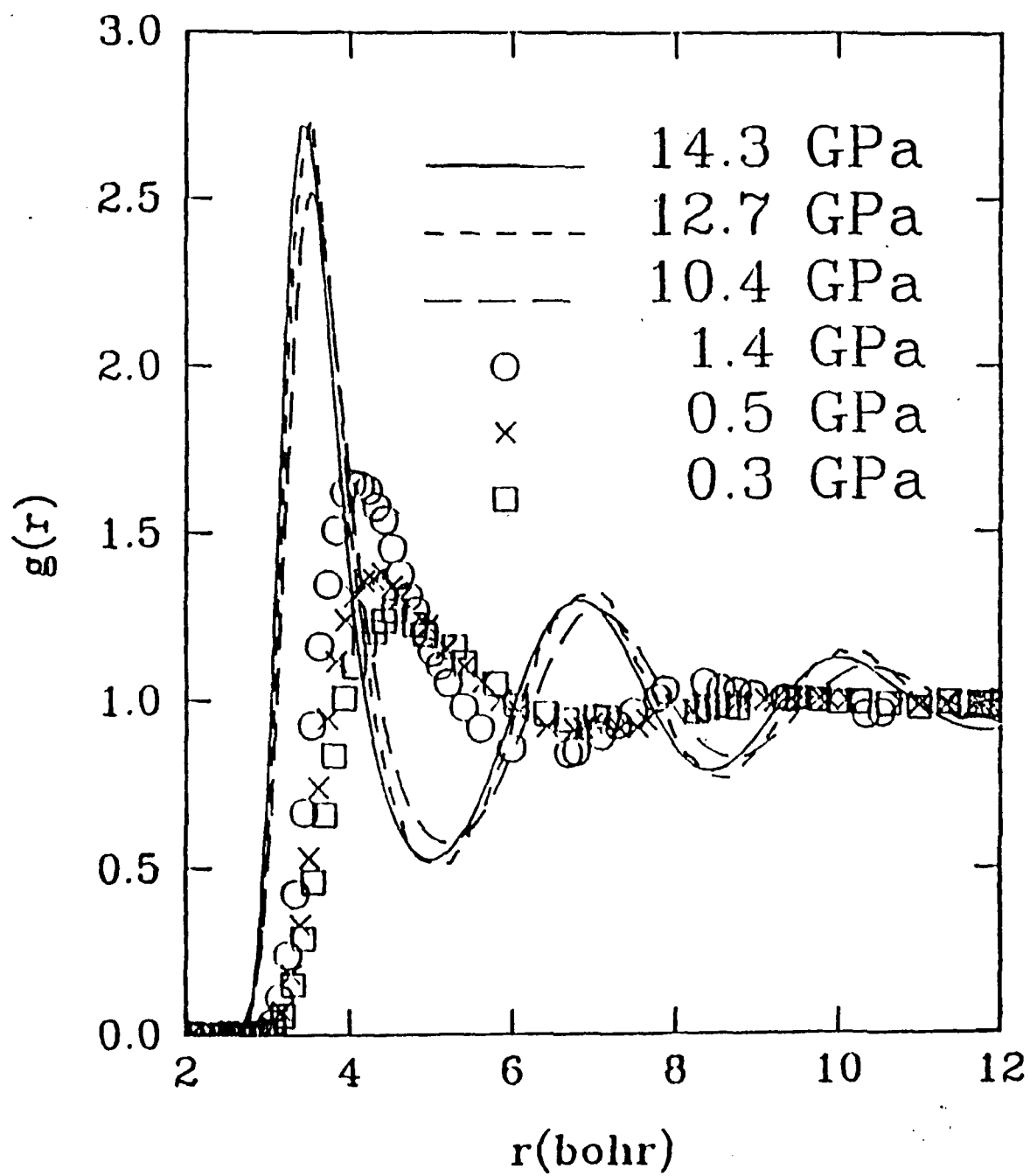


Figure 20. Fluid dynamics (VACF) of model helium as a function of pressure:

-----	14.3 GPa
- - - - -	12.7 GPa
--- --- ---	10.4 GPa
O	1.4 GPa
X	0.5 GPa
□	0.3 GPa

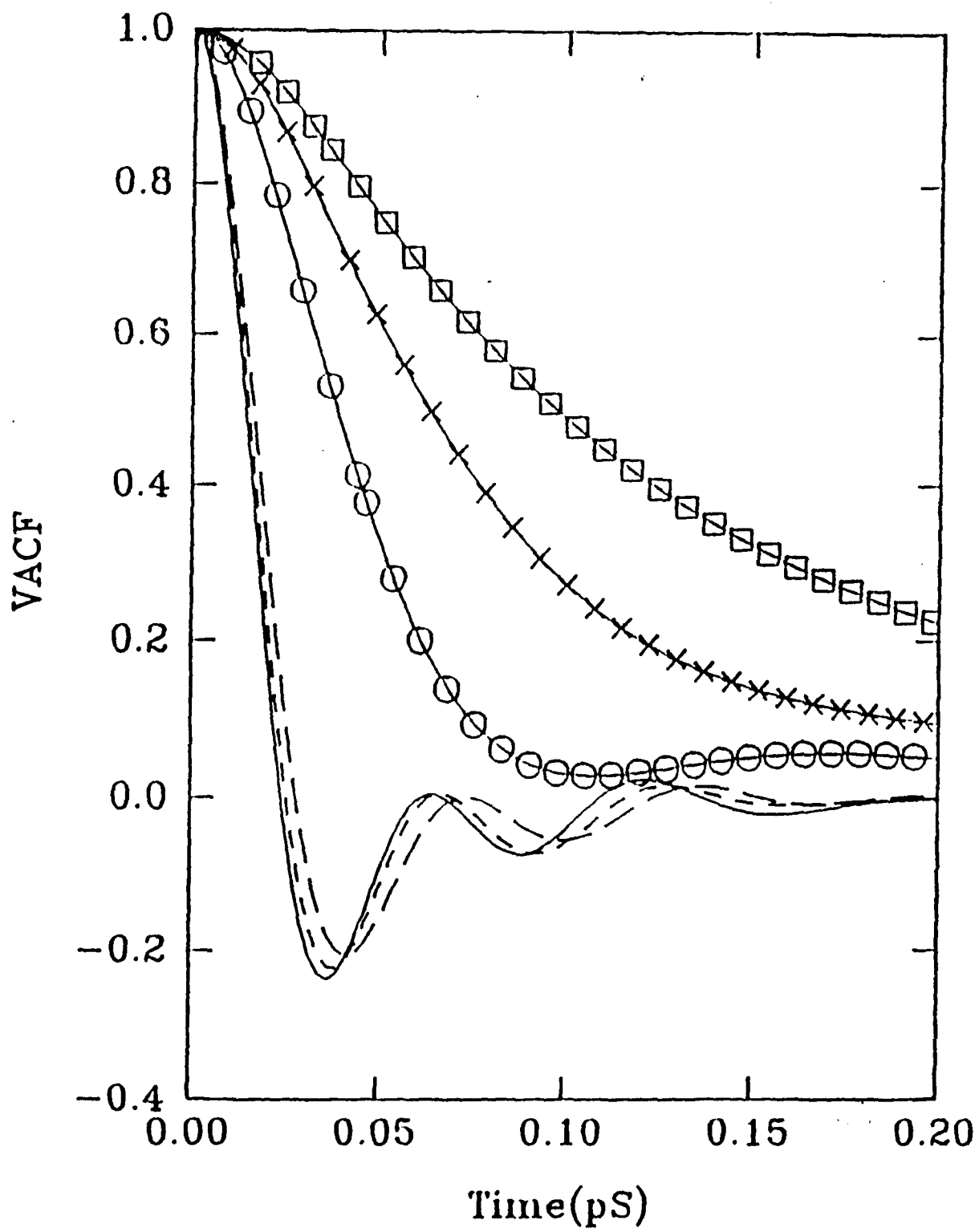


Figure 21. Variation of He(¹S) heatbath modelling (MTGLE) parameters with pressure.

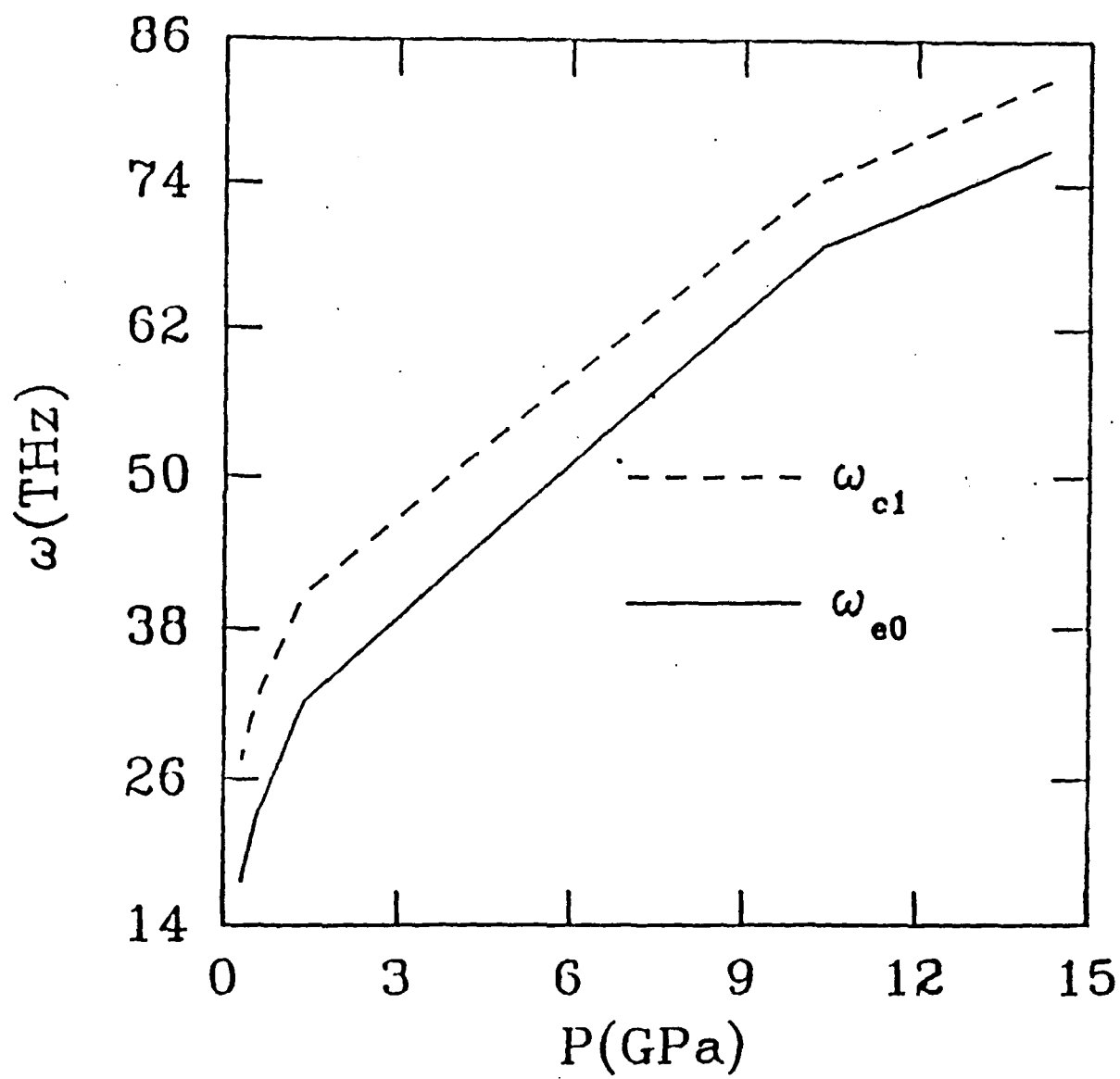


Figure 22. Comparison of pressure-dependent He(¹S) VACF obtained from MD trajectories (continuous line) and from the RDF-based gaussian friction model (dashed line).

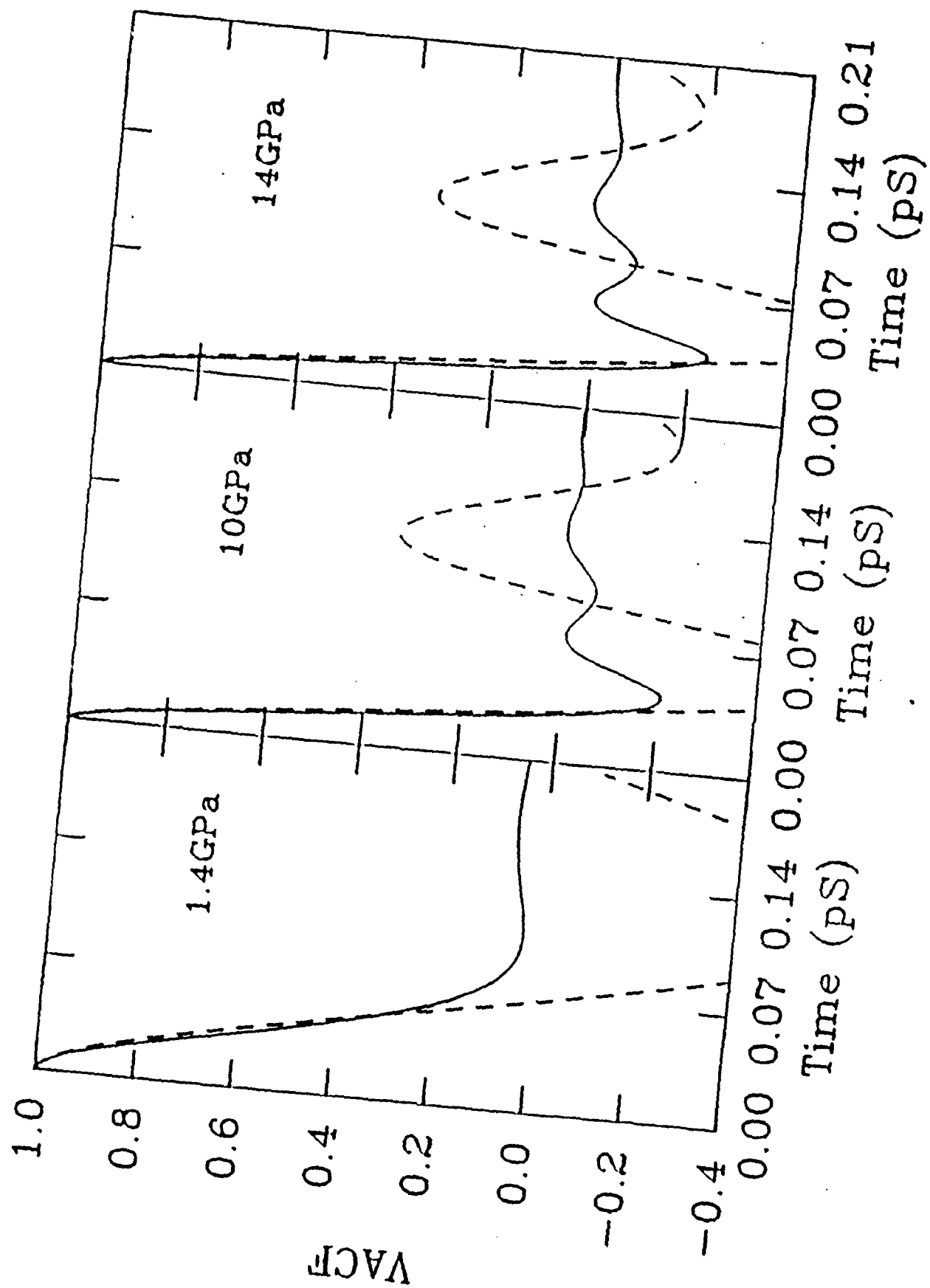


Figure 23. Effect of pressure on $\text{He}(^3\text{S})$ VACF from RDF-based gaussian friction model.

— — — — — 14 GPa
- - - - - 10 GPa
————— 1.4 GPa

Inset shows results for the RDF-based gaussian friction model of $\text{He}(^1\text{S})$ for comparison.

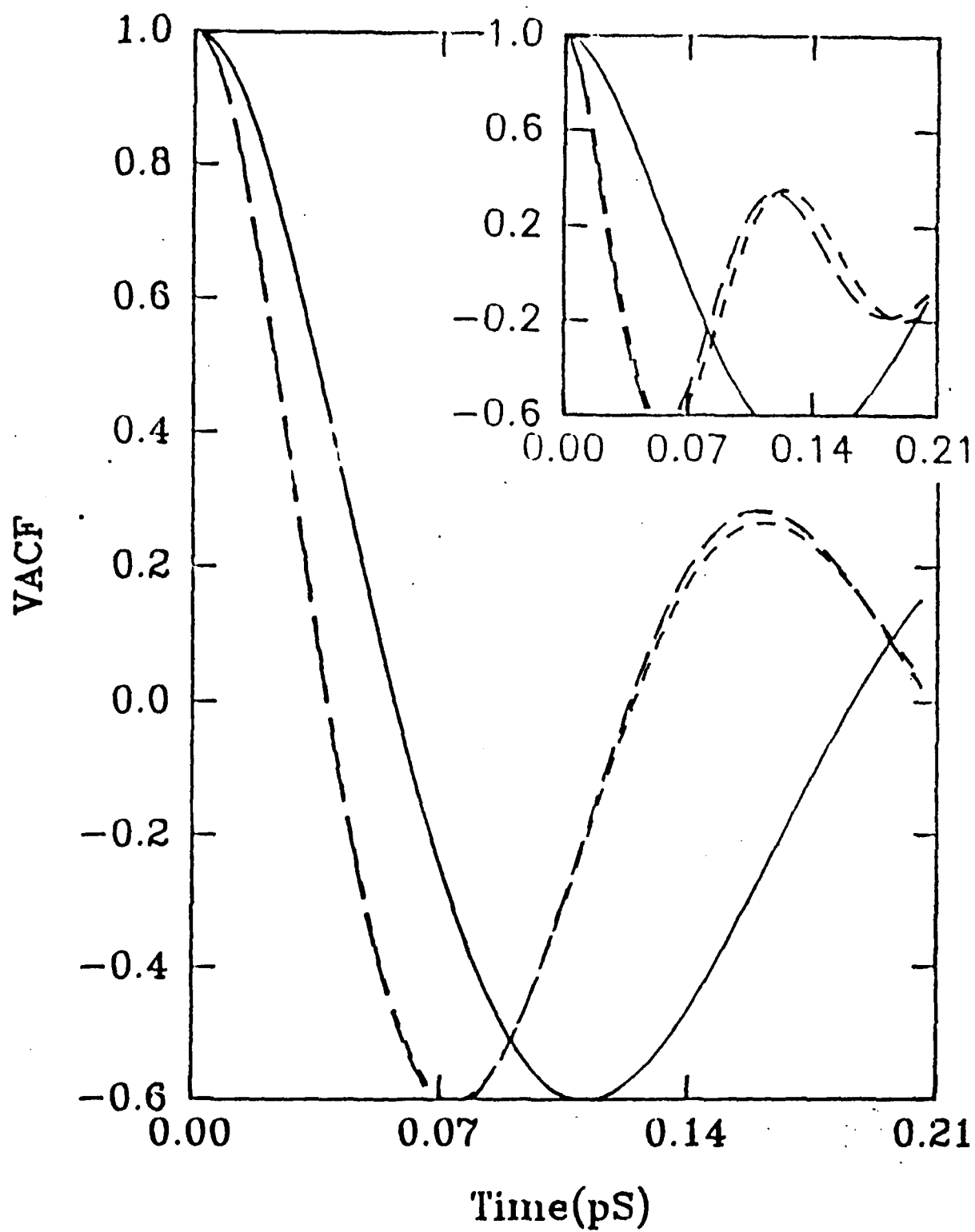


Table 5^a: Some Thermodynamic Properties of liquid ⁴He at 300K

$V_m / \text{Cm}^3 \text{mol}^{-1}$	$\langle U \rangle / \text{kJ mol}^{-1}$		$\langle P \rangle / \text{GPa}$		$\frac{PV}{RT}$
	Bulk	Solution	Bulk	Solution	
17.95	0.36	0.36	0.29	0.29	2.2
13.17	0.74	-2.0 0.85	0.55	0.55 0.57	2.9
9.02	1.9	-0.9 -2.2	1.4	1.4 1.5	5.1
4.76	11.7	10.4 11.9	10.1	10.1 10.3	19.5
4.35	16.1	14.2 15.6	14.3	13.8 13.9	25.3

(a) In the case of solution studies, first and second row values for each volume correspond to a- and c-states of He.

Table 6^a: GLE parameters for He and He* solutes in liquid He

P (GPa)	ω_{e0} (THz)			ω_{c1} (THz)		
	X-state	a-state	c-state	X-state	a-state	c-state
0.55	23, (21)	13 22	23 15	32, (39)	40 39	27 19
1.4	32, (30)	15 32	32 15	41, (48)	35 38	35 25
10.1	68, (65)	--- 47	48 ---	74, (84)	58 53	53 54
14.3	77, (68)	--- 48	49 ---	83, (86)	62 55	56 62

(a) The MTGLE parameter values for He are given as direct ensemble averages [see Eqs. (207), (208) of text] with the values in parenthesis being from the corresponding $\phi(r)$ and $g(r)$ [see Eqs. (209), (210) of text]. For a- and c-states of He, the parameters are obtained by using the corresponding $\phi(r)$ and $g(r)$ data and are reported in the first row. The second row values for a and c states correspond to mixing the $\phi(r)$ and $g(r)$ functions in Eqs. (209)-(210), with the $g(r)$ data for the state in column (a and c) and $\phi(r)$ for the other state (c and a, respectively) to which the electronic interaction is assumed to be switched.

$$\beta(t) = \omega_{e_0}^2 \exp \left\{ -\frac{1}{2} \frac{\omega_{c_1}^4}{\omega_{e_0}^2} t^2 \right\} \quad (211)$$

The normalized VACF, denoted $\dot{\chi}(t)$, is obtained from $\beta(t)$ by solving the following MTGLE response function equation:

$$\ddot{\chi}(t) = -\omega_{e_0}^2 \chi(t) - \int_0^t \dot{\beta}(t-\tau) \chi(\tau) d\tau \quad (212)$$

where dots denote time derivatives. The results shown in Fig. 22 are based on the Table 5 parameters obtained via the RDF route (Eqs. 209-210). It is seen from Fig. 22 that the gaussian model improves (by agreeing for longer times within the short-time region) with pressure, though it is not very good for the gaseous phase helium corresponding to 1.4GPa. It is worse at 0.5GPa (not shown) and this is to be expected. Although the gaussian friction model based on the direct moments (cf. Eqs. 207-208) of Table 5 led to overall better agreement with MD VACFs, but we do not present them here. The gaussian model is a good short time model at the higher densities of the liquid. Anyway, the RDF route at least allows us to obtain the VACFs for the solution of He* in He from the RDF data for He* bubble reported earlier.¹³ In Figure 23, we show the VACFs for the solution, based on the gaussian model friction for c-state helium bubble (obtained using the parameters of Table 5 and Eqs. 211-212). The key observations are:

- (i) the excited state (c-bubble) VACFs qualitatively change with increasing pressure in a way similar to the ground state VACFs (with 10GPa and 14GPa having essentially a limiting (saturated effect) behavior);
- (ii) the excited state VACFs decay on longer time scales than the ground state VACFs of Fig.22 at the corresponding pressures; and
- (iii) the pressure dependence of the excited state VACFs reflects a diminished excited state pressure sensitivity compared to the ground state (see Fig. 23 and inset for comparison).

(i) is a natural consequence of increased density of the liquid leading to more damping, whereas (ii) is related to the larger size of the excited state cage (the large bubble is formed due to the excited electron's repulsion of solvent atoms). (iii) gives a significant insight into what dynamical effects electronic excitation may lead to. (iii) is due to the farther lying atoms of the

liquid playing a primary role in the solvation effects for the large excited state atom's (cage) bubble. In this long-range region, RDFs are flat and less sensitive to the pressure, and hence so are the moments entering the gaussian model. This trend shows that long-time properties such as diffusion constants are probably more affected by pressure dependence of condensed phase influence on excited states than the present short-time dynamical properties.

4. Conclusions

The present pressure dependent simulations provide many insights. The behavior of He in the condensed phase is found quite different from the case of Argon. A predominant role is played by entropy effects in the liquid free energy of binding (reflected in the the internal energy of binding being an excess positive quantity). As pressure is increased, quantum effects become less (eg. at 10-14GPa cases reported here), and possibly, they may become relatively important only for the three lower pressures (0.3-1.4 GPa). The low pressure VACFs indicate gas-like behavior with a long hydrodynamic positive tail whereas the high pressure ones show the oscillatory structure characterizing a liquid-like condensed phase correlation. The RDFs lead to similar conclusions.

It is seen that the MTGLE parameters are quite sensitive to (and exponentially dependent on) the pressure. The gaussian friction model improves with pressure and provides VACFs for the excited atom's bubble from structural input (RDFs) alone. The sensitivity of the dynamics shown by the velocity autocorrelation functions, for He(3S) and He(1S) in comparison, reveals the change in the condensed phase dynamics occurring as a result of a sudden electronic transition to which the solvation structure has not adjusted. Electronic excitation leads to the sampling of lower frequency components of the solvating medium and this is reflected in the slower decay of VACFs upon electronic excitation. It is also found that an increase of pressure may introduce less variations in the translational dynamics of the excited He(3S) state than it does in the ground He(1S) state. The present heatbath models are being employed in stochastic dynamics calculations of electronically inelastic collision processes²¹ within the high pressure ^4He liquid.

REFERENCES

- 1 (a) W. S. Dennis, E. Durbin, Jr., W.A. Fitzsimmons, O. Heybey, and G. K. Walters, *Phys. Rev. Letts.* **23**, 1083 (1969); (b) J. C. Hill, O. Heybey, and G. K. Walters, *ibid.* **26**, 1213 (1971); (c) John L. Watkins, Jonas S. Zmuidzinas, and Gary A. Williams *Physica* **108B**, 1313 (1981); (d) A. P. Hickman, W. Steets, and N. F. Lane, *Phys. Rev.* **B12**, 3705 (1975); (e) Y. M. Shih and C-W. Woo *Phys. Rev.* **A8**, 1437 (1973); (f) G. J. Thomas, W. A. Swansiger, and M. I. Baskes, *J. Appl. Phys.* **50**, 1942 (1979); (g) G. J. Thomas and R. Bastasz, *J. Appl. Phys.* **52**, 6426 (1981).
- 2 (a) J. P. Hansen and E. L. Pollock, *Phys. Rev.* **A5**, 2214 (1972) and references therein; (b) Various articles in Rare Gas Solids, ed. M. L. Klein and J. A. Venables, (Academic, New York, 1976); (c) R. Aziz, V. P. S. Nain, J. S. Carley, W. L. Taylor, and G. T. McConville, *J. Chem. Phys.* **70**, 4330 (1979); (d) J. Talbot, J. L. Lebowitz, E. M. Waisman, D. Levesque, and J.-J. Weis, *J. Chem. Phys.* **85**, 2187 (1986).
- 3 (a) P. Loubeyre, J. M. Besson, J. P. Pinceaux, and J. P. Hansen, *Phys. Rev. Lett.* **49**, 1173 (1982); (b) J. M. Besson, R. Le Toullec, P. Loubeyre, J. P. Pinceaux, and J. P. Hansen, IX AIRAPT International High Pressure Conf. Proc. Vol. 22 of High Pressure in Science and Technology (North-Holland, Amsterdam, 1983), Chap. II, p. 13.
- 4 (a) D. Levesque, J. J. Weis, and M. L. Klein, *Phys. Rev. Lett.* **51**, 670 (1983); (b) D. Levesque, J. J. Weis, and P. Loubeyre, *Phys. Rev. B* **34**, 178 (1986); (c) D. Frenkel, *Phys. Rev. Lett.* **56**, 858 (1986); (e) P. Loubeyre, *Physica* **139&140 B**, 224 (1986); (f) P. Loubeyre, *Phys. Rev. Lett.* **58**, 1857 (1987).
- 5 (a) M. Parinello and A. Rahman, *Phys. Rev. Lett.* **45**, 1196 (1980) and *J. Appl. Phys.* **52**, 7182 (1981); (b) S. Nose and M. L. Klein, *Phys. Rev. Lett.* **50**, 1207 (1983).
- 6 D. Frenkel in Proc. of the International School of Physics "Enrico Fermi", Molecular Dynamics Simulation of Statistical-Mechanical Systems, ed. C. Ciccotti and W. G. Hoover, (North-Holland, Amsterdam 1987).
- 7 (a) see ref. 2(d); (b) see ref. 3(a); (c) see ref. 4(c).
- 8 (a) P. Loubeyre and J. P. Hansen, *Phys. Lett.* **80A**, 181 (1984); (b) see ref. 4(a), (b) see ref. 4(c), and (d) see ref. 4(f).
- 9 (a) D. M. Ceperly and H. Partridge, *J. Chem. Phys.* **84**, 820 (1986); (b) see ref. 4(c).
- 10 (a) see. ref. 4(f); (b) P. Loubeyre, *Phys. Rev. B* **37**, 5432 (1988).
- 11 (a) see ref. (3); (b) R. L. Mills, D. H. Liebenmberg, and J. C. Bronson, *Phys. Rev. B* **21**, 5137 (1980).
- 12 (a) S. A. Adelman *J. Chem. Phys.* **73**, 3145 (1980); Adv. Chem. Phys. **44**, 143 (1980); *Ibid* **53**, 611 (1983); (b) C. L. Brooks III and S. A. Adelman, *J. Chem. Phys.* **76**, 1007 (1982).
- 13 C. S. Murthy and P. K. Swaminathan, *J. Chem. Phys.* (submitted).
- 14 (a) R. M. Jordan, H. R. Siddiqui, and P. E. Siska *J. Chem. Phys.* **84**, 6719 (1986); (b) R. M. Jordan and P. E. Siska *J. Chem. Phys.* **80**, 5027 (1984).

- 15 See table II of ref. 14a except that due to a misprint, the sign of the c parameter entering Region B interaction must be changed for the a-state potential fit.
- 16 B. J. Berne and G. D. Harpe, in Adv. Chem. Phys. **17**, 63 (1970) ed. I. Prigogine and S. A. Rice, (Interscience Publishers).
- 17 M. Berkowitz, J. D. Morgan, D. J. Kouri, and J. A. McCammon, *J. Chem. Phys.* **75**, 2462 (1981).
- 18 (a) B. J. Alder and T. E. Wainwright, *Phys. Rev. A* **1**, 18 (1970); (b) A. Rahman, *Phys. Rev. A* **160**, 277, (1964).
- 19 (a) K. Singer and W. Smith, *Molec. Phys.* **57**, 761 (1986); (b) F. Barocchi, M. Neumann and M. Zoppi, *Phys. Rev. A* **36**, 2440 (1987); (c) M. Takahashi, *J. Phys. Soc. Japan*, **55**, 1952 (1986); (d) W. B. Smith and K. Singer, *Molec. Phys.* (in press).
- 20 ω_{e0} and ω_{c1} are related to the second and fourth frequency moments of the system spectral density and are defined, for eg. see ref. 12(a).
- 21 (a) B. C. Garrett, P. K. Swaminathan, C. S. Murthy, and M. J. Redmon, *J. Chem. Phys.* **87**, 3207 (1987); (b) B. C. Garrett, P. K. Swaminathan, and C. S. Murthy, *J. Chem. Phys.* **88**, 2822 (1988).

Condensed Phase Dynamics

Introduction

The condensed phase dynamical problems relevant to HEDM research involve considerable richness in possible complexity; they can also involve quite a broad range of phenomena in terms of the relevant physics and chemistry. Since the main goal of the three year program was to develop new and required methodologies using helium metastables as prototypes, our specific calculations have been determined by the relevant physics of this system. The real depth of the benefits from the three year program becomes clear only by imagining the intrinsic generality of the computer simulation techniques developed here and the fact that in coordination with the simulations, we can also employ previously existing technology such as variational transition state theory¹ to treat a wide variety of condensed phase reaction and aggregation phenomena that have now become relevant to HEDM preparation and storage issues.

The helium metastable dynamics in a high pressure helium bath can be adequately described by the SCEM+GLE technology which was developed by this effort into a tool for chemistry of species embedded in the bulk. Previous to this program, the existing technology was mainly developed for gas-surface collisions and assumed asymptotic noninteracting species undergoing a collision and separating again. The present effort began by completing our work on a variable time step integration of the stochastic equations of motion employed in the SCEM+GLE framework.²

When a "collision" occurs within the bulk, the semiclassical equations do not lead to long time asymptotic constant values of probabilities, since the heatbath is constantly interacting with the primary "collision partners" and perturbing the primary zone states into making transitions. We have adapted the SCEM+GLE methodology for liquid bulk by (1) implementing a thermal sampling of initial conditions for the "collision" in the bulk solution and (2) developing new ways to analyze the results of the semiclassical propagation to obtain observables. The second step presently involves examining appropriate time correlation functions. In particular, probability fluctuation autocorrelation functions yield information regarding lifetimes of given quantal states from their decay time. Such an analysis is soundly based on the time correlation function formalism of nonequilibrium statistical mechanics.³

The next subsection describes our dynamical calculations using the SCEM+GLE technology on the problem of metastable helium atoms trapped in condensed phase bubbles. It then summarizes the overall implications of our results in terms of what happens to the stored energy of helium metastable atoms in gas and liquid helium as a function of pressure. The subsection also finally sketches how the simulation techniques could be combined with other in-house techniques at Chemical Dynamics to address related and quite different possible fates of HEDM's in condensed phases; this type of framework is relevant to the problem of Li storage in

hydrogen or other conventional fuels such as hydrazine which are being presently explored at the astronautics laboratory (AFSC).

Dynamics of $\text{He}^*(^3\text{S})$ in Condensed Phase Bubbles

1. Solvated Dynamics

Since the metastable helium bubble, whose structure was discussed in the previous section, is too large to explicitly include all the several dozen solvent He atoms of even the first solvation shell, solvated dynamics was modelled by one solvent on either side of a collinear triatomic model, schematically shown in Fig. 24, where the central atom is the atomic metastable, $\text{He}^*(^3\text{S})$. The dynamics calculations in solution were based on employing a two state model including only a and X states along with their spin-forbidden radiative coupling. These SCEM+GLE simulations were done for different pressures (in the GPa range) and showed no significant radiative quenching on time scales much longer than that found for reactive clustering. The latter timescale was estimated from limited MD simulations of the solution system whose MC study is reported in a previous section (see p. 94). The former was manifested by a nondecaying probability fluctuation autocorrelation function for very long times. *The net conclusion is that the reactive (clustering) channel is more likely than radiative quenching in the bulk and hence the primary loss mechanism for the excited atoms.* The pressure dependence of this reactive clustering channel was revealed and investigated at length in our MC simulations.

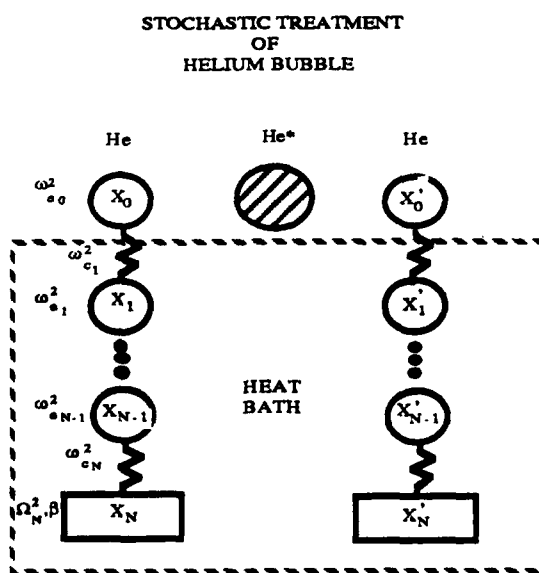


Figure 24. Schematic diagram of stochastic model with an elementary primary zone made of helium metastable atom and (effective) "ghost" atoms that represent the liquid helium heatbath.

The collinear model system was explored numerically at this stage to illustrate the basic feasibility of employing the present methodology and to display the appropriate time correlation function behavior expected in different systems with different condensed phase HEDM lifetimes. The collinear triatomic system modelling the He^* bubble in a high pressure He liquid matrix was studied using the semiclassical eikonal method for the primary zone and the generalized Langevin equation (GLE) to simulate heatbath effects. Probability fluctuation auto correlation functions (ACFs) for ^3S state of He^* are shown in Figs. 25 and 26 for 0.5GPa and 1.4GPa a-bubble which compare well to the displacement autocorrelation functions. The comparison of a variety of mode ACFs can yield information about the roles of various condensed phase modes of quenching in destabilizing the HEDM. The generalized Langevin approach correctly incorporates the local and macroscopic mode participations in primary quenching dynamics.

The dynamics shown is for radiative quenching of $\text{He}^*(^3\text{S})$ but we have employed arbitrarily increased electronic dipole couplings so as to obtain numerically facile rapid quenching behavior. As mentioned above, no radiative quenching is observed in such calculations when the actual dipole coupling strength of Chabolowski et. al.⁴ is employed since reaction occurs before quenching. Special dynamical methods are being developed for treating quenching in very long-lived HEDM species (cf. persisting ACFs), otherwise requiring long trajectories. The technology employed in this simple model may also be applied to the dynamics of vibrational relaxation in matrices; such a semiclassical, rather than classical, description is especially appropriate if $V \rightarrow V$ transfer is an important relaxation route. The adaptation of the SCEM scheme can be accomplished by expanding in a suitable joint matrix-host basis set.

2. Summary of Results on Helium Metastables

In conclusion, we summarize the overall picture already obtained from the above illustrative studies of the helium metastable quenching pathways in gas and condensed phases.

Radiative versus Nonradiative Quenching in the Gas Phase

Quenching via radiative decay in vacuum of a isolated helium atom in 2^3S state is controlled by the relativistically induced magnetic multipole couplings within the atom. Gas phase quenching at higher pressures comes from He- He^* collisions. Although the system can in principle quench nonradiatively, it was found that the related probabilities are very low, $\sim 10^{-16}$, compared to $\sim 10^{-8}$ for the radiative routes. The direct radiative route from a to X state made possible by spin-forbidden radiative coupling seems to be the dominant quenching mechanism in all our studies so far. This was also assumed for the present analysis of the condensed phase problem.

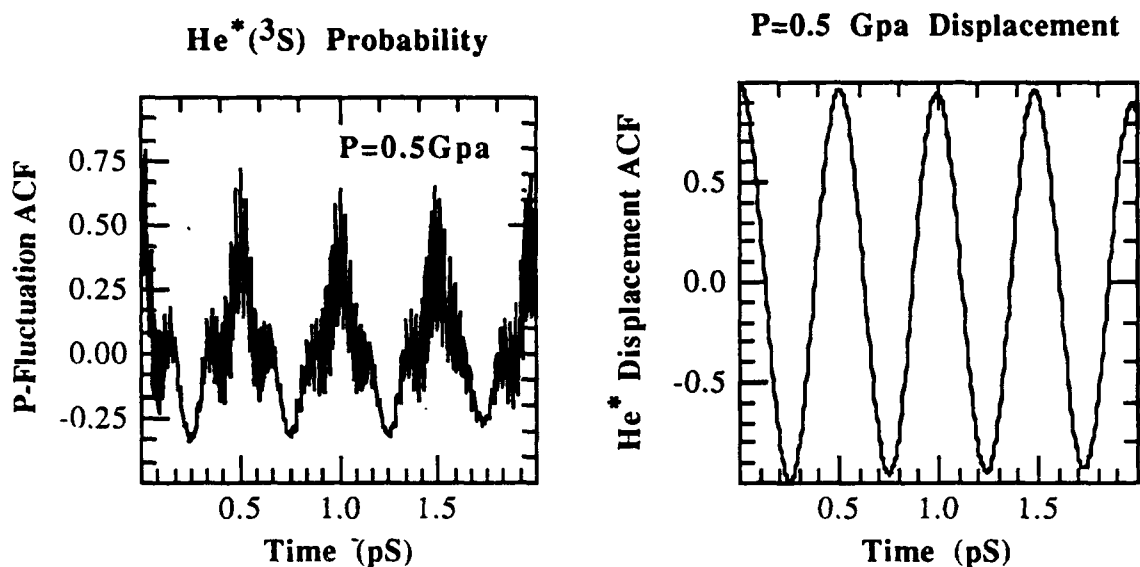


Figure 25. Results from the stochastic dynamics at 0.5 GPa showing the fluctuation autocorrelation function (of excited He*); this function will display decay of excitation due to electronically inelastic collisions within the liquid bulk. (b) the displacement autocorrelation function of the metastable He* atom in liquid.

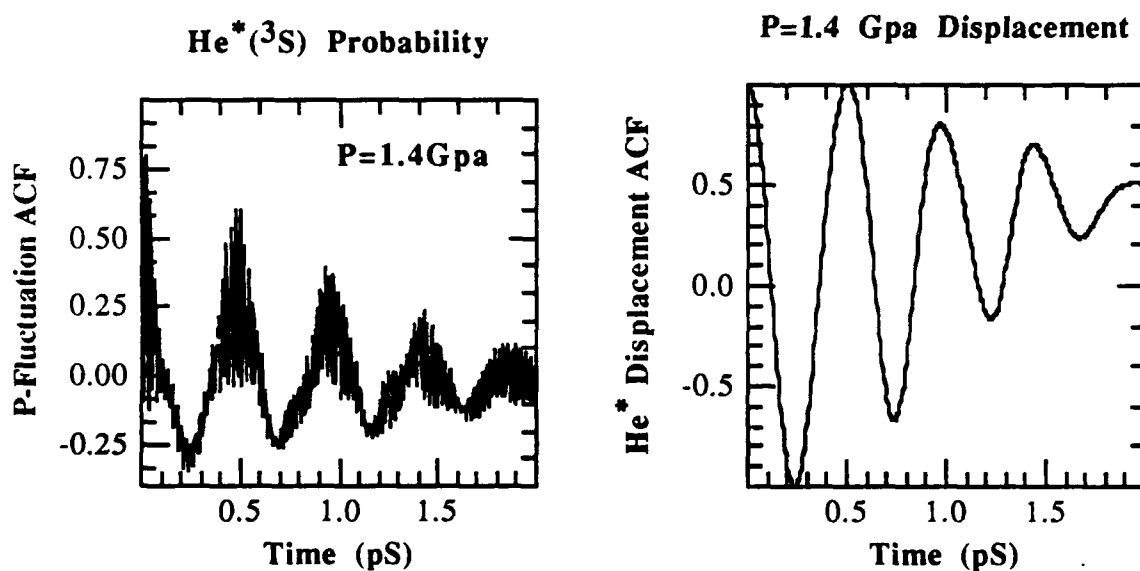


Figure 26. Same as Fig. 25 for a pressure of 1.4 GPa.

Radiative Quenching versus Reaction in Solution

The behavior of an excited atomic helium species in condensed phase involves electronically nonadiabatic solute/solvent interactions. If these are taken to be reasonably described by the gas-phase two-body potentials, estimates of condensed phase behavior may be obtained

from the computer simulations described in the previous subsections. The extremely small nonradiative and many-state collisional quenching pathways of Fig. 4 are assumed to be ignorable upon transferring to condensed phase in our present analysis. This means two-state models, such as the a and X combination used in Fig. 5, are adequate in the condensed phase and hence the a and c states are the only key potentials. Interactions of a $\text{He}^*(2^3\text{S})$ in a high pressure helium liquid lead to quantitatively different stabilities for the metastable atomic species depending on the a-state and c-state characters of solute-solvent potentials. The c-state bubble protects the atomic species up to very high pressures whereas the a-state more easily allows reaction with a solvent He atom leading to a pronounced degree of cluster formation that varies with pressure.

One remarkable feature (seen in the Monte Carlo simulation of helium bubble states) is the maintenance of a bubble structure despite the cluster formation (at least when the simulation employs reasonable pairwise additive interactions). The c- and a-states are radiatively coupled in reality and both states can play a role in determining the metastable atom's equilibrium bubble shape. The cluster formation observed here is a neutral excitation trapping process in liquid that is analogous to the charged exciton trapping phenomenon observed⁵ in rare gas halide crystals. These results indicate that stabilization of a metastable by forming clusters of it with a suitable co-species may still result in trapping into bubbles in the condensed phase. Since such bubbles can protect the species' energy from dissipation to bulk, it is useful to identify conditions for their formation in different matrices for different species.

It is verified that reaction is the dominant loss mechanism in condensed phases when compared to collision-induced radiative decay. It was found that the reaction can go on to result in formation of higher clusters, but sensitively depending on pressure and electronic state of interactions. The solution structure has been examined via computer simulations. The parameterization for a GLE heatbath description obtained that were then used in exploratory condensed phase dynamics of the HEDM. It has been found that there is no radiative quenching on the time scales within which significant reaction occurs.

Cluster Stability and Concentration Effects in Solution

Clearly, the above results show that the average degree of aggregation achieved by the clustering events depends on the thermodynamic state. Another factor in controlling their stability is the concentration of such clusters each of which could potentially release the stored energy in collisions. These studies require many-body potentials and we do not have any information pertaining to these yet. But it is believed from concentration dependence studies that dimer-dimer collisions in liquid reduce dimer lifetimes to as small as 30ms⁶ at a density of 10^{12}cm^{-3} .

Extended Studies

Solvent Shift of $2^3S \rightarrow 2^3P$ Absorption Line

Another key application of the present technology is to obtain spectral absorption and emission profiles for HEDM's in the condensed phase that include detailed solvent static and dynamical shifts and any shape changes. Such calculations can be valuable for interpreting the mechanisms controlling/modifying condensed phase experimental spectral data and in comparing to gas phase spectra. We have performed illustrative calculations using the recent helium potentials of Yarkony to reveal this capability.

One of the early key experimental observations on helium bubbles was the blue shifted nature of the above absorption line in contrast to a red shifted nature of the corresponding emission line. This was fruitfully studied in a phenomenological bubble model⁷ using adiabatic line shape theory in the static limit. Solvent static and dynamical effects can both in general play a role in shifting spectra. Although we have characterized the high pressure helium bath and deduced parameters for stochastic dynamics simulations of metastable species trapped in it, in the case of the present atomic transition, solvent dynamics can be shown to be less crucial in determining the absorption line at high pressures (a typical bath atom moves only $\sim 0.2a_0$ within a transition dipole relaxation time compared to $\sim 1.5a_0$ for the low pressure cryogenic regime where previous experiments were). *We have verified from our studies the previous experimental absorption line blue shifts* employing the quantal radial distribution function from Hansen and Pollock⁸ and Yarkony's¹ transition dipole function. We have also performed a similar calculation employing our radial distribution function for the a-bubble and the $a \leftrightarrow b$ transition dipole function to *find a large red shift for the high pressure line position* by $\sim .29\text{eV}$. This value should be modified by considering contributions due to transitions dictated by the (presently unknown radiative) coupling of the c-state to the u-manifold (outside the primary space employed by Yarkony) of the 2^3P asymptote. We have found that the *large red shift is predicted even when the contribution from the clustering region of a-bubble is subtracted*. At slightly lower pressures, the complication of reaction may be avoided and the degree of a,c mixing characterized via spectroscopic studies.

Studies on the H_2 matrix

We have conducted preliminary studies on condensed phase liquid hydrogen (high pressure, in the Gpa range, and hence classically described) with a two center Lennard-Jones (2LJC) anisotropic effective pair potential. The goal of using an anisotropic potential even though liquid hydrogen is known to be quite isotropic in behavior was to develop the codes and analysis tools for such a general diatomic condensed phase matrix.

The first step is to devise an effective anisotropic pair potential for condensed phase simulations of molecular hydrogen. MD calculations have been carried out for liquid H_2 system of 108 molecules interacting through two Lennard-Jones centers (2LJC) coincident with the positions of the atomic masses. Figures 27-29 display the center of mass (c.m.) pair correlation functions (PCFs) for special configurations and the time correlation functions (TCFs) for 2LJC-model H_2 at 265K and 4 GPa.

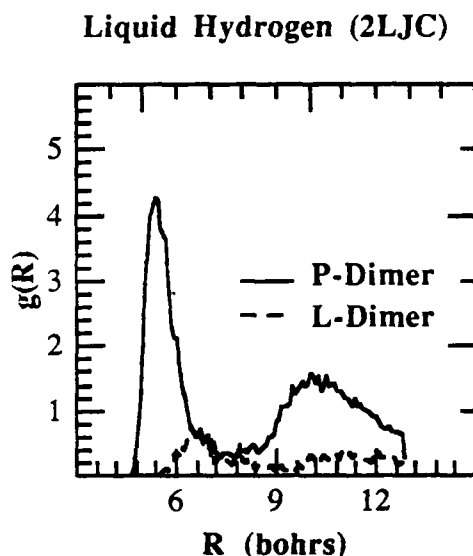


Figure 27. Simulation results for radial distribution function of parallel (P) and L-shaped hydrogen dimers in liquid.

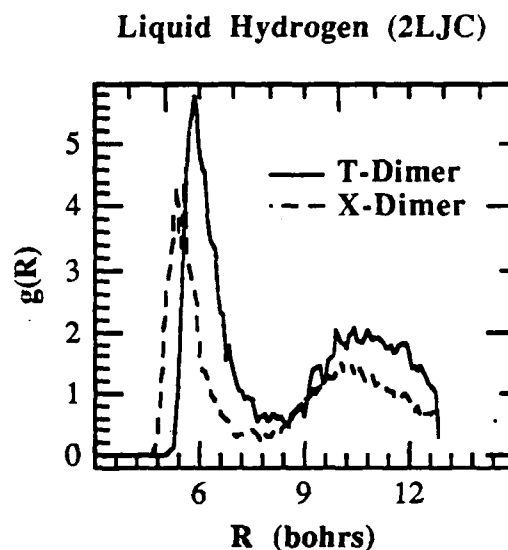


Figure 28. Simulation results for radial distribution function of T- and X- shaped hydrogen dimers in liquid.

Figures 27-28 display c.m. PCFs for configurations which lie within $\pm 10^0$ of specific relative orientations: 'X'='crossed', 'P'='parallel adjacent', 'T'='T-geometry', and 'L'='linear, or parallel end to end'. The position of the maxima of these PCFs compare well with the position of the potential energy minima for two isolated molecules in the corresponding configuration. This indicates that the presence of other molecules in the dense liquid have little effect on the minimum of the potential field which acts on adjacent molecules. By contrast, for the models of other related linear molecules, (K. Singer, A. Taylor, and J. V. L. Singer Mol. Phys. 33, 1757 (1977)) the same arrangements have been found to be almost equally stable. Figure 29 displays the c.m. and angular velocity auto-correlation functions of the 2LJC-model H_2 . In the liquid state, the VACF exhibits a negative minimum, which is interpreted as caused by back-scattering by nearest-neighbors, and a long negative tail, ascribed to a cooperative motion of the surrounding particles.

The double minimum in the c.m. VACF can be interpreted (J. Barojas, D. Levesque, and B. Quentrec Phys. Rev. A2, 1092 (1973)) as arising from the different mobility of a linear molecule parallel and at right angles to its axis. This is clear from the c.m. VACFs of velocity components parallel and perpendicular to the molecular axis. The minimum of $VACF_{\perp}$ is deeper and occurs at earlier times than that of $VACF_{\parallel}$. The presence of double minimum in $VACF_{\perp}$ was interpreted to be the result of successive negative impulses transmitted to the c.m. first by one and then by the other end of the molecule, as it encounters obstacles. The angular VACF would also exhibit negative minimum for more anisotropic systems.⁹

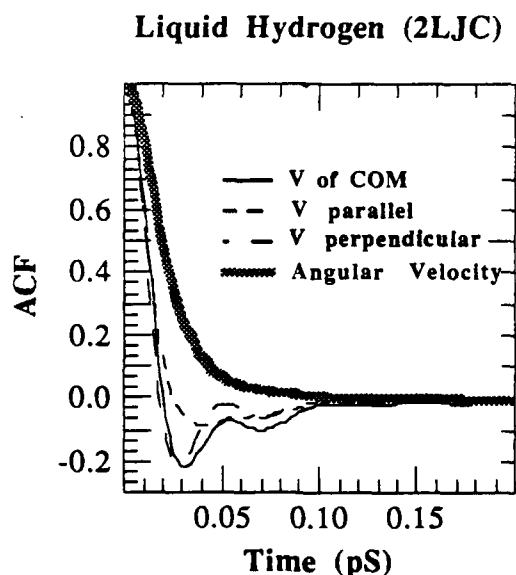


Figure 29. Simulation results for autocorrelation functions of various components of the molecular velocity in liquid hydrogen; correlation functions of center of mass, parallel, perpendicular and angular velocities are shown.

Detailed Studies of Molecular Structure:

The pair correlation function (pcf) for linear molecules is generally defined as $g(R, \theta_1, \theta_2, \phi_{12})$, where $R = |\mathbf{R}_{12}|$, \mathbf{R}_{12} being the vector joining the two centers of mass; $\cos \theta_1 = \mathbf{l}_1 \cdot \hat{\mathbf{R}}_{12}$, $\cos \theta_2 = \mathbf{l}_2 \cdot \hat{\mathbf{R}}_{12}$, and $\cos \phi_{12} = (\mathbf{l}_1 \times \hat{\mathbf{R}}_{12}) \cdot (\mathbf{l}_2 \times \hat{\mathbf{R}}_{12})$; $\mathbf{l}_1, \mathbf{l}_2$ are the bond vectors of molecules 1 and 2, and $\hat{\mathbf{R}}_{12}$ denotes unit vector. It is difficult to study the properties of such a 4-dimensional correlation function. The expansion in terms of spherical harmonics can be used to analyze the pcf of linear molecules¹⁰:

$$g(R, \theta_1, \theta_2, \phi_{12}) = 4\pi \sum_l \sum_{l'} \sum_m g_{ll'm}(R) Y_{l,m}(\theta_1, \phi_1) Y_{l',-m}(\theta_2, \phi_2) \quad (213)$$

where $Y_{l,m}$, $Y_{l',-m}$ are normalized associated Legendre functions. Although not directly measurable until very recently,¹¹ the coefficients $g_{l,l'm}$ can be obtained from the translational and rotational trajectories of the molecules in the computer "experiment".

The site (atom)-site pcf $g_s(r)$ defined by

$$\frac{N^2}{2V} g_s(r) = \lim_{\Delta r \rightarrow 0} \frac{1}{2} \sum_j \sum_s \sum_{j'} \sum_{s'} n(r < r_{isjs'} < r + \Delta r) / 4\pi r^2 \Delta r \quad (214)$$

where N is the number of molecules, V is the volume, s and s' correspond to the nonbonding sites of the pair of molecules i and j , and $n(r)$ is the histogram count. $g_s(r)$ is related by Fourier inversion to the static structure factor which can be determined by X-ray or neutron diffraction. Useful information has also been obtained from the incidence of certain special configurations as functions of molecular separation.

The site-site pcf, the first six coefficients in the above expansion and the four special configurations have been calculated for molecular H_2 at 270K (~4 GPa). The principal characteristics of these structural features are reported in Table 7.

Curves for the first six radial distributions which arise as non-vanishing coefficients in the expansion (1) are shown in Figs. 30 and 31. The general appearance of the $g_{l,l'm}$ is surprisingly similar to the long (more anisotropic) linear molecules.¹²

$g_{000}(R)$ is the c.m. pcf. The main peak occurs at 5.83 bohr which coincides with the peak of the corresponding T pcf. The second peak is at somewhat less than twice the distance of the first peak, R_{max} . It could obviously arise from two vectors of length R_{max} making a small angle with each other. There is no bulge on the left-hand side of the first peak. This is mostly the case with less anisotropic molecules such as N_2 , F_2 . Generally its range of correlation has been found to be greater than that of $g_s(r)$. As we employed 108-molecules in our preliminary simulation studies, the correlation length is restricted and does not extend beyond the second maximum. The necessity to carry out large system is thus apparent.

Table 7: Characteristics of pair correlation functions

Positions (bohrs) of maxima of pcf's for special configurations			
	X 5.29	P 5.41	T 5.83
			L 6.43
	Maxima at (bohr)	Minima at (bohr)	
$g_s(r)$	5.69, 10.57	8.09	
g_{000}	5.83, 10.6	8.05	
g_{200}	6.28	5.41	
g_{220}	5.23, 6.67	5.71	
g_{221}	6.19	5.29	

$g_{200} \approx f(R) \langle 3 \cos^2 \theta_1 - 1 \rangle_R$ has no negative lobe at small R; this is because if the centers of mass are close to one another the vector connecting them is likely to be approximately normal to the axes of both molecules -as in the configurations X and P. The maxima of these pcf's is in fact close to the minimum of g_{200} . The zeros of g_{200} result from the cancellation of positive and negative contributions to $\langle 3 \cos^2 \theta_1 - 1 \rangle_R$ arising from $\theta_1 > \cos^{-1}(\sqrt{3}/3)$; they occur at separations which are close to the main peaks of g_{000} . For the T configuration $\langle 3 \cos^2 \theta_1 - 1 \rangle$ equals either 2 or -1, and a small mean value of the angular factor for arrangements close to T is plausible. This is compatible with a large contribution of T configurations to the main peak of g_{000} .

Figure 30. Simulation results for g_{000} , g_{200} , and g_{220} coefficients of Eq. (213).

$g_{ll'm}$ coefficients

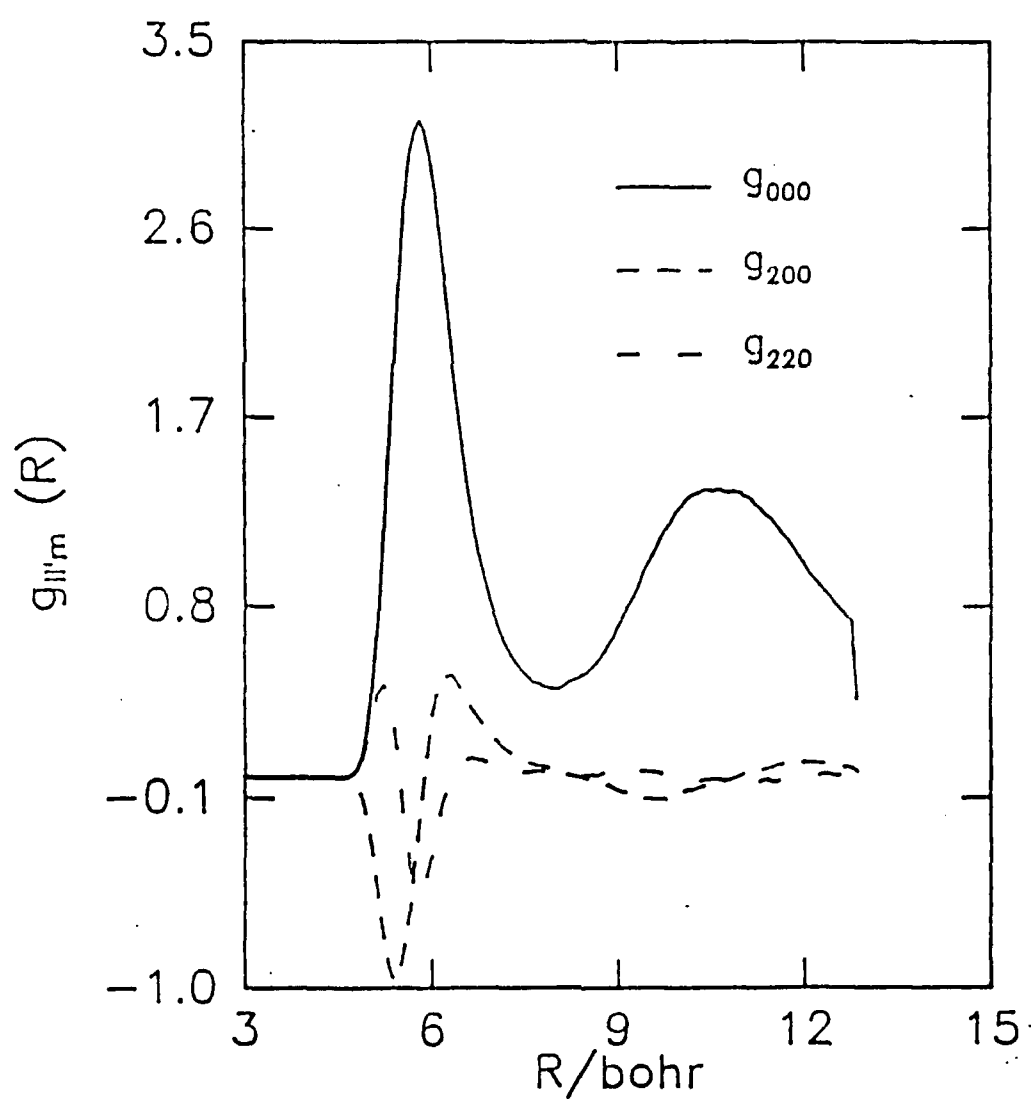
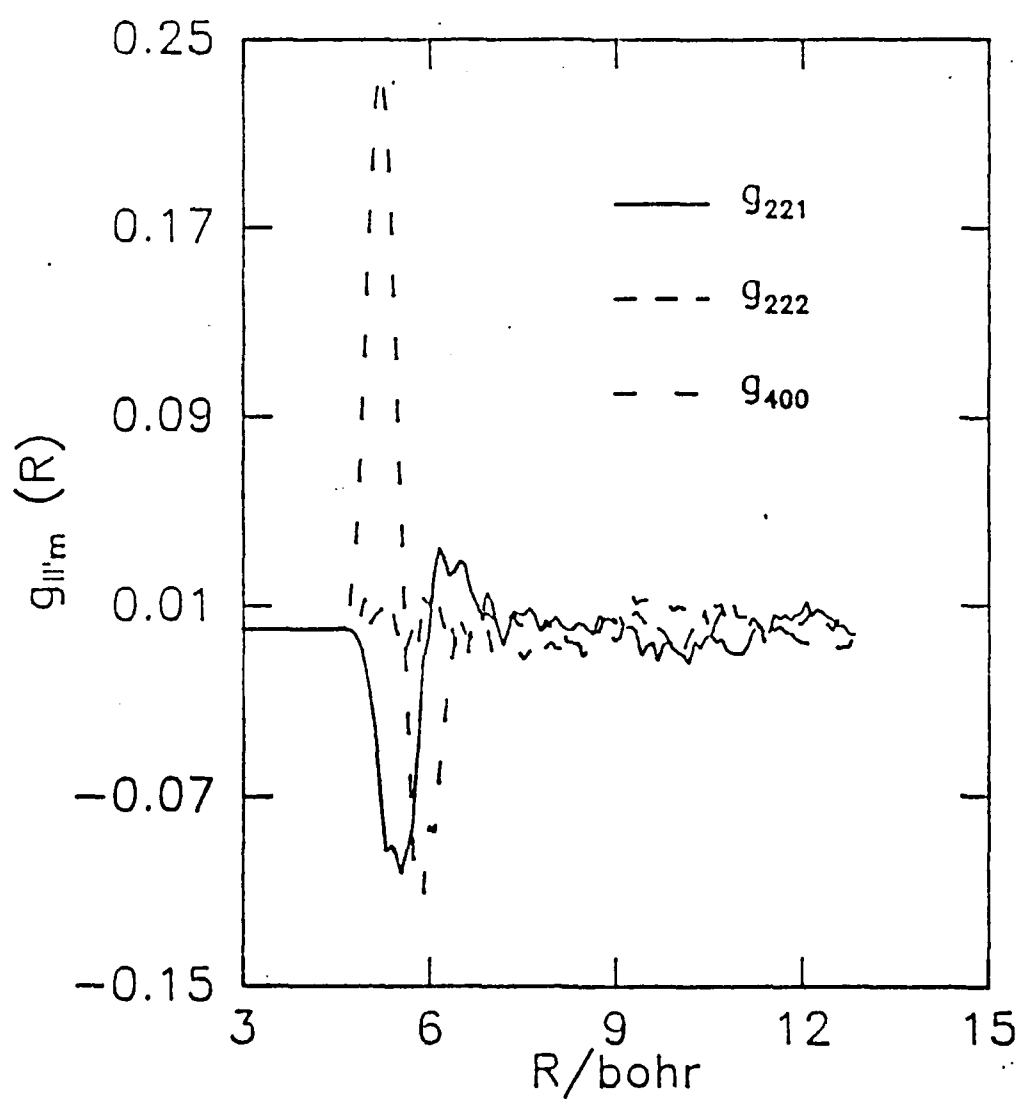


Figure 31. Simulation results for g_{221} , g_{222} , and g_{400} coefficients of Eq. (213).

$g_{ll'm}$ coefficients



For $g_{220} \approx f(R) \left\langle 3 \cos^2 \theta_1 - 1 \right\rangle \left\langle 3 \cos^2 \theta_2 - 1 \right\rangle_R$, the initial positive lobe with a maximum at 5.23 bohr indicates $\theta_1 \approx \theta_2 \approx \pi/2$, i.e. + and II like configurations. The lowest possible value of the angular factor occurs at $\theta_1 = \pi/2, \theta_2 = 0$ or vice versa, i.e. for T configuration. Table 7 shows that the minima of g_{220} almost coincides with the maxima of g_{000} . This again points to a significant incidence of T configurations at the main peak of g_{000} . The subsequent positive lobe is probably due to L-like configurations.

The geometrical interpretation of the higher expansion coefficients becomes rapidly more complicated. The theoretical significance of the expansion lies in its possible use in perturbation expansion for anisotropic potentials.

REFERENCES

- 1 D. G. Truhlar, A. D. Isaacson, and B. C. Garrett, in "Theory of Chemical Reaction Dynamics"; M. Baer, Ed.; CRC Press: Boca Raton, FL (1985); Vol. 4, p65.
- 2 B. C. Garrett, P. K. Swaminathan, C. S. Murthy and M. J. Redmon, "Implementation of Variable-Step Stochastic dynamics for electronically inelastic gas-surface collisions", J. Chem. Phys. **87**, 138 (1987).
- 3 D. McQuarrie, "Statistical Mechanics" (Harper and Row, 1976).
- 4 C. Chabalowsky, J. O. Jensen, D. R. Yarkony, and B. H. Lengsfeld III, J. Chem. Phys. **90**, 2504 (1989).
- 5 The authors thank Professor A. Apkarian for discussions concerning this topic.
- 6 J. W. Keto, M. Stockton, and W. A. Fitzsimmons, Phys. Rev. Letters **28**, 792 (1972).
- 7 A. P. Hickman, W. Steets and N. F. Lane, Phys. Rev. B **12**, 3705, 1975.
- 8 J. P. Hansen and E. L. Pollock, Phys. Rev. A **5**, 2214 (1972).
- 9 K. Singer, J. V. L. Singer, and A. J. Taylor, Mol. Phys. **37**, 1239 (1979).
- 10 W. B. Street and D. J. Tildesley, Proc. Roy. Soc. A **348**, 485 (1976).
- 11 D. Zeidler, Preprint (1988).
- 12 K. Singer, A. Taylor, and J. V. L. Singer, Molec. Phys. **33**, 1757 (1977).

CONCLUSIONS AND RECOMMENDATIONS

From our gas phase method development efforts, based on the semiclassical computational approach (within the eikonal approximation) we conclude that the approach is useful for applications to collisional problems that are difficult to treat quantum mechanically due to the large number of nuclear rovibrational states (coupled channels). The present semiclassical methodology reveals much formal flexibility, and techniques are now available for applying it to different levels of treatment of both classical and quantum dynamics of polyatomic systems. For each application, the principles validated by our research should be carefully exploited in choosing a computational strategy; the strategy should depend on the nature of the potential energy surface on which the collision dynamics evolves, the accuracy of the available potentials and couplings and the accuracy with which state-to-state results are needed. Validation studies described in this report are not exhaustive, but do illustrate of the potential of the methods. New directions for novel and efficient semiclassical computations have been formally developed by employing semiclassical wavefunctions for multidimensional electronically inelastic problems, although the validations of this new approach (studies of $O+HF$ and $Na+H_2$ collisions) have been done only for multidimensional single potential surface problems. A "primitive" version of the theory (not using semiclassical wavefunctions) was employed for most of this research, since the formal improvements were discovered towards the end of the research. The primitive method has been illustrated using the (many-surface) electronically inelastic problem of metastable helium collisions in both gas and condensed phases.

The effort on condensed phase modelling, and simulations on helium metastable structure and dynamics in liquids illustrate the power of the computational approach by revealing microscopic aspects of the phenomenon of bubble formation around an electronically excited atom in a liquid. The sensitivity of the simulation method to the potential surfaces for different electronic states shows that semiquantitative levels of treatment are possible. Even using approximate potential energy surfaces, such calculations can be used to reveal mechanistic details that are not easily accessed in experiments, and assist in the interpretation of condensed phase chemistry experiments. Our experience in building a stochastic model for the simple helium system can lead the way for treating other inert gas hosts; however, heavier inert gas systems do exhibit different phenomena and require more complex potential surface information. Systems such as the hydrogen matrix, also recently studied by us, can display more complex behavior that may be difficult to obtain accurate potential energy information on; this can happen if the excited state chemistry involves many hydrogen molecule neighbors, and atom transfer. The key requirement for

dynamical studies is potential energy surface information, and systems for which this is available are amenable to theoretical studies.

The ground state dynamics of different species in the hydrogen matrix can be treated by combining the present methods with more standard methods such as variational transition state theory. Besides computing rates for elementary chemical processes and lifetimes of species, the technology developed here is also useful for obtaining theoretical line shapes for solid matrices, a quantity directly probed in experiments.

PUBLICATIONS, MEETINGS ATTENDED, OTHER INTERACTIONS AND PERSONNEL

Publications Acknowledging this Contract

- (1) B. C. Garrett, P. K. Swaminathan, C. S. Murthy and M. J. Redmon, "Implementation of Variable Time Step Stochastic Dynamics for Electronically Inelastic Gas-Surface Collisions", J. Chem. Phys. **87**, 3207 (1987).
- (2) C. S. Murthy and P. K. Swaminathan, "Monte Carlo Simulation of Helium Bubble States", J. Chem. Phys. **90**, 2776 (1989).
- (3) P. K. Swaminathan, and C. S. Murthy, "Heatbath Models for Helium Bubble States", J. Phys. Chem. submitted.
- (4) B. C. Garrett, M. J. Redmon, and P. K. Swaminathan, "Comparison of the SCE Method and Close Coupling Results for a Model Atom-Atom Electronic Quenching Process", in preparation.
- (5) P. K. Swaminathan, B. C. Garrett, and C. S. Murthy, "Liquid Quenching of He^* Metastables in High Pressure Helium Matrix", in preparation.
- (6) B. C. Garrett, M. J. Redmon, and D. G. Truhlar, "The Quenching of $\text{Na}(3^2\text{P})$ by H_2 : A Quantal IOS calculation of Electronic to Vibrational Energy Transfer", in preparation.
- (7) P. K. Swaminathan, G. A. Natanson, B. C. Garrett, and M. J. Redmon, "The Quenching of $\text{Na}(3^2\text{P})$ by H_2 : Comparison of the SCE Method and Close Coupling Results ", in preparation.
- (8) G. A. Natanson, P. K. Swaminathan, B. C. Garrett, and M. J. Redmon, "The Quenching of $\text{Na}(3^2\text{P})$ by H_2 : Comparison of Semiclassical T-amplitudes and Close Coupling Results", in preparation.
- (9) G. A. Natanson, and P. K. Swaminathan, "Semiclassical Methodology for Computing Multichannel Eikonal Wavefunctions in Molecular Collisions: A Reformulation and Extension", for publication in Journal of Chemical Physics.

Meetings in addition to HEDM contractor's meetings:

1. Gas/Surface Interactions Gordon Conference, 1987
2. Dynamics of Molecular Collisions meeting Wheeling, W. Va. 1987
3. Structure and Dynamics of Clusters Gordon Conference, 1988.
4. Dynamics of Molecular Collisions meeting, Asilomar, CA 1989

Other Interactions:

Significant scientific interactions on the topics of the present research have occurred with the following scientists who were a part of the HEDM effort during this period. We have kept our own work coordinated and relevant in a synergistic manner with their HEDM research efforts.

Byron H. Lengsfeld III and George Adams' research group

There were close collaborations between Chemical Dynamics and the Ballistics Research Laboratory (BRL) during this period. Several visits and discussions occurred. BRL calculations, in collaboration with the Johns Hopkins effort of David Yarkony, provided information on the potential energy surfaces for helium and other helium and hydrogen metastable species. The He-He system was discussed in depth.

David R. Yarkony

There were fruitful interactions on the helium problem and the requirements expected of quantum chemistry for solving electronically inelastic radiative and nonradiative dynamical problems.

Daniel Konowalow

The main interactions were on the sensitivity of condensed phase effects on long range helium potentials and the possibility of obtaining *ab initio* potentials for use in Li/H₂ matrix simulation studies.

Marcy Rosenkrantz

The main interactions were on methods for different species-matrix interactions to be employed for dynamics studies.

Steve Rodgers

A number of significant interactions occurred regarding the important technologies for HEDM research, especially for condensed phase dynamical problems.

Ara Apkarian

Stimulating discussions took place including a visit by Dr. Apkarian to Chemical Dynamics to discuss possible theoretical support of his experimental program.

Nathan Presser

The main interaction was on the condensed-phase line shape problem of sodium in rare gas solids, a problem to which the technology developed on this project can be applied.

Gilbert Collins

Recent interactions have occurred on the problem of hydrogen atom diffusion and reaction in hydrogen matrices and how to interpret the experiments on thermal spikes and isotope effects.

The following Chemical Dynamics staff members have been partially supported during this three year contract:

Dr. Pazhayannur K. Swaminathan

Dr. Michael J. Redmon

Dr. Cheruvu S. Murthy

Dr. Bruce C. Garrett